CONFIDENTIAL

C66-7893

NOTE: This document contains information affecting the national defense of the United States within the meaning of the Espionage Laws, Title 18, USC, Sections 793 and 794. The transmission or the revelation of its contents in any manner to an unauthorized person is prohibited by law.

NASA CR-54971

GA-7061

Copy No. 21

(Title Unclassified)

DETERMINATION OF EFFECTS OF METAL OXIDE ADDITIONS ON THE SOLUBILITY OF URANIUM IN UO_2

Final Report

by

S. Langer, N. L. Baldwin, F. O. Burris, Jr., and A. W. Mosen

Prepared for

NATIONAL AERONAUTICS AND SPACE ADMINISTRATION

31 March 1966

CONTRACT NAS 3-6215

Technical Management
NASA Lewis Research Center
Cleveland, Ohio
A. Doan

During the period of this report, the following "reportable items," as defined by the article "Report of New Technology," evolved: None.

Group 1

D

RESTRICTED DATA

GENERAL ATOMIC

DIVISION OF

GENERAL DYNAMICS

JOHN JAY HOPKINS LABORATORY FOR PURE AND APPLIED SCIENCE

P.O. BOX 608, SAN DIEGO, CALIFORNIA 92112

CONFIDENTIAL

CONTENTS

Figures

Tables

ABSTRACT

5165

The temperature-composition (solubility) curve for the phase boundary separating the single-phase region UO_{2-x} (s) and the two-phase region U (liquid) + UO_2 (s) was studied by high temperature thermal analysis, and the effects of varying concentrations of the additives Y_2O_3, CaO, ThO_2, and CeO_2 on this phase boundary were determined.

It was found that:

1. The solubility of U(liquid) in UO_2 in the unstabilized U-O binary system in the range of $UO_{1.52}$ to $UO_{2.06}$ (as determined in the program) is in reasonable agreement with the results of other workers obtained by equilibration techniques; and
2. The precipitation of uranium from urania is unaffected by the presence of 15 mole percent CaO or 10 mole percent Y_2O_3, ThO_2, or CeO_2 insofar as thermal analysis can detect.

Some additional information is given on liquidus temperatures, on monotectic temperatures, and on the point of maximum solubility of uranium in urania.

SUMMARY

A phase diagram study using thermal analysis techniques in an inert atmosphere has been carried out with the following objectives:

1. Investigation of U-UO_2 diagram in the region defined by an O/U ratio ranging from 1.5 to 2.1 and temperatures ranging from about 1000°C to 2550°C with special emphasis on the location of the phase boundary between the single-phase region UO_{2-x} (solid) and the two-phase region U(liquid) + UO_2 (solid). This boundary represents the limit of solubility of uranium metal in urania as a function of temperature.

2. Determination of the effects of the oxides CaO, Y_2O_3, ThO_2, and CeO_2 at varying concentrations on this phase boundary.

The results of the thermal analysis measurements on the U-UO_2 system have been compared with data obtained by other workers who used equilibration techniques. The equilibration data generally fall on the high O/U side of the most probable location of the solubility curve based on thermal analysis data. The liquidus data determined in the present program are 100° to 200°C higher than the results of other investigators.

Within the estimated experimental errors, the temperature at which uranium segregates from substoichiometric uranium dioxide has been shown to be unaffected by the presence of the additive oxides at concentrations ranging from 2.5 to 10 mole percent (to 15 mole percent in the case of CaO). That is, no significant shift in the phase boundary occurs. Therefore, the decrease in the amount of precipitated uranium metal observed in stabilized substoichiometric samples of UO_2 cannot be attributed to a shift in the location of the phase boundary.

Two additives were volatilized at high temperature from the open crucibles. Calcia was the most volatile and yttria slightly less so. This led to scatter in the data where these additives were used. Thoria and ceria were relatively non-volatile and, from this point of view, appear to be preferable to CaO or Y_2O_3 for stabilization of UO_2 at high temperatures. The liquidus and monotectic temperatures were depressed by CaO and Y_2O_3, were not changed by CeO_2, and, possibly, were increased slightly by ThO_2.

(This page intentionally left blank.)

1. INTRODUCTION

This document constitutes the final report under National Aeronautics and Space Administration Contract NAS 3-6215. The objectives of the study were to determine, by high-temperature thermal analysis, the hypostoichiometric phase boundary of the UO_{2-x} (solid) phase as a function of temperature in the range 1000° to 2550°C and to determine the effect on this boundary of the addition of varying amounts of several metal oxides. As a consequence of the redirection of the program toward materials of greater promise after partial completion of the work, the oxygen/uranium (O/U) ranges of the additives investigated were different.

The additives, the amounts thereof, and the O/U ranges finally investigated were:

Additive	Additive Amounts (mol-%)	O/U Ratio
Yttria	2.5-10	1.5-2.1
Calcia	2.5-15	1.5-2.1
Ceria	2.5-10	1.6-2.0
Thoria	2.5-10	1.6-2.0

This report describes the experimental work performed, the materials used in the study, their analysis, and the results obtained. The experimental results are analyzed and discussed, and conclusions and recommendations are presented.

1.1. Purpose and Background

Tungsten-UO_2 cermets have been under consideration for use in fuel elements for the tungsten, water-moderated nuclear rocket. This concept has been under study by the National Aeronautics and Space Administration for several years. The operating temperature of these fuel elements is 4500°F (2500°C), in flowing hydrogen.

In closed systems, it has been shown that W and UO_2 are compatible up to the melting point of UO_2. However, thermal cycling tests (1, 2) have revealed excessive fuel losses. In addition, fuel compacts have been observed to undergo cracking after high-temperature testing. Among other factors, such as mismatched thermal expansions between W and the UO_2, high impurity contents of the UO_2, and microcracks in the W cladding, the fundamental chemical behavior of UO_2 at high temperatures has been shown to be partially responsible for these problems. Thus, the reduction of UO_2 to a substoichiometric oxide by H_2 at high temperatures (>2000°C), followed by the disproportionation of the substoichiometric oxide on cooling to yield $UO_{2.0}$ and liquid uranium metal, is responsible for cracking of the cermets or the W cladding. Also, hypostoichiometric UO_2 has been shown to have an enhanced volatility, resulting in an increased rate of fuel loss (3).

A number of methods have been proposed for decreasing the fuel loss to tolerable levels and for eliminating the cracking problem. Among these are the production of UO_2 fuel particles encapsulated with W for incorporation into the cermet body and the stabilization of UO_2 by solid solution formation. Encapsulation clearly reduces fuel loss by preventing volatilization. The addition of stabilizing oxides has reduced fuel losses in some cases (4), but the mechanism is not clear. Finally, three of the proposed stabilizing additives, CaO, Y_2O_3, and CeO_2, have been shown to reduce the amount of free U precipitated, while a fourth additive (ThO_2) has not.

Although the pragmatic objectives of reducing fuel loss and preventing cracking of the compacts appear clear, the chemical effects of the stabilizing oxides in accomplishing these ends are obscure. The research reported herein has investigated one of the possible mechanisms of stabilization; i.e., the stabilization of the UO_{2-x} phase against disproportionation by solid solution formation. This concept is discussed below.

As noted above, other studies have shown that the amount of U precipitated from substoichiometric urania can be reduced by the addition of oxides of varying cationic charge, possibly by valence compensation of the

O deficiency. It was the purpose of this research to determine whether this stabilization is the result of a shift in the substoichiometric phase boundary of urania; and if so, to determine the magnitude of the shift as a function of the additive and its concentration. The problem can also be stated as a measurement of the solubility of U in urania as a function of temperature, oxide additive, and additive concentration.

1.2. The U-Urania Phase Diagram

A tentative phase diagram for the U-urania system was published by Martin and Edwards (5), and more recently was updated by them (6). This latter version of the phase diagram is reproduced in Fig. 1 and will be used as a basis for discussion of the phase behavior of the system throughout this report.

The principal features of the phase diagram which are of importance to this study are (6):

1. A wide miscibility gap in which U (liquid) + UO_{2-x} (solid) coexist is present below the monotectic temperature.
2. The monotectic liquid (L_2) is in equilibrium with UO_{2-x} at temperatures above $2470^{\circ} \pm 25^{\circ}C$.
3. The monotectic liquid has an O/U ratio of 1.3 ± 0.1 and is in equilibrium with $UO_{0.05 \pm 0.01}$ (liquid) and $UO_{1.60 \pm 0.02}$ (solid) at the monotectic temperature.
4. The hypostoichiometric UO_2 phase becomes less oxygen deficient with decreasing temperature and approaches $UO_{2.0}$ at $\sim 1000^{\circ}C$.

The studies of the hypostoichiometric boundary by Edwards and Martin were carried out by equilibrating liquid U in UO_2 crucibles at temperatures between 1600° and $2470^{\circ}C$ and analyzing the growths of hypostoichiometric UO_2 which formed between the liquid and the crucible. A similar procedure was followed by Bates and Daniel (7). The hypostoichiometric boundary was also investigated by the General Electric Nuclear Material and Propulsion Operation (GE-NMPO) by determination of the O/U ratio of the urania phase in equilibrium with liquid uranium (actually URe_2) annealed in Re capsules at various temperatures (4).* The agreement between these various sets of data was quite good considering the difficult experimental conditions. A comparison of these data is shown in Fig. 2.

All of the data presented above were obtained by equilibration techniques which basically depend on the establishment of equilibrium at elevated temperatures followed by quenching to room temperature. It is assumed that

*These data actually yield the O/U ratio of the oxide phase in equilibrium with URe_2 at the annealing temperature. These data were then corrected by studying the vapor pressure of U(gas) over URe_2 (8).

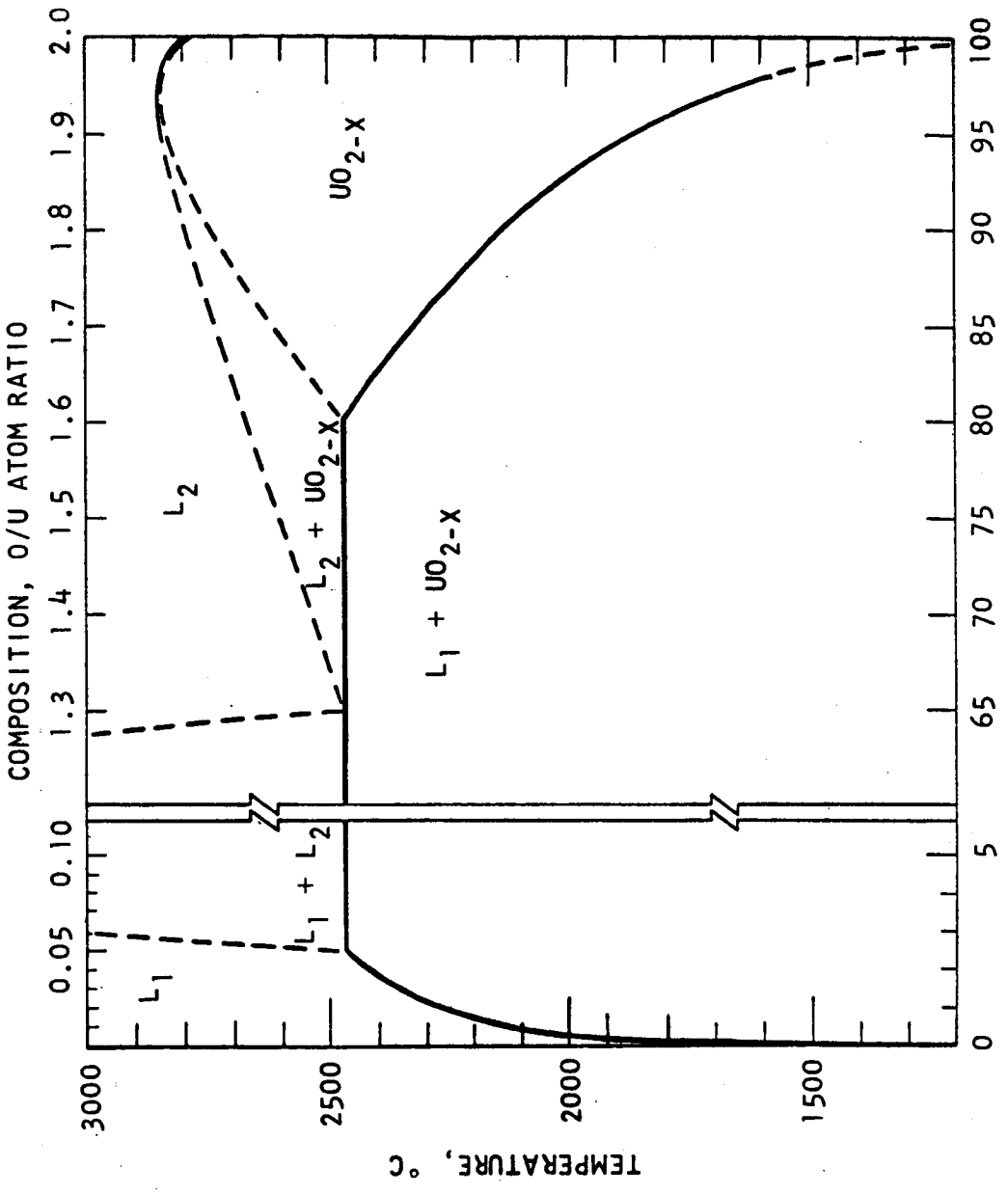

Fig. 1--Phase diagram of the uranium-urania system (5,6)

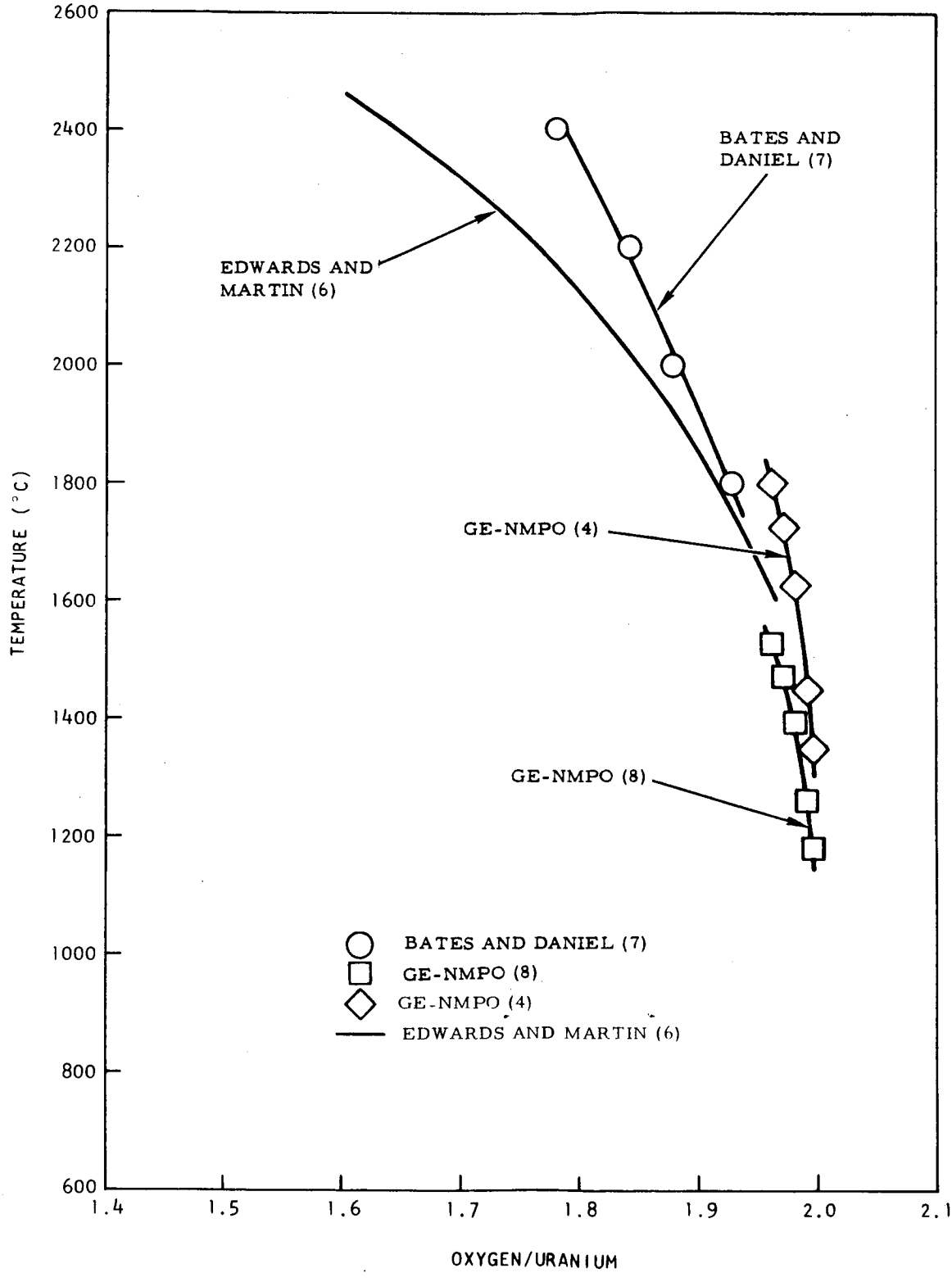

Fig. 2--Solubility of U in UO_2 (7, 8, 9)

the quenching process is sufficiently rapid to prevent composition changes during the cooling process which make the room temperature sample, which is analyzed, significantly different from the equilibrium sample at elevated temperatures. In contrast, the research reported herein studied the hypostoichiometric phase boundary of UO_{2-x} by the dynamic technique of thermal analysis, which depends on detection of the heat liberated (or absorbed) as U is precipitated (or dissolved) from the UO_{2-x} matrix.

It should be noted, however, that study of the boundary by thermal analysis is likely to be somewhat difficult since the phase change which is detected is not an isothermal process described by the initial (high temperature) and final (room temperature) species:

$$UO_{2-x}(\text{solid}) = (1 - \tfrac{x}{2})\, UO_{2.0}(\text{solid}) + \tfrac{x}{2}\, U(\text{solid}) \quad 0 < x \leq \sim 0.4 \ , \qquad (1)$$

or even the species above 1100°C

$$UO_{2-x}(\text{solid}) = (1 - \tfrac{x}{2})\, UO_{2.0}(\text{solid}) + \tfrac{x}{2}\, U(\text{liquid}) \quad 0 < x \leq \sim 0.4 \ . \qquad (2)$$

The phase change takes place over a range of temperatures depending upon the O/U ratio of the sample, and the isothermal process can more accurately be written as:

$$UO_{2-x}(\text{solid}) = \frac{(2 - x + \delta)}{2}\, UO_{2-x+\delta} + \frac{x - \delta}{2}\, U(\text{liquid, saturated with oxygen}) \quad 0 < x \leq \sim 0.4 \ , \qquad (3)$$

where δ is an infinitesimally small number.

From the above discussion and the thermodynamic data discussed below, it is clear that $UO_{2.0}$ is unstable with respect to a substoichiometric oxide at high temperatures in an oxygen-deficient or reducing atmosphere. In hydrogen, the equilibrium involved is

$$UO_2(\text{solid}) + xH_2(\text{gas}) = UO_{2-x}(\text{solid}) + xH_2O(\text{gas}) \quad (0 \leq x < \sim 0.4) \ . \qquad (4)$$

This reaction will proceed to the right until the hypostoichiometric phase boundary is reached. At this boundary the hypostoichiometric oxide will be further reduced to liquid uranium metal according to the equation:

$$UO_{2-x}(\text{solid}) + (2-x)\, H_2(\text{gas}) = U(\text{liquid}) + (2-x)\, H_2O(\text{gas}) \quad (0 \leq x \leq \sim 0.4) \ . \qquad (5)$$

Combining Eqs. (4) and (5) yields the net reaction taking place:

$$UO_2(\text{solid}) + 2H_2(\text{gas}) = U(\text{liquid}) + 2H_2O(\text{gas}) \quad . \qquad (6)$$

The data for this reduction reaction have been given in the literature (9) and are reproduced with additional calculations to 2800°C in Table 1. Since these data are for the direct reduction of stoichiometric UO_2, which is not a stable phase in contact with liquid U at these temperatures, they are not a quantitative measure of any observable equilibrium pressure. They show nevertheless that at 2500°C an H_2O/H_2 ratio of the order of 10^{-4} is necessary to prevent the reduction of UO_2 by hydrogen.

Table 1

REDUCTION EQUILIBRIA FOR $UO_{2.0}$(s)

Temp (°K)	ΔF° (kcal/mole)	P_{H_2O}/P_{H_2}
1500	119.6[a]	2.1×10^{-9}[a]
1800	114.8[a]	1.1×10^{-7}[a]
2000	111.9[a]	7.7×10^{-7}[a]
2100	110.5	1.8×10^{-6}
2200	109.1	3.8×10^{-6}
2300	107.7	7.7×10^{-6}
2400	106.3	1.4×10^{-5}
2500	104.8	2.6×10^{-5}
2600	103.4	4.5×10^{-5}
2700	102.0	7.4×10^{-5}
2800	100.6	1.2×10^{-4}

[a] From Ref. (9).

It should also be noted from Table 1 that the calculated pressure ratio changes with temperature, so that as a sample is cooled from 2500° to 1500°C the water content of the hydrogen must be reduced from ~100 to 0.1 ppm to prevent a change of O/U ratio in the condensed phase. In the region of the phase diagram where only the single-phase UO_{2-x} is present, the O/U ratio of the substoichiometric phase would change toward higher values if the equilibrium pressure at 2500°C were maintained as the sample cooled.

Below the phase boundary separating the two-phase and single-phase regions, the liquid U would tend to react with the H_2O if the same P_{H_2O}/P_{H_2} were maintained. Even if the variation of the partial molar free energy of oxygen in the substoichiometric UO_2 phase were considered, it is clear from these data that meaningful thermal analysis results cannot be obtained in a hydrogen atmosphere, even with a controlled water content, and that it is obviously impractical to attempt to vary the content of the buffer gas during an experiment. It was, therefore, necessary to carry out the thermal analyses in an inert atmosphere to reduce the expected volatilization of UO_2 and in which oxygen impurity (O_2 + H_2O) was maintained at a low level to prevent oxidation of the sample.

2. EQUIPMENT

The design and operation of the thermal analysis apparatus and the performance and calibration of the optical pyrometers is discussed in this section.

2.1. Thermal Analysis Apparatus

The design of the thermal analysis apparatus as utilized in other studies has been described previously (10). However, since the earlier work was largely concerned with carbides and graphite a number of modifications were necessary to adapt the system for the study of oxides. The design and operation of the equipment as utilized in the present study is discussed below.

The thermal analysis equipment is shown in Figs. 3 and 4. The oxide sample is placed in a tungsten crucible and is supported on a tungsten pedestal whose relative position in the induction coil can be closely adjusted by use of the threaded tungsten support rod. The tungsten crucible is shielded on the sides by seven turns of 0.002-in. tungsten foil; on the top by the tungsten lid and six layers of 0.005-in. tungsten foil; and on the bottom by the crucible support. The tungsten sight tube projects through the top shielding and is supported on a recessed lip by the crucible lid. The tube is 0.25 in. o.d. by 0.020-in. wall thickness by 4-in. long, and was fabricated by chemical vapor deposition. The components and the crucible assembly are shown in Figs. 5, 6, and 7.

In earlier studies, the metallic shielding was surrounded by inverted graphite cups to minimize the radiant emission from the metallic shielding. Since the use of graphite in these studies was precluded by the requirement of minimal contamination of the system by carbon, an attempt was made early in this program to utilize inverted UO_2 crucibles* as external shielding. These attempts were unsuccessful, however, because of the sensitivity of these crucibles to the thermal shock imposed on the system by the high heating and cooling rates. Several crucibles were completely shattered on the initial heating.

For the reasons outlined above, the outer ceramic shielding was eliminated and other methods of reducing the effects of radiation emanating from the metallic parts were investigated. Finally, the placement of an

*Several other refractory oxide materials including zirconia, thoria, and alumina were also tested with similar results.

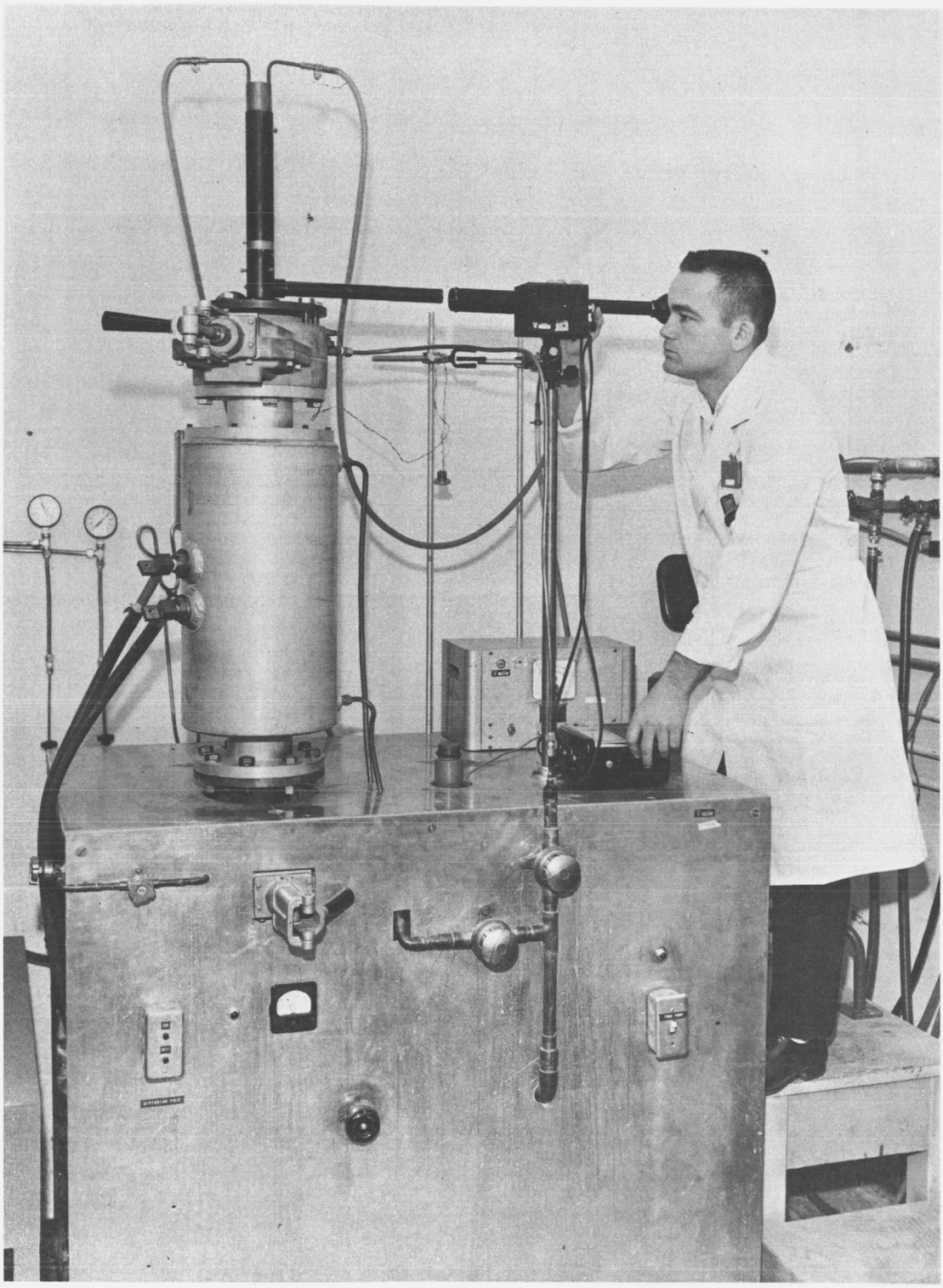

AC-26224

Fig. 3--Thermal analysis apparatus (photo)

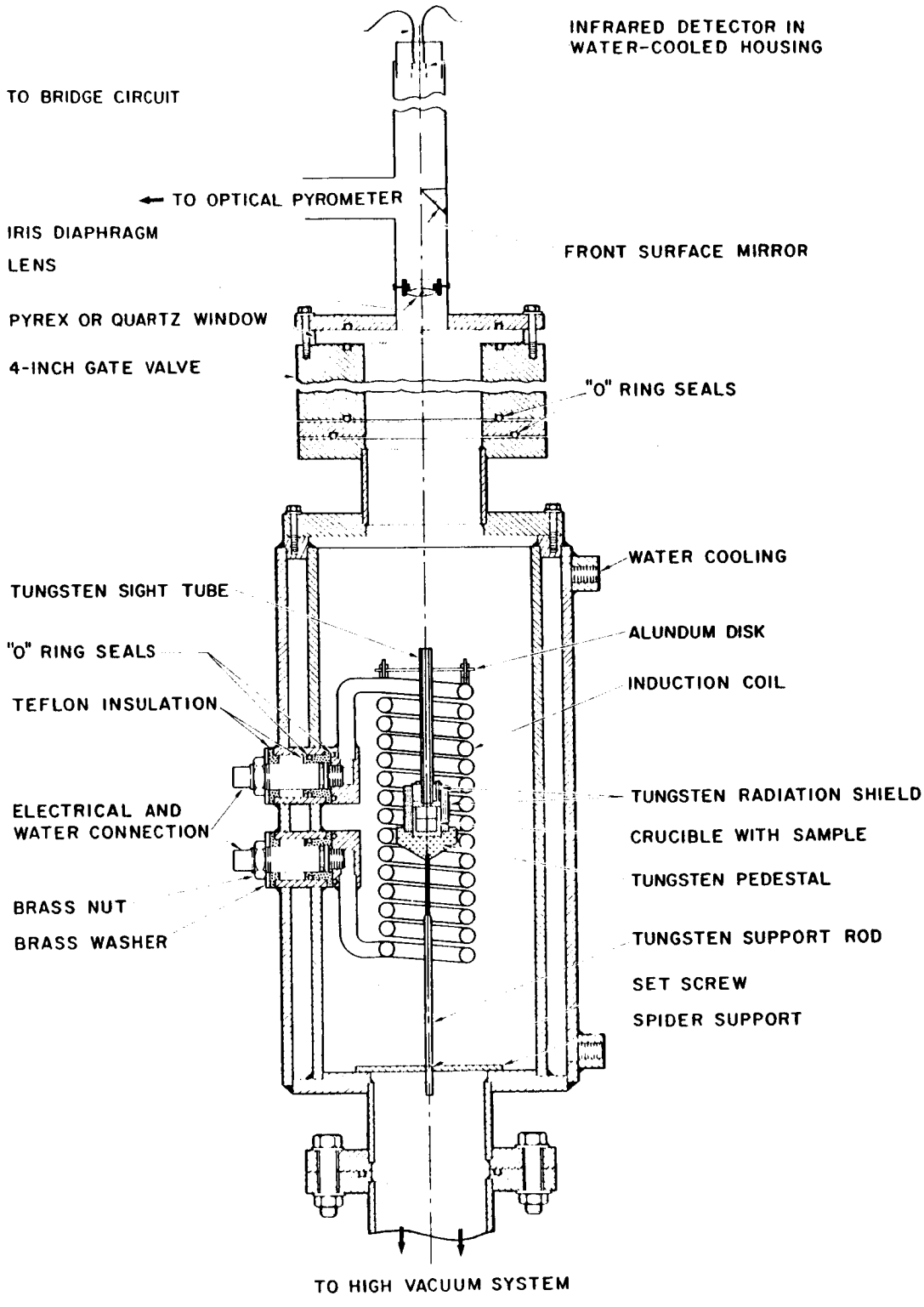

Fig. 4--Thermal analysis apparatus (schematic)

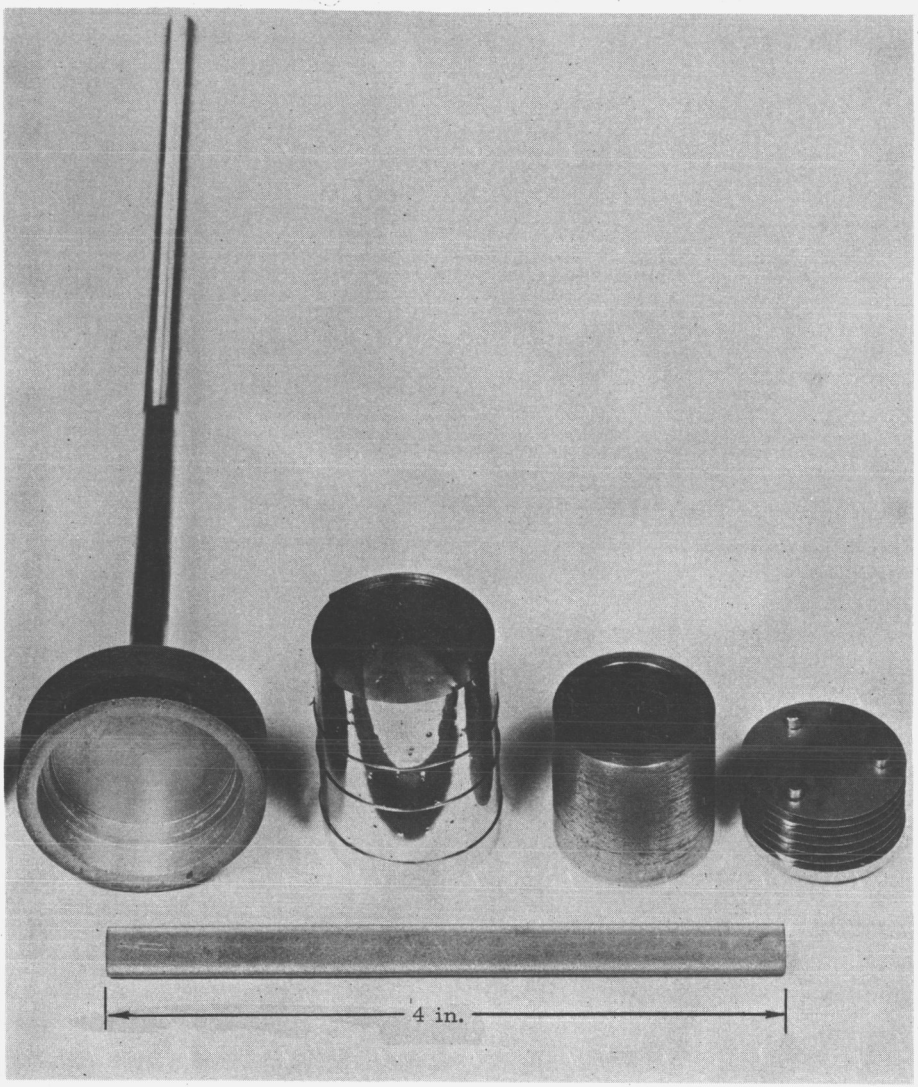

G-37,259

Fig. 5--Components of crucible assembly

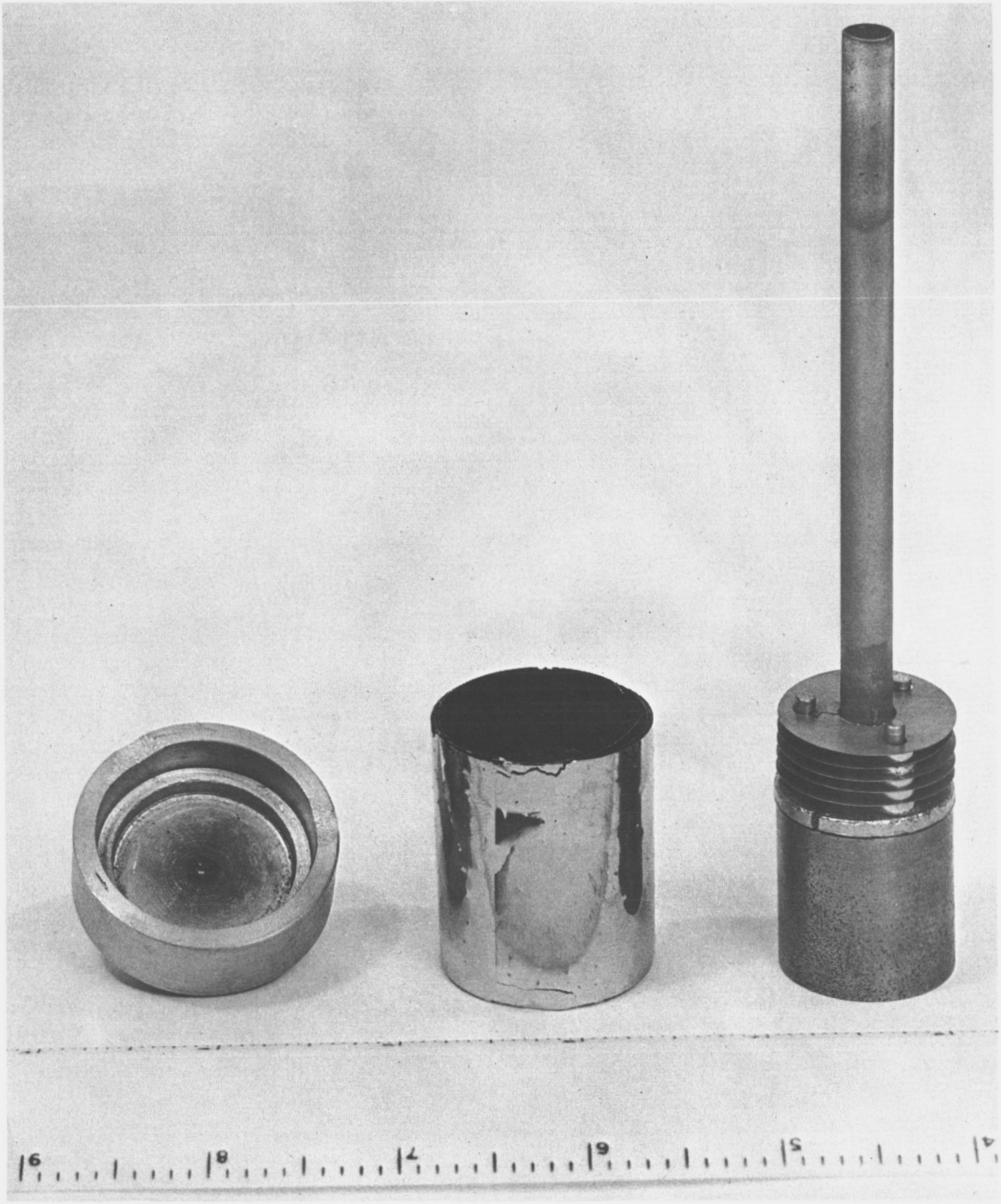

Fig. 6--Components of crucible assembly

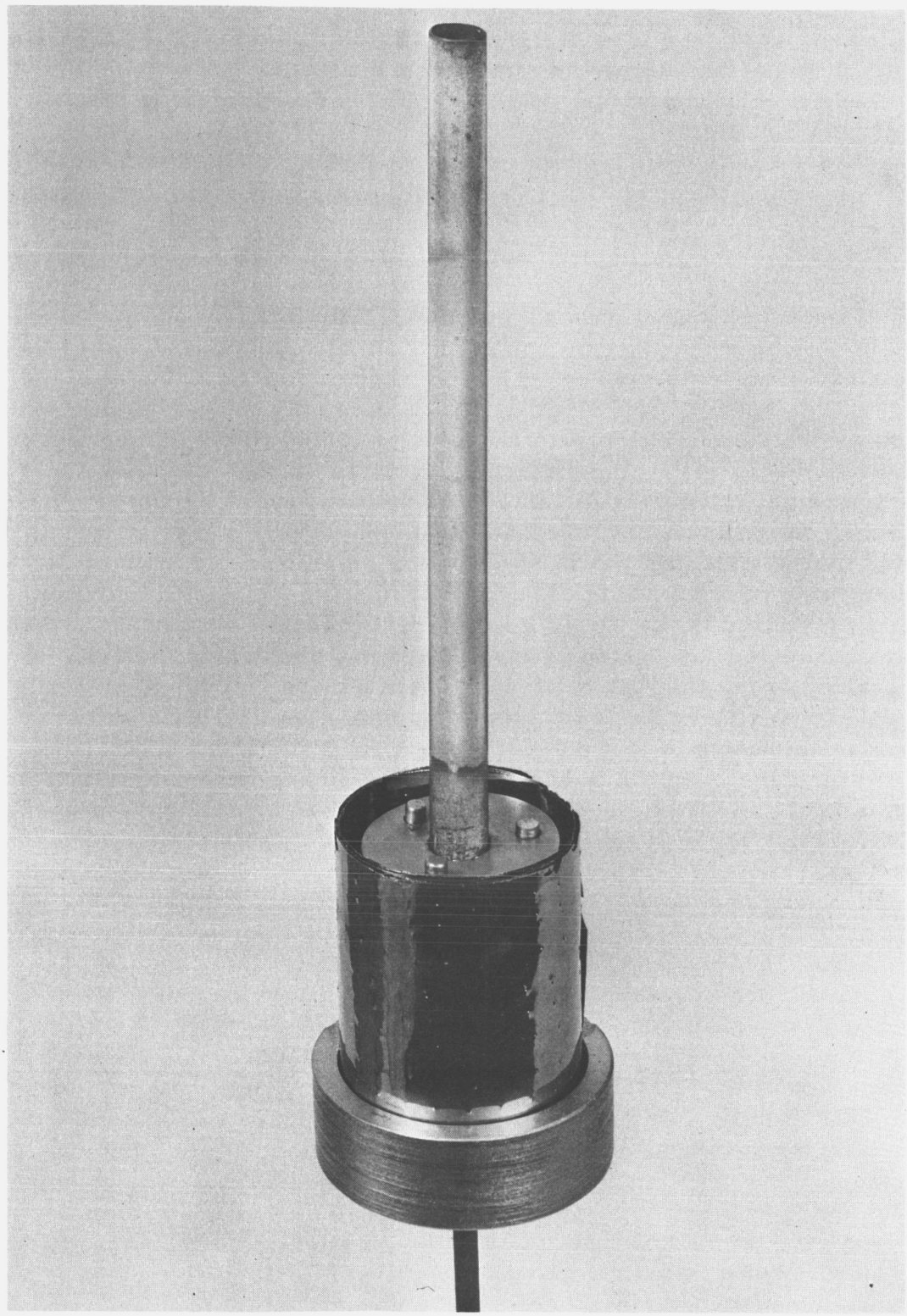

Fig. 7--Components of crucible assembly

alundum disk on the top turn of the induction coil some three inches above the crucible was found to be the simplest and most effective means of limiting the radiation falling on the detector. This arrangement is shown schematically in Fig. 8.

In practice, the oxide sample in the tungsten crucible is heated inside the vacuum chamber by a 10-kc, 30-kw induction heater. The radiation emitted by the sample passes through the optical system, composed of a variable iris diaphragm and a condensing lens, and is focused on the surface of a photoconductive infrared detector. The detector is connected as one leg of a simple Wheatstone bridge circuit whose output is fed to the Y_1 axis of a two-pen, x-y recorder. In this manner, relative heating and cooling curves of the sample can be obtained rapidly. The absolute temperature of the sample is determined using a standard brightness pyrometer in conjunction with the front-surfaced reflecting mirror in the optical path. Temperature calibration marks based on the brightness pyrometer readings are scribed on the margin of the chart paper by a pen that is remotely activated by the operator. A differentiating circuit on the input to the Y_1 axis of the recorder generates the time derivative of the thermal analysis curve, which is fed to the Y_2 axis of the recorder and plotted at the same time as the thermal analysis curve.* The detailed design, construction, and operation of the thermal analysis apparatus are discussed by Langer, Baldwin, and Kester (11). With this equipment, heating and cooling curves from room temperature to 2600°C and back to ~200°C can be obtained in times of the order of 6 min. The present design has detected solid state transformations in which the total energy absorbed or released amounts to about 3 calories in samples weighing about 25 g. It should be emphasized, however, that the ease with which a transition can be detected is greatly dependent on the phenomenology of the process. Thus, a polymorphic transition that occurs isothermally can be detected quite readily, whereas a process that involves the precipitation of a quantity of a second phase over a range of temperatures may not be as readily apparent.

2.2. Temperature Measurement and Pyrometer Performance

In past studies using the thermal analysis apparatus, a standard brightness pyrometer has been used for measurement of the absolute temperature. It was planned, under the present contract, to attempt to utilize a two-color optical pyrometer for plotting the heating and cooling curves and to obtain absolute temperatures that would not require emittance corrections. While this attempt was unsuccessful, preliminary experiments with the two-color pyrometer yielded information of great value

* Also, differential thermal analysis is possible by utilizing two-holed crucibles containing the sample and a standard, and a system which contains a mirror and chopper, which alternately focuses the radiation emitted by the sample and the radiation emitted by the standard on the surface of the detector.

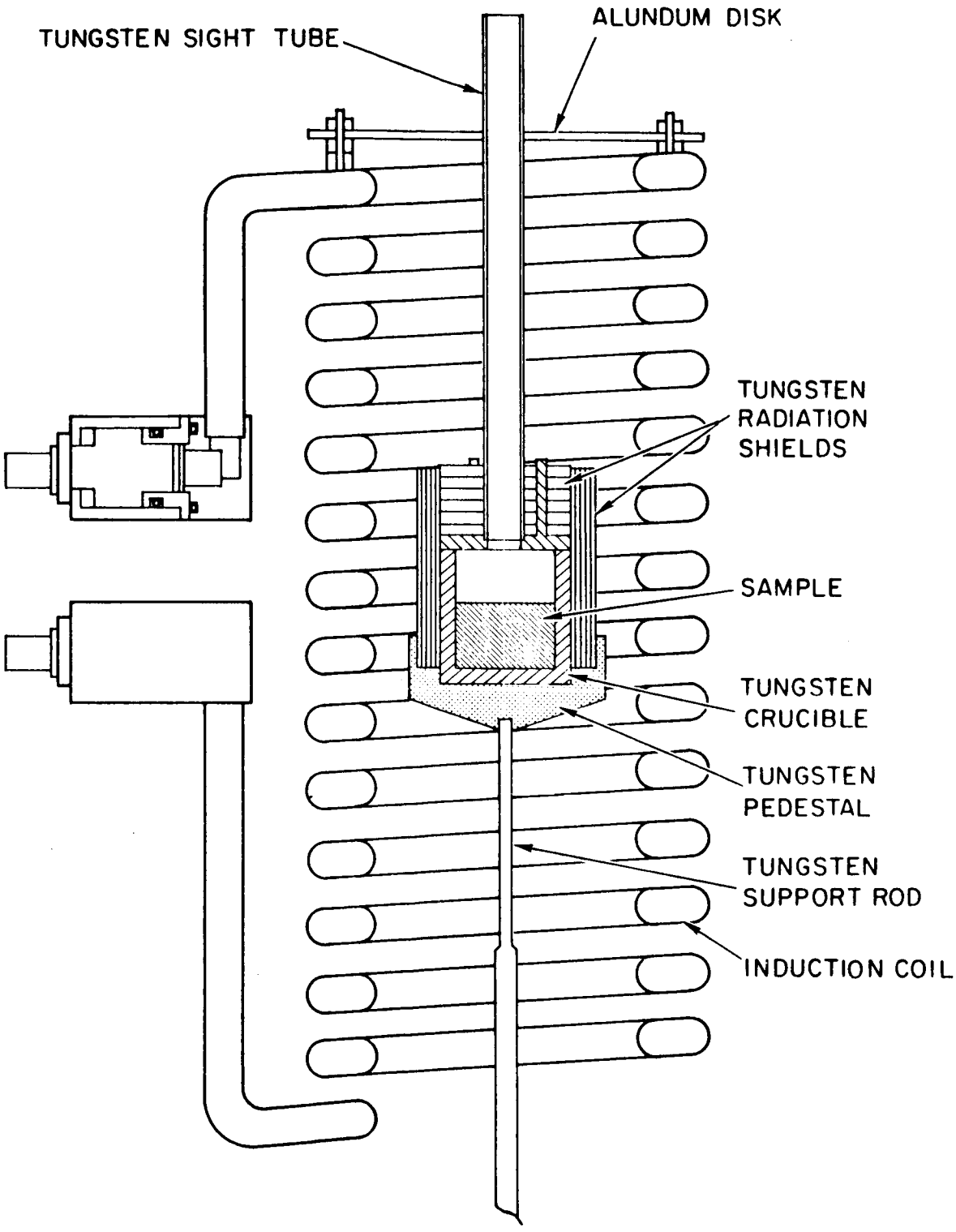

Fig. 8--Schematic of present crucible assembly

regarding interpretation of the thermal analysis curves. It was found that differences in the appearance of the thermal analysis curves obtained using the different methods of detection aided in associating thermal arrests with specific features of the phase diagram (this is discussed in Section 2.2.2.).

A two-color optical pyrometer was loaned to General Atomic by the National Aeronautics and Space Administration's Lewis Research Center for use on this contract. It was hoped that the use of this pyrometer would avoid the problem of the unknown emittance of UO_2 and simplify the determination of the absolute temperatures, since brightness matching by an operator would not be required. The optics of the pyrometer were modified so that it could be used at the same distance from the sample as the brightness pyrometer. Unfortunately, unforseen and unavoidable delays allowed four months of the contract period to pass before these modifications were complete. Consequently, insufficient time was available to permit careful comparison and calibration of the two-color pyrometer against the brightness pyrometer. In view of the contractual requirements of the contract which required reporting approximately half of the data points by the end of the initial six months, it was necessary to proceed with the measurements utilizing the brightness pyrometer for temperature measurement. An emittance of unity was assumed in lieu of a proper value for UO_2 under the conditions present in the experiments. The error introduced by this assumption is considerably smaller than the probable error in the data resulting from hysteresis and compositional uncertainties.

2.2.1. Brightness Pyrometer Calibration

The micro-optical brightness pyrometer was calibrated using standard techniques in the calibration section of the General Atomic Standards Laboratory against a tungsten filament lamp certified by the U.S. National Bureau of Standards. The calibration was carried out twice during the contract period.

The temperature measurements were made as described in Section 2.2. In calculating the true temperature from the observed temperature corrections were applied to the observed pyrometer readings to compensate for the absorptions of the window and the front surface mirror. A correction for the pyrometer calibration was also applied. The window correction curves are given in Figs. A.1 through A.4, the mirror correction curve in Fig. A.5, and the pyrometer calibration curves in Figs. A.6 and A.7, of Appendix A.

In addition to the above corrections, the window was examined at the end of each experiment to determine whether volatile material had condensed on the window during the experiment, thus lowering its transmission. This calibration was made by reading the temperature of a tungsten filament

with and without the window in the optical path. Deposition of material on the window was indicated by an absorption above that obtained in the calibration experiment with the clean window.

2.2.2. Appearance of Thermal Analysis Curves Obtained from Different Instruments

A number of preliminary experiments were carried out utilizing the brightness pyrometer and infrared detectors for temperature measurement and curve plotting, respectively, and also using the two-color pyrometer both for temperature measurement and for curve plotting. These experiments have served to emphasize the difference in response of the two instruments.

The thermal analysis curve (recorded using the lead sulfide infrared detector) for a $UO_{1.7}$ sample containing 2.5 mol-% Y_2O_3 is shown in Fig. 9. The curve during heating shows an apparent instantaneous decrease in temperature of the sample at the liquidus temperature. This apparent decrease is a synthetic effect generated by the detector. Since the emittance of the liquid is less than the emittance of the solid, the infrared detector sees the change of emittance as an apparent decrease in the temperature of the sample. On cooling, the reverse process occurs and the infrared detector interprets the emittance change accompanying the formation of the first film of solid on the surface as a large increase in temperature. These phenomena are clearly evident in Fig. 9.

The curve during heating and cooling obtained for the same sample using the two-color pyrometer is shown in Fig. 10. The absence of the instantaneous changes in apparent temperature accompanying the appearance or disappearance of a solid phase that was observed when the infrared detector was used, emphasizes the relative independence of the two-color pyrometer from the emittance. The curve resembles the heating and cooling curves usually determined with thermocouples. The change of slope is indicative of the absorption or liberation of the heat of fusion. The absence of the instantaneous change indicates that the ratio of the emittance at the two wave-lengths utilized by the pyrometer (4700 Å and 6400 Å) does not change greatly from the solid to the liquid.

The marked changes of emittance between the solid and liquid shown in Fig. 9 also emphasize the advantage to be gained if it had been possible to utilize the two-color pyrometer for temperature measurements. The observed rapid variation in emittance shows that the temperatures observed depend on the measured emittance and that the tungsten sight tube does not actually constitute a good black-body hole. Thus, temperatures observed with the brightness pyrometer are subject to emittance corrections. Unfortunately, emittance values for UO_2 under conditions similar to those in the present experiment were not available. The data in Section 7 are, therefore,

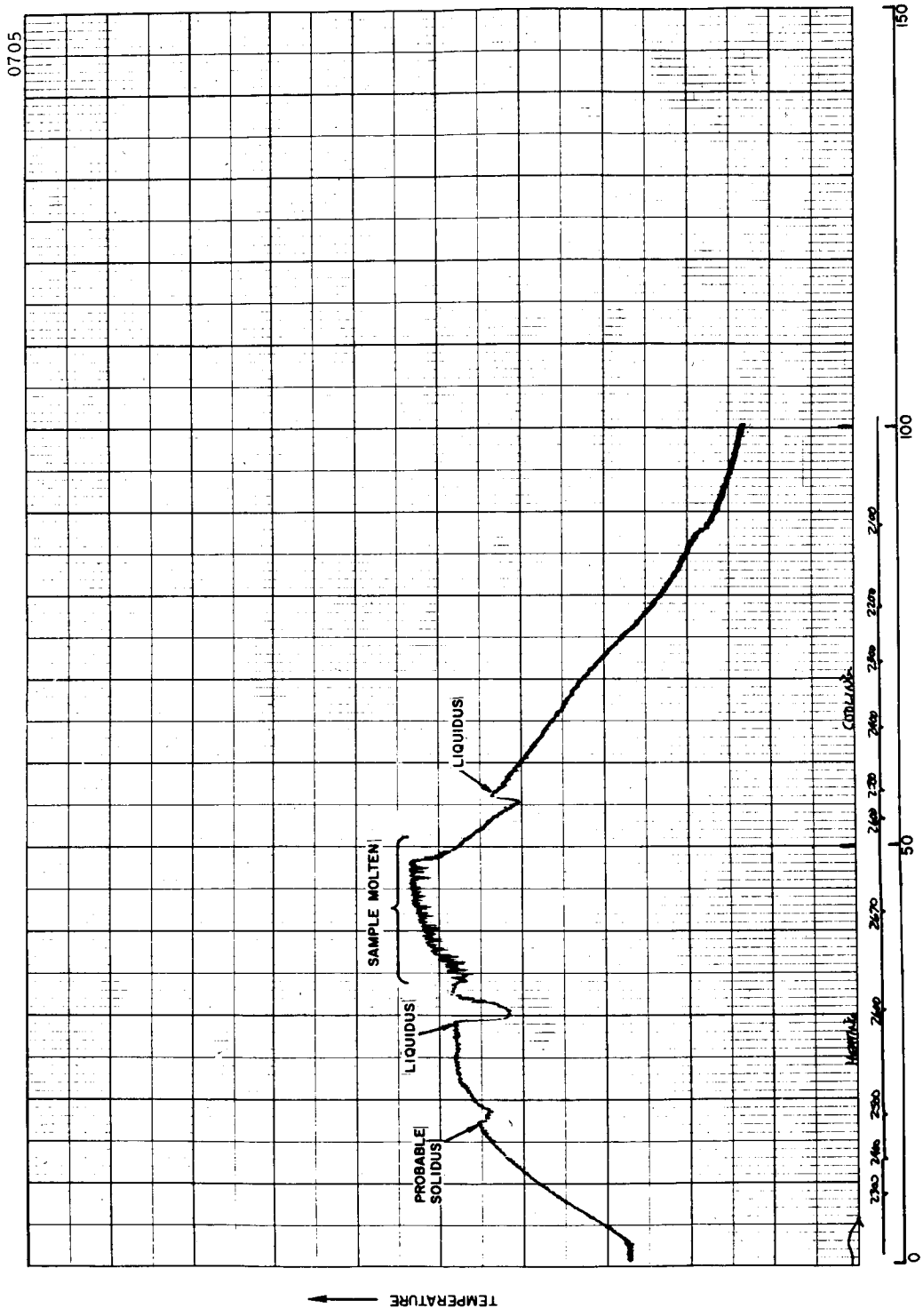

Fig. 9--Thermal analysis curve for ~$UO_{1.7}$ (2.5 mol-% Y_2O_3) infrared detector

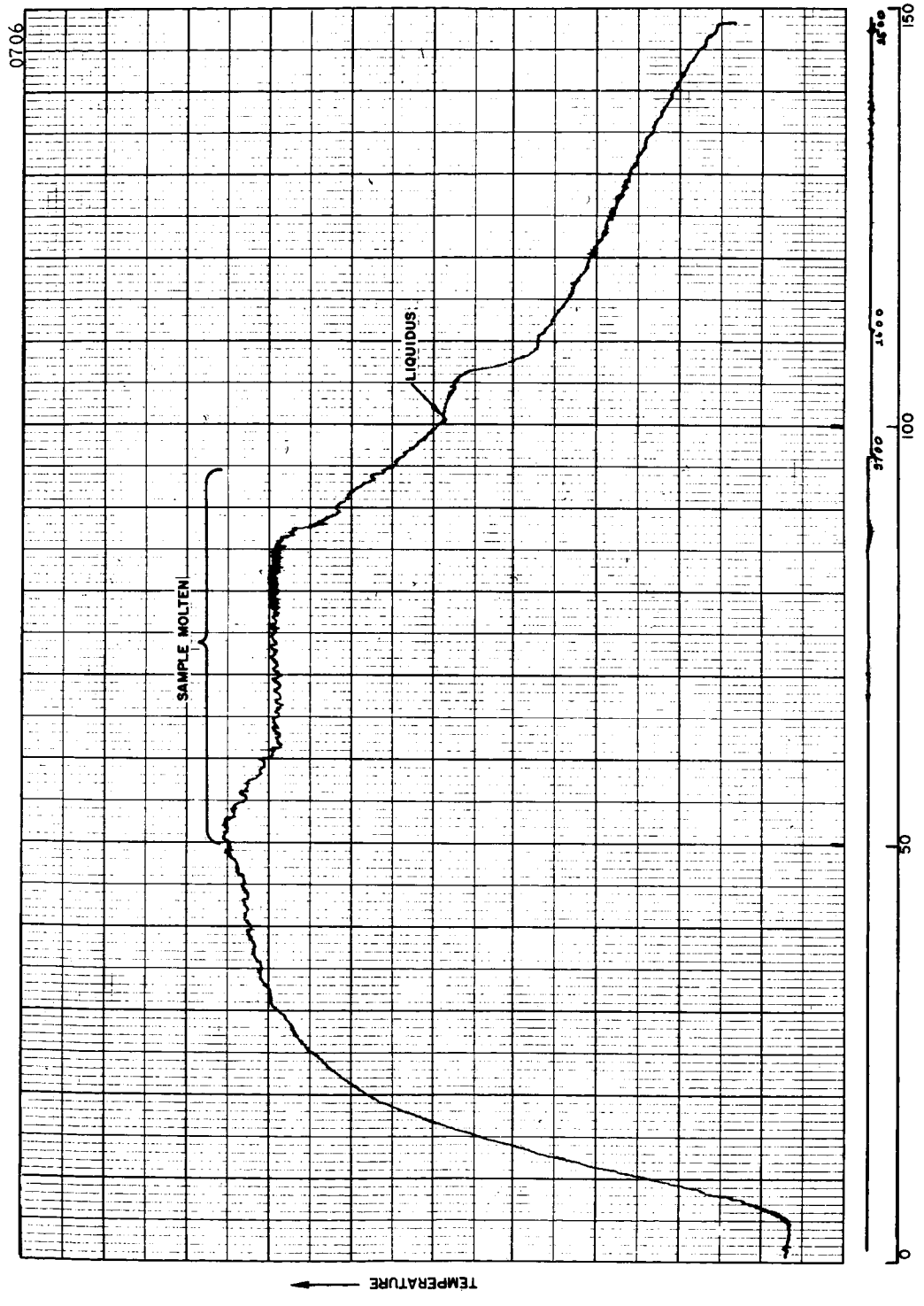

Fig. 10--Thermal analysis curve for ~$UO_{1.7}$ (2.5 mol-% Y_2O_3) two-color pyrometer

reported assuming an emittance of unity, which introduces a probable error of less than ±40°C, which is considerably smaller than the error resulting from hysteresis and the compositional uncertainties.

On the other hand, the sensitivity of the infrared detector to emittance changes made measurements of the liquidus temperatures possible. Prior to this study, the probability of the successful measurement of these temperatures had not been considered very good because of the extreme temperatures involved. The emittance changes on formation or disappearance of a solid phase facilitated these measurements. In some cases, it has also been possible to determine the solidus temperature. The liquidus and solidus temperatures are presented in Section 7.2.1.

3. MATERIALS PURITY

This section discusses the specifications for the materials utilized in the present program and the results of the chemical analyses required to establish their quality. The analytical procedures themselves are given in Appendix B.

The contractual requirements of the present study imposed the following restrictions on the materials utilized in this program:

> "No single impurity shall be present in any of the materials at greater than 50 parts per million by weight; however, carbon contaminants should be less than 20 parts per million; except for uranium metal which will be the best purity commercially available."

Considerable difficulty was experienced in finding suppliers who could meet these specifications.

Preliminary chemical analyses at General Atomic indicated that none of the oxide materials had an acceptably low-carbon content. In addition, the calcia and yttria contained large sintered particles which analyses indicated contained the bulk of the metallic impurities. This latter problem was solved by screening out the material with large particle size in those materials. It was also shown that the carbon content of all of the oxides could be reduced to acceptable levels by heating in hydrogen for several hours; thus, lending support to the theory that the initial high-carbon contents were due to the adsorption of CO_2 on the finely divided material. The final analyses for the oxides are given in Tables 2 through 6.

The uranium metal could not be obtained at a purity level equivalent to that of the oxides at a reasonable cost. Therefore, the principal impurity content of the samples was contributed by the uranium metal. Actually, after cleaning, the uranium bar stock was hydrided, dehydrided, and rehydrided to convert it to a finely powdered form and to facilitate the addition of uranium with a fairly well-known oxygen content. The uranium was therefore analyzed as the hydride and these results are given in Table 7.

The tungsten bar stock from which the crucibles were fabricated was high-purity material prepared by hydrogen reduction of WF_6. Some

Table 2

ANALYTICAL RESULTS: URANIUM DIOXIDE

Element	Impurity Content[a, b]	Element	Impurity Content[a, b]
Ag	N < 1	Mo	N < 2
Al	N < 1	Na	10
As	N < 40	Ni	N < 1
Au	N < 4	P	N < 50
B	N < 0.1	Pb	10
Ba	N < 6	Pd	N < 4
Bi	N < 1	Rb	N < 2
Ca	1	Sb	N < 8
Cd	N < 0.2	Si	N < 1
Co	N < 2	Sn	N < 1
Cr	1	Sr	N < 60
Cu	2	Te	N < 8
Fe	10	Ti	N < 60
Ge	N < 1	V	N < 100
Hg	N < 8	Zn	N < 8
In	N < 2		
K	N < 8	U	86.5%
Li	N < 1	O/U	2.17
Mg	4	C[c]	12 ± 2 ppm
Mn	N < 1	C[d]	9 ± 2 ppm

[a] In parts per million by weight except where noted.

[b] The following notation system is used:

20 means impurity content is 20 ppm ± 20%;

< 20 means impurity content is < 20 ppm;

N < 20 means not detected with a lower detection limit of 20 ppm.

[c] Annealed in vacuum at 1400°C.

[d] Annealed in H_2 at 1400°C.

Table 3

ANALYTICAL RESULTS: THORIUM DIOXIDE

Element	Impurity Content[a, b]	Element	Impurity Content[a, b]
Ag	N < 1	Mo	N < 1
Al	N < 1	Na	40
As	N < 20	Ni	N < 1
B	N < 1	Pb	20
Ba	N < 1	Sb	N < 8
Bi	N < 1	Si	1
Ca	N < 100	Sn	N < 1
Cd	N < 20	Sr	N < 40
Co	N < 1	Te	N < 40
Cr	1	Ti	N < 40
Cu	< 1	Tl	N < 1
Fe	1	V	N < 10
Ge	N < 1	Zn	N < 40
Hg	N < 20	Th	87.5%
In	N < 1	O/Th	2.02 ± .02
K	2	C[c]	24 ± 4 ppm
Li	1	C[d]	24 ± 3 ppm
Mg	1		
Mn	N < 1		

[a] In parts per million by weight except where noted.
[b] The following notation system is used:
20 means impurity content is 20 ppm ± 20%;
< 20 means impurity content is < 20 ppm;
N < 20 means not detected with a lower detection limit of 20 ppm.
[c] Annealed in vacuum at 1400°C.
[d] Annealed in H_2 at 1400°C.

Table 4

ANALYTICAL RESULTS: YTTRIUM OXIDE

Element	Impurity Content[a, b]	Element	Impurity Content[a, b]
Ag	N < 5	Rh	N < 200
Al	N < 40	Ru	N < 100
As	N < 400	Sb	N < 100
Au	N < 60	Sc	N < 10
B	N < 10	Si	20
Ba	N < 5	Sn	N < 100
Bi	N < 40	Sr	N < 600
Ca	10	Ta	N < 400
Cd	N < 200	Te	N < 600
Co	N < 100	Th	N < 100
Cr	N < 600	Ti	N < 40
Cu	N < 100	Tl	N < 400
Fe	N < 60	V	N < 40
Ga	N < 60	W	N < 600
Ge	N < 80	Zn	N < 600
Hf	N < 400	Zr	N < 10
Hg	N < 80	Pr	N < 60
In	N < 200	Nd	N < 80
Ir	N < 400	Sm	N < 40
K	N < 200	Eu	N < 40
La	N < 40	Gd	N < 1000
Li	N < 40	Tb	N < 80
Mg	10	Dy	N < 60
Mn	N < 20	Ho	N < 1000
Mo	N < 100	Er	N < 40
Na	N < 80	Tm	N < 100
Nb	N < 100	Yb	N < 20
Ni	N < 80	Lu	N < 60
P	N < 1000	Ce	N < 100
Pb	N < 400		
Pd	N < 100	Y	78.5%
Pt	N < 80	O/Y	1.53 ± 0.02
Rb	N < 200	C[c]	95

[a] In parts per million by weight except where noted.

[b] The following notation system is used:
20 means impurity content is 20 ppm ± 20%;
< 20 means impurity content is < 20 ppm;
N < 20 means not detected with a lower detection limit of 20 ppm.

[c] Annealed in H_2 at 1400°C for 2 hr. Carbon level can apparently be further lowered by longer annealing times.

Table 5

ANALYTICAL RESULTS: CALCIUM OXIDE

Element	Impurity Content[a, b]	Element	Impurity Content[a, b]
Ag	N < 5	Rh	N < 200
Al	100	Ru	N < 100
As	N < 400	Sb	N < 100
Au	N < 60	Sc	N < 10
B	N < 10	Si	20
Ba	N < 5	Sn	N < 80
Bi	N < 40	Sr	N < 600
Cd	N < 200	Ta	N < 400
Co	N < 100	Te	N < 600
Cr	N < 600	Th	N < 100
Cu	N < 100	Ti	N < 40
Fe	N < 60	Tl	N < 400
Ga	N < 60	V	N < 40
Ge	N < 80	W	N < 600
Hf	N < 400	Y	N < 10
Hg	N < 80	Zn	N < 600
In	N < 200	Zr	N < 10
Ir	N < 400	Pr	N < 100
K	N < 200	Nd	N < 100
La	N < 40	Sm	N < 100
Li	N < 40	Eu	N < 100
Mg	< 5	Gd	N < 100
Mn	200	Tb	N < 100
Mo	N < 100	Dy	N < 100
Na	N < 80	Ho	N < 1000
Nb	N < 100	Er	N < 100
Ni	N < 80	Tm	N < 100
P	N < 1000	Yb	N < 100
Pb	N < 400	Lu	N < 100
Pd	N < 100	Ce	N < 100
Pt	N < 80	C[c]	52 ± 17
Rb	N < 200		

[a] In parts per million by weight except where noted.

[b] The following notation system is used:
20 means impurity content is 20 ppm ±20%
< 20 means impurity contents is < 20 ppm;
N < 20 means not detected with a lower detection limit of 20 ppm.

[c] Annealed in H_2 at 1400°C for 2 hr. Carbon level can apparently be further lowered by longer annealing times.

NOTE: O/Ca ratio cannot be determined because of its volatility and gettering action of the calcium, and the lower stability of the carbide.

Table 6

ANALYTICAL RESULTS: CERIUM OXIDE

Element	Impurity Content[a, b]	Element	Impurity Content
Ag	N < 5	Nb	N < 100
Al	N < 40	Ni	N < 80
As	N < 400	P	N < 1000
Au	N < 60	Pb	N < 100
B	N < 10	Pd	N < 100
Ba	N < 5	Pt	N < 80
Be	N < 5	Rh	N < 200
Bi	N < 40	Ru	N < 100
Ca	N < 200	Sb	N < 100
Cd	N < 200	Si	300
Co	N < 100	Sn	N < 100
Cr	N < 600	Sr	N < 600
Cu	N < 100	Ta	N < 400
Fe	N < 60	Te	N < 600
Ga	N < 60	Th	N < 100
Ge	N < 80	Ti	N < 40
Hf	N < 400	Tl	N < 400
Hg	N < 80	V	N < 40
In	N < 200	W	N < 600
In	N < 400	Zn	N < 10
Mg	200	Zn	N < 10
Mn	N < 20	Ce	81.7%
Mo	N < 100	O/Ce	2.00
Na	N < 80	C	33[c]

[a] In ppm by weight, except where noted.

[b] The following notation system is used: 20 means impurity content is 20 ppm ±20%; <20 means impurity content is <20 ppm; and N < 20 means not detected with a lower detection limit of 20 ppm.

[c] Annealed in vacuum at 1400°C for 1 hr.

Table 7

ANALYTICAL RESULTS: URANIUM HYDRIDE

Element	Impurity Content[a, b]	Element	Impurity Content[a, b]
Ag	< 1	Na	N < 60
Al	100	Ni	60
As	N < 40	P	N < 5
Au	N < 4	Pb	N < 10
B	0.1	Pd	N < 10
Ba	N < 6	Sb	N < 8
Be		Si	60
Bi	N < 1	Sn	N < 1
Ca		Sr	N < 60
Cd	N < 0.4	Te	N < 8
Co	N < 2	Ti	N < 60
Cr	N < 10	V	N < 100
Cu	4	Zn	N < 8
Fe	200	U	98.25%
Ge	N < 1	H/U	3.01
In	N < 2	O	0.55 ± 0.02%
Mg	600	N	739 ± 13 ppm
Mn	40	C	840 ± 100 ppm
Mo	N < 2		

[a] In parts per million by weight except where noted.

[b] The following notation system is used:

20 means impurity content is 20 ppm ± 20%;
< 20 means impurity content is < 20 ppm;
N < 20 means not detected with a lower detection limit of 20 ppm.

difficulty was experienced in obtaining a reliable number for the molybdenum content. General carrier spectrographic analysis yielded a value of 60 ±20 ppm while instrumental neutron activation analysis using 14-Mev neutrons found <66 ppm. A final determination using thermal neutron activation analysis followed by separation of the molybdenum by precipitation of MoS_2 yielded a value of <50 ppm. The analytical data for the tungsten metal are given in Table 8.

Examination of the impurity levels of the stabilizing oxides reported in Tables 3 to 6 shows that even 10 mole percent of the additive oxide does not result in an impurity content of >50 ppm in the solid solution as a result of the impurities in the additive oxide. The impurities in uranium metal, however, do increase the nitrogen and magnesium content of $UO_{1.5}$ samples to ~200 and 125 ppm, respectively. The location of the phase boundary is insensitive to impurity levels as low as those present in this work.

Table 8

ANALYTICAL RESULTS: TUNGSTEN BAR STOCK

Element	Impurity Content[a, b]	Element	Impurity Content[a, b]
Ag	N < 1	Ni	< 1
Al	< 1	Pb	N < 1
As	N < 10	Sb	N < 2
B	N < 2	Si	< 1
Ba	N < 1	Sn	N < 1
Be	N < 1	Sr	N < 10
Bi	N < 1	Te	N < 40
Ca	N < 6	Ti	20
Cd	N < 4	Tl	N < 8
Co	N < 1	V	N < 8
Cr	N < 6	Zn	N < 10
Cu	< 1	Zr	N < 10
Fe	< 1	C	11 ± 1 ppm
Ga	N < 4	H_2	7 ± 5 ppm
Hg	N < 8	N_2	< 1
In	N < 20	O_2	21 ± 10 ppm
Mg	< 1	F	21 ± 15 ppm
Mo	< 50[c]		
Na	N < 20		

[a] In parts per million by weight except where noted.

[b] The following notation system is used:

20 means impurity content is 20 ppm ± 20%;
< 20 means impurity content is < 20 ppm;
N < 20 means not detected with a lower detection limit of 20 ppm.

[c] Result obtained by neutron activation analysis using thermal neutrons.

4. SAMPLE PREPARATION

The preparation of samples for thermal analysis was carried out with the objective of minimizing both the contamination by impurities and the pickup of oxygen (or CO_2) by adsorption.

The samples were based on 0.1 mole of $UO_{2.17}$ (27.0 g). To this quantity of UO_2 the amount of uranium hydride necessary to yield the desired O/U ratio was added. The weighing and addition of the uranium hydride was carried out in an argon atmosphere glove box. Finally, the quantity of stabilizing oxide needed to yield the desired metal oxide content was added, again under inert atmosphere conditions. The mixture was removed from the glove box and blended for 10 min in a mixer. The blending operation was carried out in a plastic mixing jar sealed with tape; the vial being further protected from the atmosphere by a sealed plastic bag. Chemical analyses of representative samples for carbon after the completion of the thermal analyses showed, in all but one instance, that the carbon contents were markedly lower than that calculated from the amount of carbon present in the uranium hydride. These data indicate that carbon is lost, probably as CO, during the thermal analysis experiment.*

After completion of the blending operation, the sample vial was returned to the inert atmosphere glove box. The sample was loaded into an 11/16-in. diameter steel die, and then sealed in a plastic bag before removal from the glove box for the pressing operation. Compaction of the powder to a cylindrical sample that can be readily loaded into a crucible was accomplished with a laboratory-sized hydraulic press at about 10,000 psig. The pressed pellets were stored in the glove box until needed.

*The presence of carbon in the starting material has no effect on the O/U ratios, since the latter were determined after completion of the thermal analysis experiment.

5. EXPERIMENTAL PROCEDURE

The procedures by which the prepared samples were homogenized and the thermal analyses performed are discussed in this section. Also, the reduction of the thermal analysis curves to yield the data given in Tables 17 to 26 and Figs. 17 to 46 are described below. (These tables and figures are presented in Section 7.)

5.1. Sample Homogenization

The cold-pressed oxide pellets were loaded into tungsten crucibles in the inert atmosphere glove box. Tungsten shielding, as described in Section 2.1, was added and the crucible assembly transferred rapidly to the thermal analysis apparatus. During this transfer operation, the sample is necessarily exposed to the room atmosphere and thus is partially oxidized. The exposure period was minimized, however, and it is estimated that this exposure did not exceed one minute.

The system was evacuated and pumpdown was continued at room temperature until a pressure of 10^{-5} torr was reached. Helium was then admitted to the furnace chamber to limit vaporization and heating was initiated slowly to decompose the uranium hydride. The heating continued under flowing helium until the sample reached 1800°C and then was annealed for one-half hour. Even this procedure was insufficient to insure solid solution homogeneity, so the sample was then taken to the melting point. The electromagnetic stirring action of the induction field helped insure thorough mixing.

5.2. Thermal Analysis

Once the uniformity of the sample was assured, thermal analysis was begun. The liquidus and solidus temperatures were studied first; the sample was maintained at high temperature (>~ 1800°C) continuously for 10 to 20 min. Consequently, it is most probable that the greatest changes in composition (both in the O/U ratio and metal additive content) took place during this period. At least two attempts to determine (on both heating and cooling) the liquidus and solidus temperature were made for each sample.

After the liquidus and solidus determinations were completed, thermal analysis runs were carried out at lower temperatures. As shown in Section 7,

the decomposition of UO_2 was normally observed in the range from O/U ≅ 1.63 to O/U ≅ 1.95. During these analyses, the temperature of the sample was high for only short periods of time and it was frequently below the lowest visible temperature (~750°C). It is likely, therefore, that changes in the sample composition were minimal during this period. At least two attempts to determine the decomposition temperature were made, both on the heating and the cooling cycles.

As noted in Section 7, it was frequently not possible to determine a thermal halt on the heating cycle while it could be easily observed on the cooling cycle. This was most frequently true for the solidus or monotectic temperatures and occurred less often for the decomposition temperatures. Occasionally, it was not possible to determine the liquidus temperature on both heating and cooling cycles.

On completion of the thermal analysis, the crucible assembly was removed from the furnace chamber and returned to the glove box with a minimum exposure to the atmosphere. The sample was removed from the crucible, a portion (5 g) was removed for analytical samples, and the balance retained for submission to NASA as the contract required.

5.3. Evaluation of Temperatures

This section describes the procedures by which the temperatures and cooling curves recorded on the chart paper are converted into the data presented in Tables 17 through 26 of Section 7.

The graph paper on which the heating and cooling curves were recorded was mounted on a drafting table in such a manner that the coordinate system of the paper was parallel to the mechanical arm of the table. The temperature calibration marks which span the temperature of the indicated transition were transferred from the lower margin of the paper to each thermal analysis curve. The temperature scale between the two calibration marks on either side of the indicated thermal arrest was assumed to be linear, and the uncorrected temperature of the thermal arrest was found by interpolation. This procedure was followed for each thermal arrest noted and was carried out for both the standard and the derivative thermal analysis curves.

The temperature of the thermal arrest as determined above was corrected by application of the corrections for window absorption, mirror absorption, and pyrometer calibration from data given in Appendix A. The individual measurements of each thermal arrest were then averaged to yield values of the temperature of the arrest for the standard and derivative curves on both heating and cooling cycles. These values are given in Tables 17 through 26 of Section 7

It will be noted that it has not been possible to obtain temperature measurements on all thermal arrests for the standard and derivative curves on both heating and cooling cycles. In many cases, the enthalpy changes associated with the thermal arrest are small and the thermal effect cannot be detected on the standard curve. Thus, temperatures can be determined only from the derivative curve. In a few cases, the rapidly changing slope of the derivative curve makes determination of the temperature of the inflection difficult and thus less reliable. In such cases, only the data from the standard curve are used.

In summarizing the data, the temperatures determined from the standard thermal analysis curve during heating and cooling are averaged, as are the analogous temperatures from the derivative curve. This procedure is necessary to compensate for the observed hysteresis on heating and cooling. For solid state transformations, the hysteresis loops can vary widely as shown by Wolten (12) and are independent of time. Similar behavior has been observed in the present studies. The average of heating and cooling temperatures from the standard thermal analysis curves agrees quite well with the analogous average obtained from the derivative curves. Finally, the heating and cooling average temperatures from the two types of curves are averaged.

6. COMPOSITION OF MATERIALS

Samples for investigation in this study were intended to have O/U ratios which were integral multiples of 0.1 in the range $1.5 < O/U < 2.1$. Partially as a result of the susceptibility of the uranium hydride to oxidation during handling, the as-prepared samples differed from the desired compositions. In addition, the O/U ratio changed again during the thermal analysis experiment; most likely during the initial study of the liquidus and solidus temperatures. Thus, the final composition of the sample was sometimes quite different from the composition originally desired. Finally, the loss of metal oxide additive from some of the samples by volatilization during the thermal analysis experiments resulted in metal oxide contents which varied from the prescribed composition. This section discusses the composition of the samples and the reasons for the deviation of these compositions from those initially desired.

6.1. Sample Compositions and Chemical Analysis

The analytical data on all five series of samples are given in Tables 9 through 13. These tables list the desired compositions in terms of O/U ratio, mol-% additive oxide, and the final compositions, as determined by chemical analysis. The latter consists of the O/U ratio, the amount of stabilizing oxide, the amount of tungsten contamination, if any, and the carbon content of representative samples. Since the metals, carbon and oxygen are all determined directly, the mass balance is also given. For a number of samples in the unstabilized uranium-oxygen series, the initial (or as-prepared) composition is also given. This latter analysis was carried out to determine the reasons for deviation of the final from the desired compositions.

Prior to the chemical analyses, the samples were stored as large pieces in the inert atmosphere dry box. Every effort was made to complete the oxygen determination within three days after the completion of the experiment. Several samples which were stored for extended periods of time, showed oxygen contents which increased with storage time, especially when in a powdered form. This is in agreement with results reported by the General Electric Nuclear Materials and Propulsion Operation which showed that CeO_2-UO_2, Nd_2O_3-UO_2, and Yb_2O_3-UO_2 samples oxidized at room temperature (13).

The oxygen was determined by the inert-gas-fusion method. This procedure consisted of heating the sample in a graphite crucible to 2300°C in a flowing stream of argon. The CO_2 content of the gas was then determined

Table 9

ANALYTICAL DATA FOR THE URANIUM-OXYGEN SAMPLES

Exp. No.	Desired Comp. O/U Ratio	Initial Comp. O/U Ratio	Final Comp. O/U Ratio	Final Composition		Mass Balance	
				Tungsten (wt-%)	Carbon (ppm)	Initial Comp. (wt-%)	Final Comp. (wt-%)
1.1-1	1.5		1.52		115	101.14	99.30
1.15-1	1.55		1.62	ND[a]	132		99.07
1.3-2	1.6	1.72	1.67			100.27	99.85
1.3-3	1.6		1.67				99.40
1.5-1	1.7	1.76	1.71			100.30	99.98
1.5-5	1.7		1.73				99.60
1.5-4	1.7	1.75	1.75			100.06	100.23
1.7-3	1.8		1.77				98.99
1.17-1	1.75		1.80	ND			98.87
1.7-2	1.8	1.83	1.80			100.19	100.04
1.9-3	1.9	1.93	1.83			100.04	99.58
1.9-4	1.9		1.84		150[b]		98.82
1.9-4'	1.9		1.87	ND			98.98
1.9-5	1.9		1.90	ND			99.97
1.11-3	2.0		1.92	ND			99.27
1.9-2	1.9	1.93	1.95			100.23	100.21
1.11-2	2.0		2.02				99.61
1.11-2'	2.0		2.02	<0.5			99.12
1.13-1	2.1		2.06	2.			98.00

[a] ND indicates that tungsten was not detected ($\leq 0.2\%$).

[b] This sample appears to have an anomalously high carbon content which cannot be accounted for. Analysis of this sample by the NASA Lewis Research Center yielded an average value of 11 ppm carbon. The NASA value for carbon content is taken as correct.

Table 10

ANALYTICAL DATA FOR THE URANIUM-CALCIUM-OXYGEN SAMPLES

Exp. No.	Desired Composition		Final Composition				
	CaO (mol-%)	O/U Ratio	O/U Ratio	CaO (mol-%)	Carbon (ppm)	Tungsten (wt-%)	Mass Balance (wt-%)
2.0-1	2.5	1.4	1.61	1.30		ND	99.95
2.15-1	5.0	1.5	1.63	1.94	139	<0.20	100.18
2.1-1	2.5	1.5	1.66	1.30	135	<0.20	100.35
2.17-1	5.0	1.6	1.67	2.60		ND[a]	100.27
2.3-1	2.5	1.6	1.72	1.95		<0.20	100.30
2.5-1	2.5	1.7	1.75	1.97		<0.20	100.43
2.5-2	2.5	1.7	1.83	1.33	38	ND	99.72
2.7-2	2.5	1.8	1.89	1.32		ND	99.62
2.7-1	2.5	1.8	1.90	1.99		ND	100.15
2.9-1	2.5	1.9	1.92	2.00		<0.20	99.83
2.11-1	2.5	2.0	1.95	1.99		0.40	99.34
2.13-1	2.5	2.1	2.02	2.04		1.80	98.81
2.14-1	5.0	1.4	1.63	3.51		ND	99.88
2.15-2	5.0	1.5	1.67	3.86		ND	99.93
2.19-1	5.0	1.7	1.74	3.23		ND	100.03
2.23-1	5.0	1.9	1.79	3.26		ND	99.41
2.21-1	5.0	1.8	1.81	3.25		ND	100.23
2.21-2	5.0	1.8	1.91	3.91		ND	100.09
2.25-1	5.0	2.0	1.99	3.89		ND	100.01
2.27-1	5.0	2.1	2.03	3.38		3.0	100.40
2.28-1	10.0	1.4	1.66	7.98	207	ND	100.64
2.29-1	10.0	1.5	1.67	5.37		ND	100.00
2.31-1	10.0	1.6	1.76	6.35		ND	99.48
2.33-1	10.0	1.7	1.84	6.98		ND	99.19
2.35-1	10.0	1.8	1.90	7.01		ND	99.26
2.39-1	10.0	2.0	1.96	7.42		1.0	99.30
2.37-1	10.0	1.9	1.97	7.09		1.0	99.50
2.41-1	10.0	2.1	2.02	7.24		3.0	99.63
2.43-1	15.0	1.5	1.74	9.22			100.07
2.45-1	15.0	1.6	1.80	10.15			99.73
2.47-1	15.0	1.7	1.84	11.35			99.20
2.49-1	15.0	1.8	1.95	11.65		0.25	99.55
2.55-1	15.0	2.1	1.97	12.24		3.55	100.41
2.53-1	15.0	2.0	1.98	12.05		1.25	99.90
2.51-1	15.0	1.9	1.99	12.01		0.70	99.00

[a] ND indicates that tungsten was not detected ($\leq 0.2\%$).

Table 11

ANALYTICAL DATA FOR THE URANIUM-YTTRIUM-OXYGEN SAMPLES

Exp. No.	Desired Composition		Final Composition				
	Y_2O_3 (mol-%)	O/U Ratio	O/U Ratio	Y_2O_3 (mol-%)	Carbon (ppm)	Tungsten (wt-%)	Mass Balance (wt-%)
3.2-1	2.5	1.4	1.57	2.51		ND	
3.1-1	2.5	1.5	1.61	2.09	143	ND[a]	100.74
3.3-1	2.5	1.6	1.73	2.61	48	0.50	99.21
3.5-1	2.5	1.7	1.74	2.62		ND	99.63
3.7-2	2.5	1.8	1.84	2.48		ND	
3.7-1	2.5	1.8	1.88	1.96	49	ND	99.92
3.9-1	2.5	1.9	1.92	2.62	70	0.60	99.86
3.11-1	2.5	2.0	2.03	2.64	52	0.80	99.91
3.13-1	2.5	2.1	2.04	2.27		1.40	99.53
3.15-2	5.0	1.5	1.64	4.89		ND	100.57
3.17-2	5.0	1.6	1.70	4.51		ND	100.21
3.19-3	5.0	1.7	1.81	4.79		ND	
3.19-2	5.0	1.7	1.83	4.59		ND	99.28
3.21-2	5.0	1.8	1.88	4.59		ND	99.58
3.21-3	5.0	1.8	1.88	4.83		ND	
3.23-2	5.0	1.9	1.93	4.58		ND	100.13
3.25-1	5.0	2.0	2.02	4.89		0.40	99.57
3.27-1	5.0	2.1	2.10	4.86		2.0	99.14
3.29-2	10.0	1.5	1.58	8.79		ND	99.88
3.31-2	10.0	1.6	1.68	8.94		ND	99.32
3.33-2	10.0	1.7	1.80	9.17		ND	99.77
3.35-2	10.0	1.8	1.86	8.78		ND	100.06
3.37-2	10.0	1.9	1.94	8.82		ND	100.00
3.39-1	10.0	2.0	2.08	8.58		1.40	99.31
3.41-1	10.0	2.1	2.14	9.06		2.50	99.07

[a] ND indicates that tungsten was not detected ($\leq 0.2\%$).

Table 12

ANALYTICAL DATA FOR THE URANIUM-THORIUM-OXYGEN SAMPLES

Exp. No.	Desired Composition		Final Composition				
	ThO_2 (mol-%)	O/U Ratio	O/U Ratio	ThO_2 (mol-%)	Carbon (ppm)	Tungsten (wt-%)	Mass Balance (wt-%)
4.3-1	2.5	1.6	1.68	2.50		ND[a]	101.17
4.5-1	2.5	1.7	1.75	2.50		ND	101.05
4.7-1	2.5	1.8	1.83	2.38	56	ND	100.04
4.9-1	2.5	1.9	1.92	2.28	63	ND	101.08
4.11-1	2.5	2.0	1.98	2.41	64	ND	100.27
4.17-1	5.0	1.6	1.67	5.02		ND	100.47
4.19-1	5.0	1.7	1.81	4.90		ND	100.84
4.21-1	5.0	1.8	1.85	4.92		ND	100.92
4.23-1	5.0	1.9	1.92	4.85		ND	100.30
4.25-1	5.0	2.0	1.95	4.88		ND	99.81
4.29-1	10.0	1.5	1.58	9.91		ND	99.78
4.31-1	10.0	1.6	1.69	10.00		ND	100.42
4.33-2	10.0	1.7	1.76	9.89		ND	100.27
4.35-1	10.0	1.8	1.86	9.83		ND	100.92
4.37-1	10.0	1.9	1.90	9.98		ND	99.65
4.39-1	10.0	2.0	1.96	9.56		ND	98.83

[a]ND indicates that tungsten contamination was not detected ($\leq$ 0.3 wt-%).

Table 13

ANALYTICAL DATA FOR THE URANIUM-CERIUM-OXYGEN SAMPLES

Exp. No.	Desired Composition		Final Composition				
	CeO_2 (mol-%)	O/U Ratio	O/U Ratio	CeO_2 (mol-%)	Carbon (ppm)	Tungsten (wt-%)	Mass Balance (wt-%)
5.1-1	2.5	1.5	1.55	2.44		ND[a]	99.73
5.3-1	2.5	1.6	1.68	2.64	91	ND	99.67
5.5-1	2.5	1.7	1.75	2.42		ND	99.53
5.7-1	2.5	1.8	1.83	2.44		ND	99.33
5.11-1	2.5	2.0	1.92	2.31	37	0.8	99.20
5.9-1	2.5	1.9	1.93	2.40		ND	99.31
5.15-1	5.0	1.5	1.53	5.06		0.3	99.87
5.17-1	5.0	1.6	1.71	4.65	55	ND	99.94
5.19-1	5.0	1.7	1.76	5.13		ND	99.67
5.21-1	5.0	1.8	1.82	5.07		ND	99.86
5.25-1	5.0	2.0	1.89	4.89	25	0.8	99.01
5.23-1	5.0	1.9	1.91	5.13		ND	99.55
5.29-1	10.0	1.5	1.56	9.77		0.3	100.02
5.31-1	10.0	1.6	1.68	9.93	60	ND	100.30
5.33-1	10.0	1.7	1.76	10.14		ND	100.19
5.35-1	10.0	1.8	1.89	9.86		ND	100.45
5.39-1	10.0	2.0	1.94	9.95	44	1.3	99.63
5.37-1	10.0	1.9	2.01	9.95		0.6	100.66

[a] ND indicates that tungsten contamination was not detected ($\leq$ 0.3 wt-%).

gravimetrically. It is estimated that oxygen was determined to ±1%. This analytical error resulted in a propagated error of ±0.02 in the O/U ratio.

Uranium and the additive metal contents were determined by x-ray spectrographic analysis. The sample was first fused into a borax bead, which was mounted in the x-ray beam. The intensity of the x-ray lines, as determined by the spectrograph, were then compared with known standards. It was estimated that uranium could be determined to ±1 wt-%. The 1 wt-% error in the uranium determination propagated into an error of ±0.02 in the O/U ratio. When combined with the estimated error in the oxygen analysis, a standard error of ±0.04 in the O/U ratio was calculated, exclusive of the errors introduced by the invalidity of the assumptions regarding the oxidation state of the tungsten contamination which is discussed below. Carbon was determined using an analyzer which determines carbon as CO_2 using a thermal conductivity detector. The detailed procedures for these analyses are given in Appendix B.

The propagation of the analytical errors in the determination of the additive metals have been calculated and the results are given in Table 14. It is noted that the precision with which these metals can be determined varies with the amount of additive present and that the precision improves with increasing amounts of additive.

A number of the samples were found to contain tungsten as a contaminant, and consequently tungsten was regularly determined in each sample, except for a number of the initial samples in the U-O system. The tungsten was assumed to be present in the metallic state in the sample, as discussed below, for the purpose of calculating the O/U ratio. It is known, from electron microprobe studies, that this assumption is not entirely true, and a subsequent possible error of ±0.05 in O/U per 1 wt-% tungsten is thus introduced into the reported ratios for those samples that contain tungsten as a contaminant (see Section 6.4).

The tungsten contamination primarily affects the samples with high O/U ratios, although one yttria-stabilized sample with O/U = 1.73 had a tungsten content of 0.5 wt-%. Conversely, none of the thoria-stabilized samples showed any tungsten contamination. Tungsten contamination was minimal below O/U ~1.92, and since the decomposition reaction is no longer observed above O/U ~1.95, only those samples with $1.92 < O/U < 1.95$ could have been affected by the tungsten. The tungsten contamination may appear to be responsible for an apparent reversal in final composition of the O/U = 1.9 and 2.0 samples in each of the ceria-stabilized series. The samples, which were prepared to be $UO_{2.0}$ have considerably larger tungsten contents than the samples prepared is $UO_{1.9}$. However, statistical analysis indicates that, within the limits of the analytical errors, the compositions are identical, and the apparent reversals of the type noted are to be statistically expected.

Table 14

ESTIMATED ERRORS IN COMPOSITION OF STABILIZED URANIA

Additive	Nominal Amount of Additive		Analytical Error (wt-%)	Propagated Error[a] (mol-%)
	Metal Oxide (mol-%)	Metal (wt-%)		
Y_2O_3	2.5	1.8	±10	±0.3
	5.0	3.4	±10	±0.5
	10.0	6.5	±1	±0.1
CaO	2.5	0.3	±10	±0.2
	5.0	0.6	±5	±0.2
	10.0	1.1	±5	±0.5
CeO_2	2.5	1.3	±10	±0.2
	5.0	2.7	±5	±0.2
	10.0	5.4	±2	±0.2
ThO_2	2.5	2.2	±5	±0.1
	5.0	4.3	±3	±0.1
	10.0	8.6	±2	±0.2

[a] Calculated according to the procedure given in Ref. 14.

The mass balances given in the final columns of Tables 9 through 13 are given as an index of the precision of the analytical data. In view of the fact that the metals and oxygen were determined directly, the mass balances in the tables must be considered exceptionally good.

The final carbon contents of several samples in each series were determined in an effort to maintain control of procedures that might lead to C contamination of the sample; and these contents are given in Tables 9 through 13. It is thought that the primary source of C in these samples was the uranium hydride, which was shown to contain 840 ±100 ppm of carbon. The data in these tables indicate that most of this carbon was lost, probably as CO, during the thermal analysis experiment. As noted earlier, the O/U ratio is unaffected since it was determined after completion of the experiment.

6.2. Variation of the O/U Ratio

The preparation of samples for the thermal analysis experiments and the precautions taken to avoid contamination by oxygen have been described in Section 5. In spite of these efforts, the as-prepared samples varied from the desired composition. This is indicated by the data in Table 9 (for the U-O system) which shows the variation of the initial (as-prepared) O/U

ratios of 5 samples from the desired (or calculated make-up) composition. The accuracy with which the UO_2 and UH_3 were weighed (±0.001 g) precluded weighing errors from being responsible for the composition variances. In addition, the data show that in all cases, the O/U ratio was higher than the desired composition. It is likely, therefore, that oxygen absorption by the UH_3 during sample preparation, and in spite of handling in the glove box, is responsible for the increased oxygen content of the as-prepared samples.

Additional changes in the O/U ratios of the samples occurred during the thermal analysis experiments. As was noted in Section 5.2, it is most likely that these composition shifts occurred during the initial phases of the experiments as a result of free vaporization of the samples into the helium atmosphere. During these initial thermal analyses, heating and cooling curves were being run between 2400° and 3100°C to determine the liquidus and solidus temperature. The total time during which the sample is above 2500°C is of the order of 6-10 min. The ensuing experiments which studied the decomposition temperature were carried out between room temperature and 2400°C, with only a short time at the higher temperatures. The composition changes during this period were thus clearly less than during the high temperature study. The net result of the composition changes was almost invariably a shift toward higher O/U ratios for samples in the range O/U <1.9. Conversely, stoichiometric or hyperstoichiometric UO_2 samples normally decreased in O/U ratio during the experiment. Since the principal composition change probably occurred during the initial studies of the liquidus and solidus temperatures rather than during studies of the decomposition temperatures, the final O/U ratio, as determined by subsequent chemical analysis, most closely represents the composition of the sample at the time of the decomposition studies. Therefore, the O/U ratio determined by this analysis has been used in all evaluations of the data.

In samples containing the stabilizing oxides CeO_2, ThO_2, Y_2O_3, and CaO, it was assumed that the oxidation state of the additive metals remained unchanged in the solid solution and that the oxidation state was that given by the stoichiometric formula. Formation of hypostoichiometric oxides is possible, at least in the rare earth and actinide oxides. However, investigation of the average oxidation state of these metals in the solid solution was beyond the scope of the contract. In the case of ceria, it is known that CeO_2 can be reduced to essentially stoichiometric Ce_2O_3. The error in calculated O/U ratio which would be introduced if a 10 mol-% CeO_2 sample were completely reduced to Ce_2O_3 is about ±0.05 units in O/U ratio, and well within the experimental error in the ceria-stabilized systems.

6.3. Variation of the Metal Oxide Additive Content

The volatilization of the oxide additive during the thermal analysis experiments produced variations in the concentration of stabilizing oxide from the desired concentrations in both the yttria- and calcia-stabilized systems. However, the variation was serious and troublesome only in the calcia-containing system, although in the yttria-stabilized samples small, yet significant changes in additive oxide concentration were observed, especially in those samples containing the larger amounts of yttria. No changes in the stabilizing oxide contents were observed in the ceria-or thoria-stabilized series.

It was suspected that the decrease in content of the stabilizing oxide was due to preferential volatilization of the oxide during the homogenization anneal, the melting process, and the thermal analysis studies at high temperatures. However, the observed calcia losses could not be reconciled with published data on the vapor pressures of the pure materials (15, 16). Therefore, a mass spectrometer study of the equilibrium vaporization of calcium- and uranium-containing species from a tungsten Knudsen cell was undertaken.*

The vaporization study was carried out in a Nier-type 12-in. radius of curvature, 60-degree sector, single-focusing mass spectrometer. The sample used in the study contained 10 mol-% calcia and had an inital O/U ratio of 1.7. The sample was held at 2018°K until the ion signals no longer changed with time. The species observed, their intensities, relative pressures, and the relative amounts volatilized from the crucible are given in Table 15.

The ion-signals were converted to relative pressures, P, using the equation:

$$P = \frac{IT\sqrt{M}}{E\gamma} ,$$

where I is the ion signal corrected for isotopic abundances, T the absolute temperature, M the mass of the ion measured, E the energy above the appearance potential at which the ion was measured (in electron volts), and γ the relative electron cross section from Otvos and Stenvenson (17). Since the number of moles of calcium-containing species effusing from the Knudsen cell per unit time exceeds the moles of uranium-containing species, it is clear that the vapor phase was enhanced in calcium. Calcium was thus lost preferentially from the sample and the calcium content of the condensed phase decreased with time, in agreement with the observations of the study.

*These studies were carried out by Dr. John H. Norman and H. G. Staley.

Similar behavior has been observed at the General Electric Nuclear Materials and Propulsion Operation where the depletion of calcia in samples annealed at 1800°C has been observed (18).

Table 15

VAPOR SPECIES OBSERVED ABOVE URANIA-10 MOL-% CALCIA AT 2018°K

Ion	Mass	Intensity (V)	Relative Pressure (arbitrary units)	Moles[a] Vaporizing
Ca	40	0.412	6.93	2.44×10^{-2}
CaO	56	0.057	1.16	3.45×10^{-3}
U	238	0.066	2.29	3.20×10^{-3}
UO	254	0.384	12.6	1.76×10^{-2}
UF_2	257	0.065	2.31	3.21×10^{-3}
UO_2	270	0.029	0.930	1.26×10^{-3}
UOF	273	0.013	0.456	6.15×10^{-4}
UF_2	276	0.003	0.101	1.35×10^{-4}

[a]The number of moles vaporizing per unit time is proportional to $P/\sqrt{TM}$.

Although it was possible to explain the loss of calcia from the thermal analysis samples on the basis of the mass spectrometer results, the large and nonuniform losses, especially in the 5 and 10 mol-% series made analysis of the data difficult. It was therefore decided that a fourth series, containing initially 15 mol-% calcia should be studied to aid in interpreting the data as a function of calcia content. The data on the 15 mol-% series are also given in Table 10, but unfortunately the large losses of calcia by volatilization resulted in widely scattered thermal analysis data. The added series was thus of little additional value in extending the range of calcia contents for interpretive convenience.

6.4. Examination of Samples with the Electron Microprobe Analyzer

One sample from each of the U-Ca-O and U-Y-O systems was submitted for electron microprobe analysis. The objectives of the analysis

were: (1) to determine whether there was preferential segregation of the additive metal in the oxide matrix or whether it was uniformly distributed in the uranium metal phase also, and (2) to determine whether tungsten was present as the oxide in the UO_2 matrix or whether it was dissolved by the liquid uranium metal and was therefore present in the metallic state.

The yttria-containing sample had an initial composition of $UO_{1.62}$* and a nominal Y_2O_3 content of 5 mol-%. After the experiment, microprobe analysis of this sample showed three phases to be present. The UO_2 matrix contained about 2 wt-% yttrium (uncorrected microprobe intensity), which was uniformly distributed. In addition, there were two grain-boundary phases. The predominant grain-boundary phase was essentially pure uranium metal. This is shown as the white area in Fig. 11a. (The continuation of the white area into the black streak is probably a void produced by polishing.) The minor grain-boundary phase (black area in Fig. 11b) was found to be high in yttrium. This is in agreement with the reported low mutual solubilities of uranium and yttrium metals(19). No tungsten contamination was found in this sample, which is in agreement with the analytical results on the x-ray spectrograph, and with the general observation that tungsten was found only in samples with higher O/U ratios.

The U-Ca-O sample initially contained 2.5 mol-% CaO with an O/U ratio of 2.1. Chemical analysis of the sample after the thermal analysis experiment yielded an O/U ratio of 2.02 and a CaO content of 2.04 mol-%. The microprobe analysis showed no uranium-metal phase to be present, in agreement with the chemical analysis. Calcium was found to be uniformly dispersed throughout the sample. In this sample the grain boundaries of the UO_2 matrix also contained two phases: tungsten and a tungsten-oxide phase. The tungsten metal is the white phase shown in Figs. 12a and 12b and the tungsten oxide is the black phase in the grain boundaries. The detection of tungsten by microprobe analysis confirmed the x-ray spectrographic determination of 1.8 wt-% tungsten in this sample. Further, it emphasizes the difficulty in calculating the O/U ratio in samples containing tungsten contaminant, since the amount of oxygen combined with the tungsten is uncertain, thus introducing an error of ±0.05 in the O/U ratio for a sample containing 1 wt-% tungsten.

*Final composition, $UO_{1.64}$.

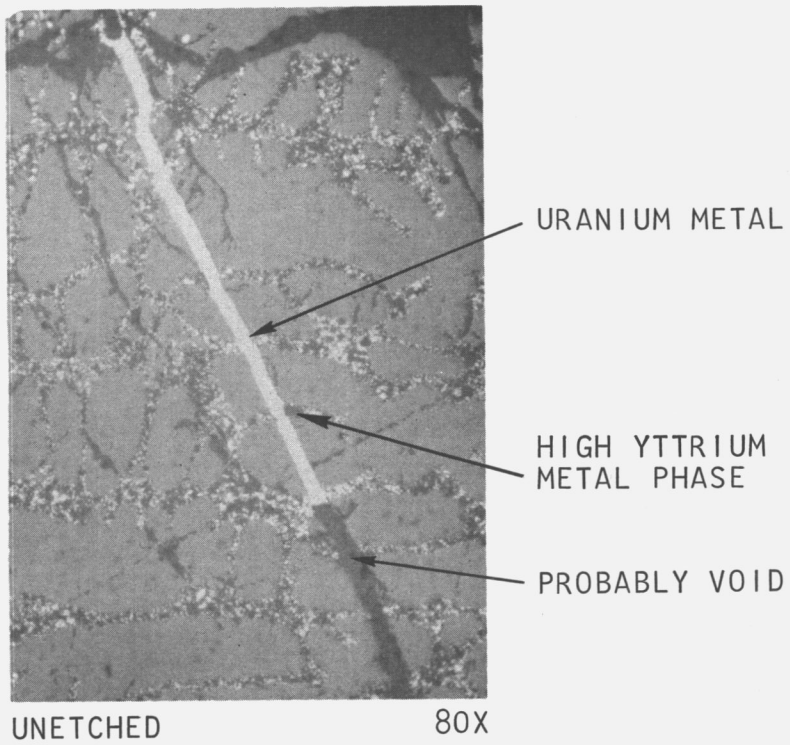

Fig. 11a--Photomicrograph of $UO_{1.64}$ (5 mol-% Y_2O_3)

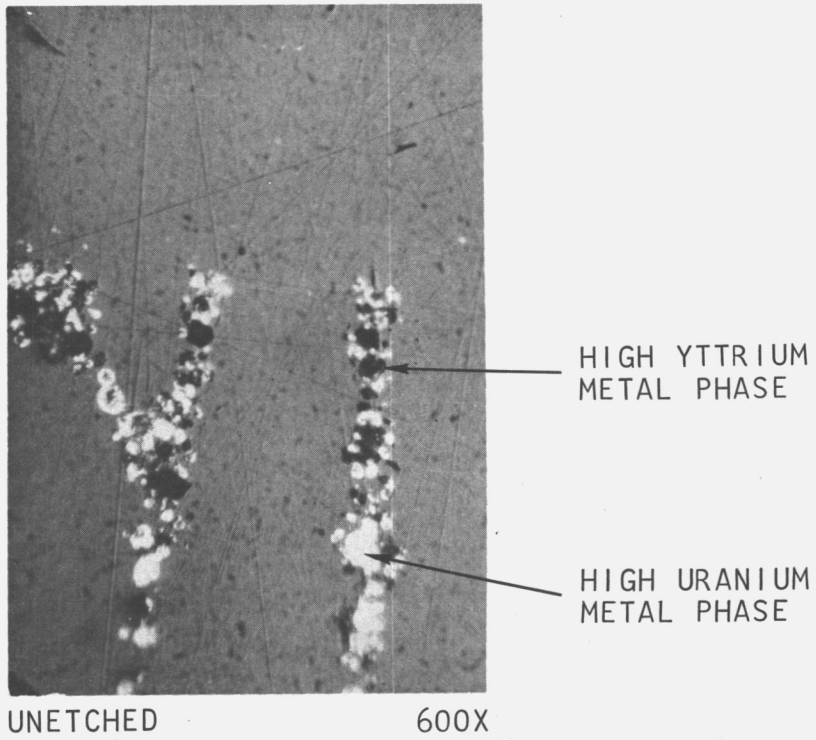

Fig. 11b--Photomicrograph of $UO_{1.64}$ (5 mol-% Y_2O_3)

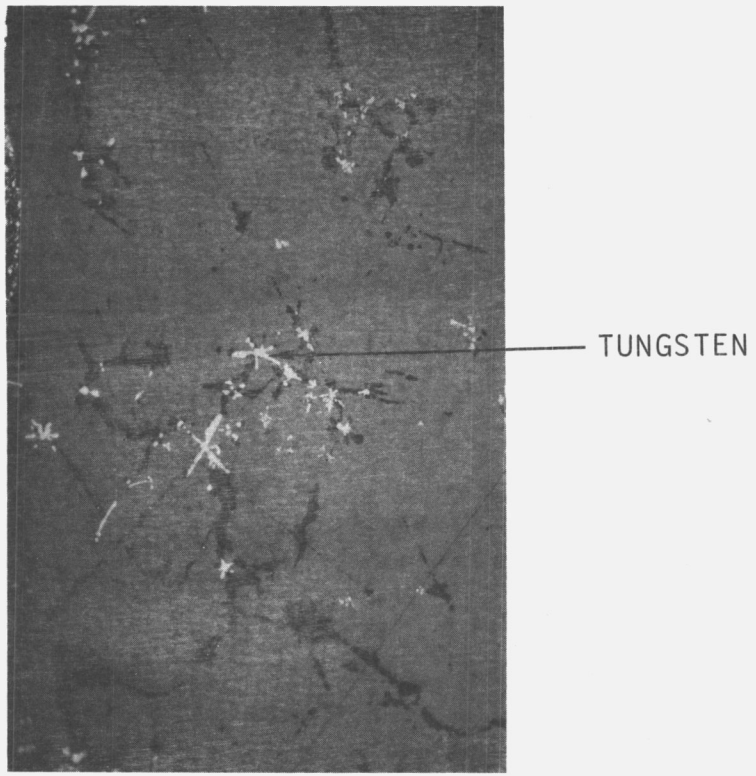

Fig. 12a--Photomicrograph of $UO_{2.02}$ (2.04 mol-% CaO)

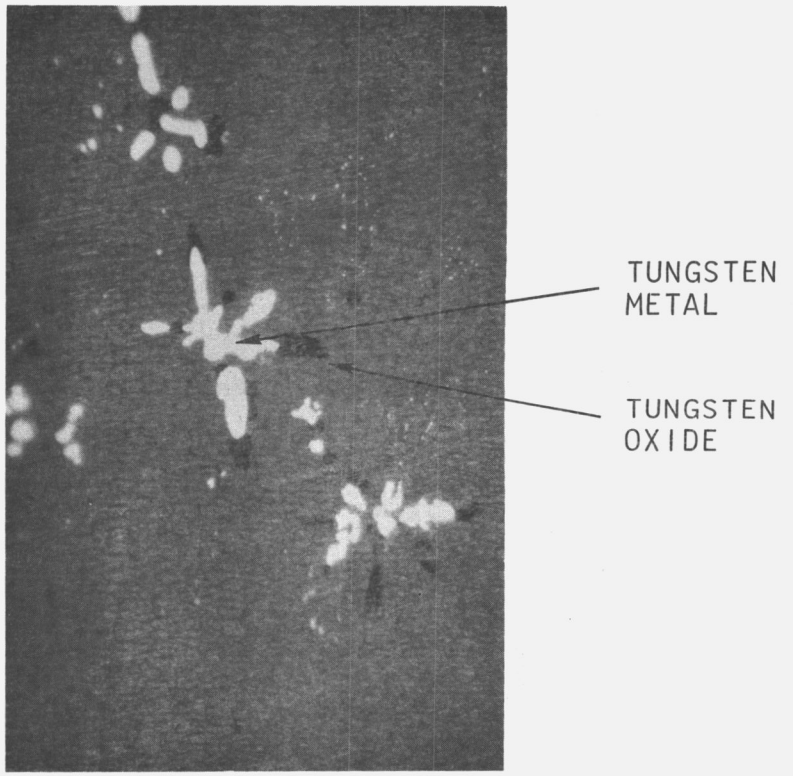

Fig. 12b--Photomicrograph of $UO_{2.02}$ (2.04 mol-% CaO)

7. THERMAL ANALYSIS DATA

The results of the thermal analyses of the five systems studied in the present program are presented in this section. The general type of cooling curves expected for various regions of the phase diagram are discussed first as an aid in interpreting the data.

7.1. Idealized Thermal Analysis Curves

It is possible, by reference to the U-O phase diagram of Edwards and Martin (6) (Fig. 1), to draw idealized cooling (or heating) curves for the two regions of the phase diagram of interest to this study.

7.1.1. Composition with $1.3 < O/U < \sim 1.60$

In the range $1.3 < O/U < \sim 1.60$, the system undergoes monotectic melting. An idealized cooling curve for a sample within this range is shown in Fig. 13. This curve shows changes in slope corresponding to the crossing of two phase boundaries: the liquidus temperature and the monotectic temperature. The lengths of the various sections of the curves will depend upon the precise composition of the sample. For those samples with O/U ratios close to that of the monotectic composition, the monotectic halt will be distinct and the change in slope at the liquidus temperature may not be seen at all. The initial change in slope is thus likely to correspond to the monotectic temperature. Conversely, samples with O/U ratios close to 1.60 will show short, if any, monotectic halts. The initial change of slope in the curve will correspond to the liquidus temperature. The heating curves for the above samples will be mirror images of the cooling curves reflected in the temperature axis.

Thermal analysis curves for samples in the region $1.5 < O/U < 1.60$ actually showed a behavior roughly comparable to the idealized curve in Fig. 13, but with much more curvature and no distinct changes in slope. They also differed in actual appearance, because of the step increase in apparent temperature due to the emittance change on freezing. No thermal effects that could be attributed to the decomposition of the substoichiometric UO_2 phase were observed in samples within the above composition region.

7.1.2. Compositions with $\sim 1.60 < O/U < 2.0$

Samples with O/U ratios $> \sim 1.60$ do not exhibit monotectic melting. But, the solidus temperature varies with composition. At lower temperatures

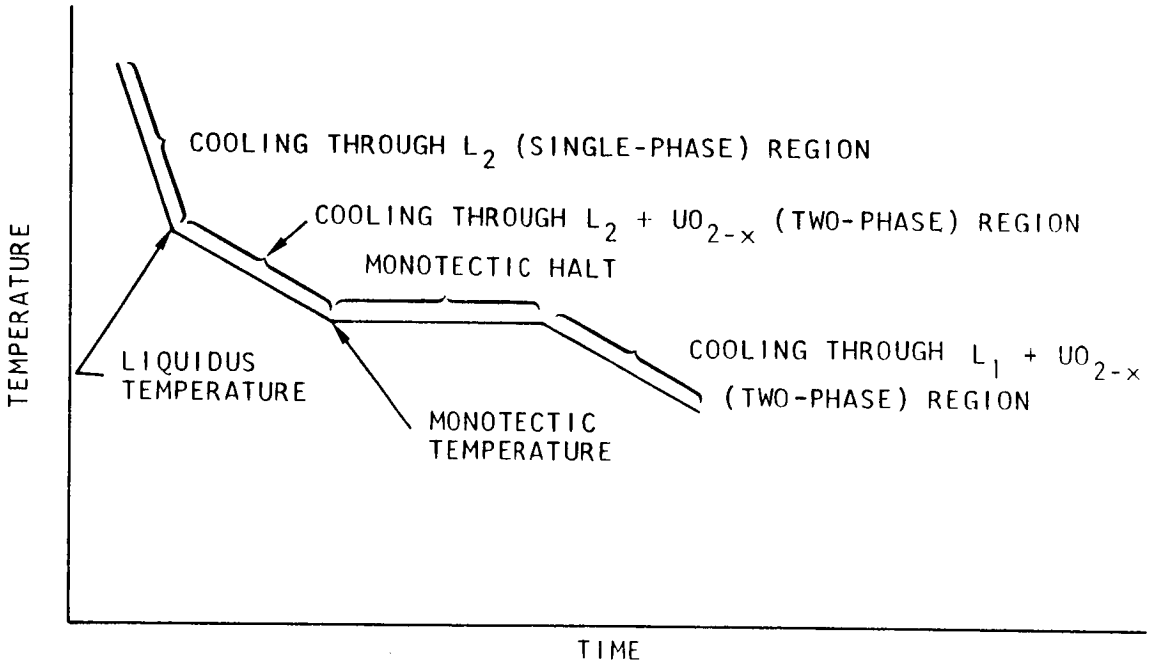

Fig. 13--Idealized cooling curve for compositions with $1.3 < O/U < 1.65$

the solid-solution phase UO_{2-x} decomposes to U(liquid) + $UO_{2-x+\delta}$, where δ is an infinitesimally small number. Determination of the temperature-composition dependence of this decomposition reaction was the primary objective of the present study.

An idealized cooling curve for compositions in the range O/U $>\sim$ 1.60 is shown in Fig. 14. This curve shows changes in slope corresponding to the crossing of three-phase boundaries: the liquidus temperature, the solidus temperature, and the decomposition temperature. Once again, the lengths of the various sections of the curve will depend upon the precise composition of the sample. It is likely that only either the liquidus or, rarely, the solidus may be apparent. For compositions very close to $UO_{1.60}$, the decomposition temperature may be difficult to detect. This may also be true near $UO_{2.0}$, where this phase boundary becomes nearly vertical, indicating a very small change with temperature in the solubility of U(liquid) in UO_2. Since only a very small amount of material is precipitated, and, further, over a range of temperature, the phase boundary should be difficult to detect.

Thermal analysis curves of samples in the composition range $UO_{1.60}$ to $UO_{2.0}$ were generally found to be similar to the curve in Fig. 14, but once again there was considerable curvature and no distinct changes in slope. Heating and cooling curves from 1000° to about 2000°C are shown in Fig. 15 for $UO_{1.95}$. The decomposition reaction is barely perceptible on the heating and cooling curves, but is readily seen on the time derivative of the temperature curves.

The thermal analyses in this region were carried on down to quite low temperatures in order to utilize the thermal arrests associated with transitions in uranium metal as confirmatory evidence for the presence or absence of free uranium metal in a given composition. These thermal arrests, quite unexpectedly, were observed in the earliest experiments with substoichiometric UO_2 samples. The small amount of uranium metal calculated to be present in some of these samples (1.6 g of uranium metal in 23 g of $UO_{1.84}$) made it quite unlikely that the freezing and polymorphic transitions could be detected. However, thermal analysis curves between 600° and 1300°C quite clearly show all three transitions. One of these curves for $UO_{1.75}$ is shown in Fig. 16. While only the γU to U(liquid) transition is detectable on the standard heating curve, all three transitions are apparent on the derivative curve. On cooling, the freezing of the liquid U and the $\gamma U \leftrightarrow \beta U$ transition can be distinguished on both the standard and derivative curves.* Since the two solid-state transitions occur at temperatures below the minimum useful range of optical pyrometers, the temperatures

*The cooling curve was not continued down to the $\beta U \leftrightarrow \gamma U$ transition temperature.

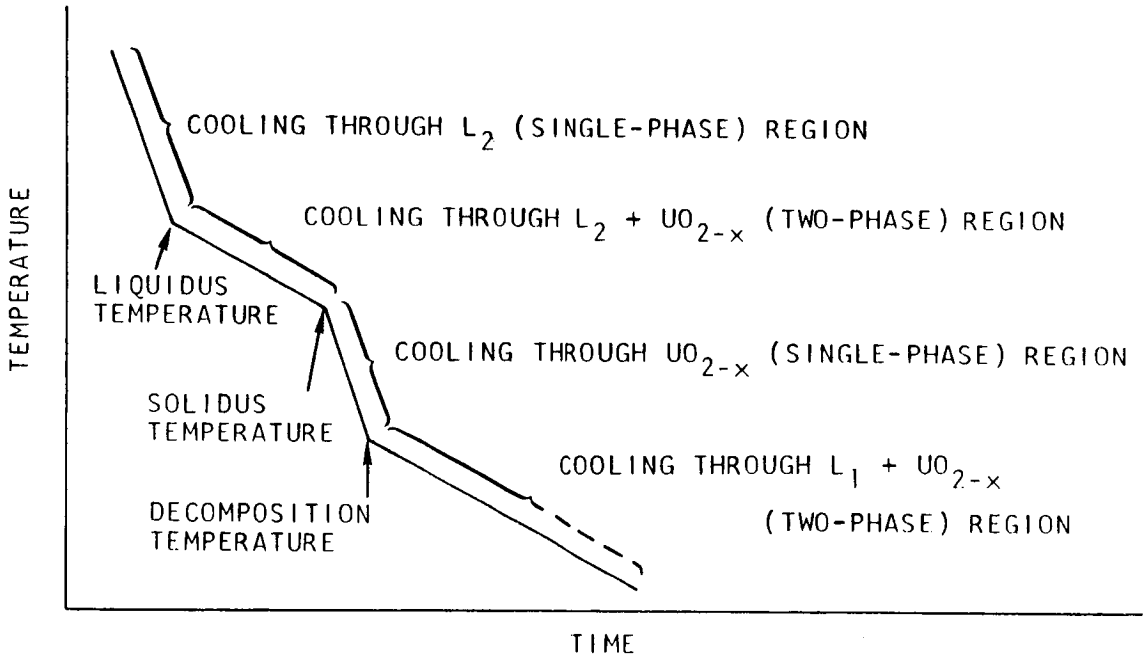

Fig. 14--Idealized cooling curve for compositions with $1.60 < O/U < 2.0$

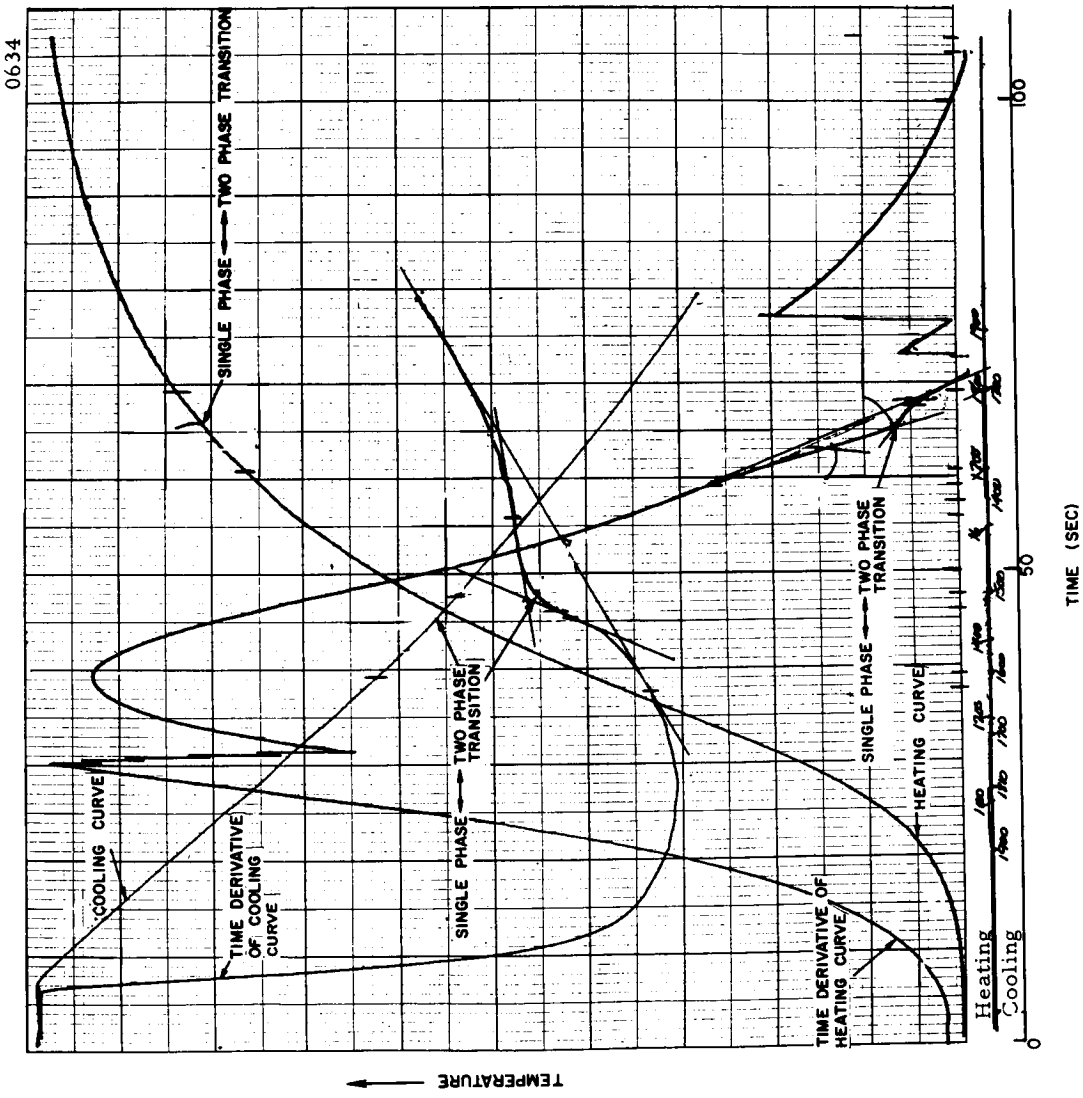

Fig. 15--Thermal analysis curve for $UO_{1.95}$

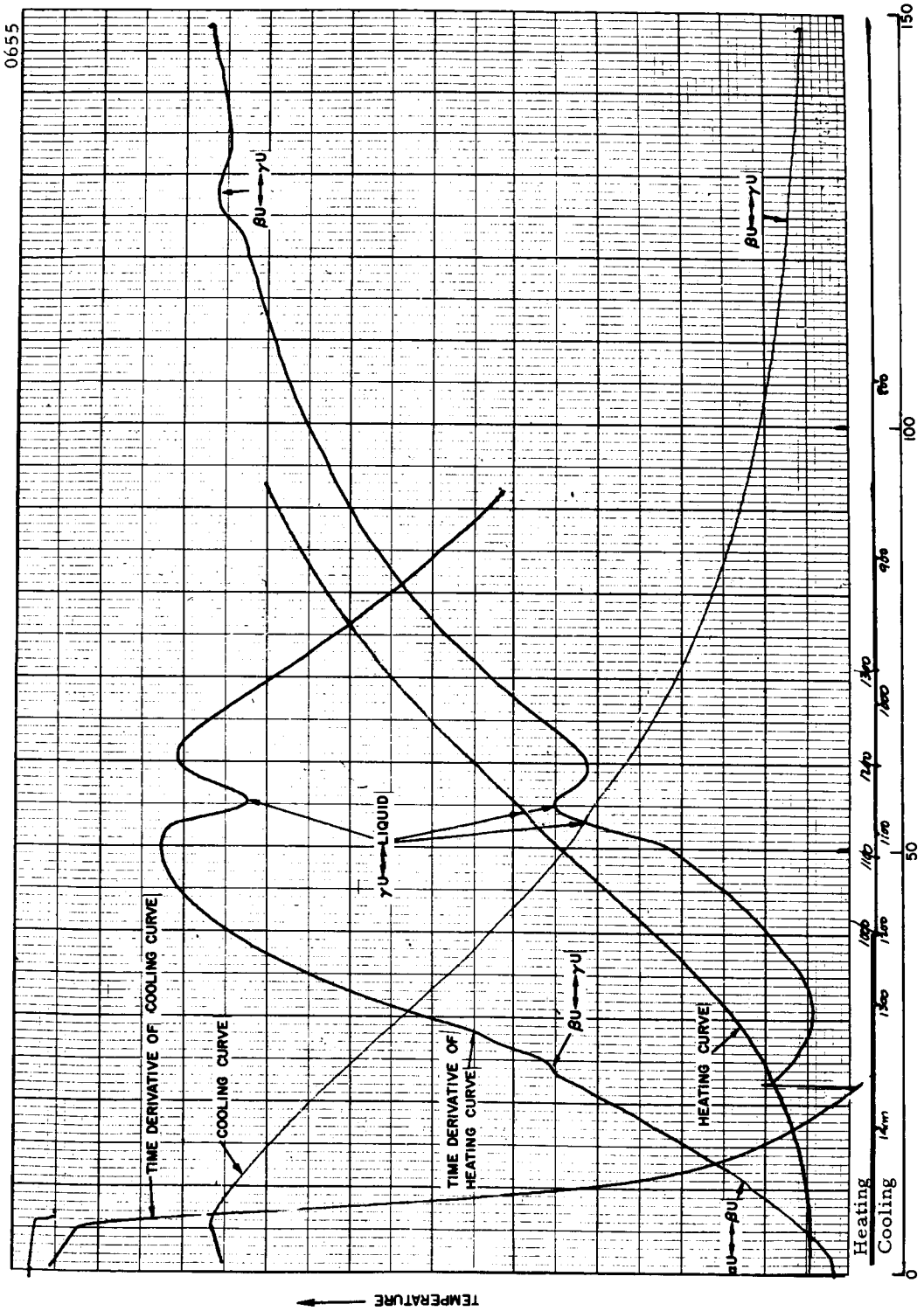

Fig. 16--Thermal analysis curve for $UO_{1.75}$

of these transitions cannot be determined from these curves. However, it was possible, in separate experiments, to measure the temperature of these thermal arrests by placing a Pt/Pt-10% Rh thermocouple directly into the UO_2 samples. This was done in samples of composition $UO_{1.67}$ and $UO_{1.84}$ and the data are given in Table 16. The thermocouple was not sufficiently sensitive to detect the solid state transition, but it was used to measure the temperature of the UO_2 as the infrared detector plotted the thermal analysis curves on which the transitions are detectable. The temperatures observed on heating are above the accepted equilibrium temperatures for the transitions, whereas those observed on cooling are below. The correspondence, however, leaves little doubt that the transitions being observed are those of uranium metal. The data in Table 16 show that isothermal enthalpy changes of <8 calories in a sample can be detected by the thermal analysis apparatus. The temperatures and enthalpy changes associated with the transitions observed in $UO_{1.67}$ and $UO_{1.84}$ are also given.

Table 16

TRANSITIONS IN URANIUM METAL

Transition	Temp (°C)			Enthalpy Change (cal/mole)[19]	$UO_{1.67}$ Sample		$UO_{1.84}$ Sample	
	Literature[19]	Observed[a]			Calculated Weight of U in Sample (g)	Calculated Heat (cal)	Calculated Weight of U in Sample (g)	Calculated Heat (cal)
		Heating	Cooling					
$\alpha \leftrightarrow \beta$	668	742	----	700	3.1	9.	[c]	[c]
$\beta \leftrightarrow \gamma$	775	790	717[b]	1150	3.1	15.	1.6	<8.
$\gamma \leftrightarrow$ liquid	1132	1144	1126	2500	3.1	33.	1.6	17.

[a] These measurements are the average of data from the standard and the derivative thermal analysis curves, except where indicated.

[b] From standard thermal analysis curve only.

[c] Thermal analysis not carried out at sufficiently low temperatures to observe the $\alpha \leftrightarrow \beta$ transition.

7.2. Experimental Data

The large amount of experimental data obtained in this study on the five systems and covering four composition ranges makes its presentation in a coherent manner difficult. The choice of the major subheadings under which to present the data and the large number of curves is necessarily arbitrary. However, the objective has been to keep measurements of the same type together, thus facilitating comparisons between systems. Thus, the decomposition temperatures are presented first, followed by a subsection dealing with the liquidus temperatures. The solidus temperatures, although measured when possible, are believed to have very large errors associated with them and are thus of limited reliability. They are presented in the interest of providing a complete record of the research, but are utilized

only as an aid in locating the monotectic temperatures and the p-tristeric* point.

7.2.1. Decomposition Temperatures

The decomposition temperatures of hypostoichiometric UO_2 were measured for the pure U-UO_2 system and for the system stabilized with CaO, Y_2O_3, CeO_2, and ThO_2. The decomposition temperatures, as determined on heating and cooling from both the standard and the derivative thermal analysis curves, are given in Tables 17 to 21.

For the unstabilized U-O system, the decomposition temperatures from the standard thermal analyses curve from columns 3 and 4 of Table 17 are plotted in Fig. 17. The data from the derivative curve (columns 5 and 6) are plotted in Fig. 18. Because of the large number of experiments in the U-O system, it was necessary to present the derivative and standard data on separate plots to obtain an uncluttered figure. (Both sets of data are presented in the same plot for the stabilized systems.) The points at O/U = 1.95 are in disagreement with the balance of the data. In this region of high O/U ratio, the hysteresis error is also large. Several monotectic temperature points, obtained from Table 22 (Section 7.2.2), have been included in the figure. This is done throughout this section as an aid in locating the terminus of the decomposition curve at the monotectic temperature.

The decomposition and monotectic temperatures of the four calcia-stabilized series are given in Figs. 19 to 22. Figure 19 contains the data from both the standard and derivative curves for samples containing nominally 2.5 mol-% calcia. Figure 20 contains the same data for samples with a nominal calcia content of 5.0 mol-%. Figure 21 shows these data for 10.0 mol-% calcia content and Figure 22 for the 15.0 mol-% calcia samples. As a consequence of the volatilization problems with calcia-containing samples, discussed in Section 6.3, the data for all the calcia series are more scattered than the data for series containing other stabilizers.

The decomposition and monotectic temperatures in the yttria-stabilized systems are given in Figs. 23 through 25, for the 2.5, 5.0, and 10.0 mol-% yttria contents, respectively. Similar data for the 2.5, 5.0, and 10.0 mol-% thoria-stabilized series are given in Figs. 26 through 28. The data for the

*The term p-tristeric point has been suggested by Marsh (21) to describe a point where a solidus curve and a solubility curve meet at the monotectic temperature. In the present case, it represents the composition with the lowest O/U ratio which can still exist as single phase UO_{2-x}. The derivation of the term is given by Marsh.

Table 17

DECOMPOSITION TEMPERATURES IN THE URANIUM-OXYGEN SYSTEM

Exp. No.	Final Composition O/U Ratio	Decomposition Temperatures[a] (°C)				Avg. of Heating and Cooling (°C)		Avg. of Standard and Derivative (°C)
		Standard Curve		Derivative Curve		Standard Curve	Derivative Curve	
		Heating	Cooling	Heating	Cooling			
1.1-1	1.52	[b]						
1.15-1	1.62	[b]						
1.3-2	1.67	----	----	2284	2338	----	2311	2311[c]
1.3-3	1.67	----	2384	----	2398	----	----	----
1.5-1	1.71	2284	2057	2341	2215	2170	2278	2224
1.5-5	1.73	2250	2223	2230	2238	2236	2234	2235
1.5-4	1.75	----	----	2354	2307	----	2331	2331[c]
1.7-3	1.77	----	1971	2060	1990	----	2025	1998
1.7-2	1.80	2174	2050	2181	2077	2112	2129	2121
1.17-1	1.80	2159	2115	2159	2122	2137	2141	2139
1.9-3	1.83	----	1661	1722	1667	----	1695	1678
1.9-4	1.84	1812	1732	1777	1735	1772	1756	1764
1.9-4'	1.87	1774	1742	1795	1739	1758	1767	1763
1.9-5	1.90	----	----	1437	1476	----	1457	1457[c]
1.11-3	1.92	[b]						
1.9-2	1.95	1900	1624	1902	1655	1762	1779	1770
1.11-2	2.02	[b]						
1.11-2'	2.02	[b]						
1.13-1	2.06	[b]						

[a] Temperatures listed are normally the average of at least two determinations.

[b] Liquidus and solidus temperatures only (see Table 22).

[c] Over-all average is from derivative curve only.

Table 18

DECOMPOSITION TEMPERATURES IN THE URANIUM-CALCIUM-OXYGEN SYSTEM

Exp. No.	Final Composition		Decomposition Temperatures[a] (°C)				Avg. of Heating and Cooling (°C)		Avg. of Standard and Derivative (°C)
			Standard Curve		Derivative Curve				
	CaO (mol-%)	O/U Ratio	Heating	Cooling	Heating	Cooling	Standard Curve	Derivative Curve	
2.15-1	1.94	1.63	[b]						
2.1-1	1.30	1.66	[b]						
2.17-1	2.60	1.67		2183		2203	2183[c]	2203[c]	2193[c]
2.3-1	1.95	1.72		2288		2317	2288[c]	2317[c]	2303[c]
2.5-1	1.97	1.75			2289	2110		2199	2199[d]
2.5-2	1.33	1.83			2024	1947		1991	1991[d]
2.7-2	1.32	1.89			1959	1772		1866	1866[d]
2.7-1	1.99	1.90			2104	1906		2005	2005[d]
2.9-1	2.00	1.92	No Data - Excessive Volatilization						
2.11-1	1.99	1.95	No Data - Excessive Volatilization						
2.13-1	2.04	2.04	No Data - Excessive Volatilization						
2.14-1	3.51	1.63		2163		2140	2163[c]	2140[c]	2152[c]
2.15-2	3.86	1.67		2254		2231	2254[c]	2231[c]	2243[c]
2.19-1	3.23	1.74			2259	2125		2192	2192[d]
2.23-1	3.26	1.79			1748			1748[e]	1748[d, e]
2.21-1	3.25	1.81			1961	1734		1848	1848[d]
2.21-2	3.91	1.91			1914	1665		1790	1790[d]
2.25-1	3.89	1.99	[b]						
2.27-1	3.38	2.03	[b]						
2.28-1	7.98	1.66		2250	2276	2217	2250[c]	2247	2247[d]
2.29-1	5.37	1.67		2236		2237	2236[c]	2237[c]	2237[d]
2.31-1	6.35	1.76		2074	2298	2076	2074[c]	2187	2187[d]
2.33-1	6.98	1.84		1849	1965	1865	1849[c]	1915	1915[d]
2.35-1	7.01	1.90	1441	1559	1385	1471	1500	1428	1464
2.39-1	7.42	1.96	[b]						
2.37-1	7.09	1.97	[b]						
2.41-1	7.24	2.02	[b]						
2.43-1	9.22	1.74		2154		2136	2154[c]	2136[c]	2145[c]
2.45-1	10.15	1.80			2302	2208		2255	2255[d]
2.47-1	11.35	1.84			1686	1624		1655	1655[d]
2.49-1	11.65	1.95			1589	1404		1497	1497[d]
2.55-1	12.24	1.97	[b]						
2.53-1	12.05	1.98	[b]						
2.51-1	12.01	1.99	[b]						

[a] The temperatures listed are normally the average of two or more determinations.
[b] Liquidus and solidus temperatures only. See Table 10.
[c] From cooling curve only. No heating curve data available.
[d] From derivative curve only. No average standard curve data available.
[e] From heating curve only. No cooling curve data available.

Table 19

DECOMPOSITION TEMPERATURES IN THE URANIUM-YTTRIUM-OXYGEN SYSTEM

Exp. No.	Final Composition		Decomposition Temperatures[a] (°C)				Avg. of Heating and Cooling (°C)		Avg. of Standard and Derivative (°C)
			Standard Curve		Derivative Curve				
	Y_2O_3 (mol-%)	O/U Ratio	Heating	Cooling	Heating	Cooling	Standard Curve	Derivative Curve	
3.1-1	2.09	1.61	(b)						
3.3-1	2.61	1.73	----	2463	----	2466	2463[c]	2466[c]	2465[c]
3.5-1	2.62	1.74	2337	2197	2269	2148	2267	2209	2238
3.7-1	1.96	1.88	----	1753	2188	1934	1753[c]	2061	2061[d]
3.9-1	2.62	1.92	1596	1490	1580	1487	1543	1534	1539
3.11-1	2.64	2.03	(b)						
3.13-1	2.27	2.04	(b)						
3.15-2	4.89	1.64	(b)						
3.17-2	4.51	1.70	----	2285	2376	2259	2285[c]	2318	2318[d]
3.19-3	4.79	1.81	----	----	2033	2025	----	2029	2029[d]
3.19-2	4.59	1.83	----	----	2340	2077	----	2209	2209[d]
3.21-2	4.59	1.88	----	----	----	1585	----	1585[c]	1585[c, d]
3.21-3	4.83	1.88	----	----	1946	1591	----	1769	1769[d]
3.23-2	4.58	1.93	(b)						
3.25-1	4.89	2.02	(b)						
3.27-1	4.86	2.10	(b)						
3.29-2	8.79	1.58	(b)						
3.31-2	8.81	1.68	----	----	2424	2220	----	2324	2324[d]
3.33-2	8.78	1.80	----	----	----	2095	----	2095[c]	2095[c, d]
3.35-2	8.78	1.86	----	----	1725	1585	----	1655	1655[d]
3.37-2	8.82	1.94	----	----	----	1221	----	1221[c]	1221[c, d]
3.39-1	8.58	2.08	(b)						
3.41-1	9.06	2.14	(b)						

[a] Temperatures listed are normally the average of two or more determinations.
[b] Liquidus and solidus temperatures only (see Table 24).
[c] From cooling curve only. No heating curve data available.
[d] From derivative curve only. No average standard curve data available.

Table 20

DECOMPOSITION TEMPERATURES IN THE URANIUM-THORIUM-OXYGEN SYSTEM

Exp. No.	Final Composition		Decomposition Temperatures[a] (°C)				Average of Heating and Cooling (°C)		Avg. of Standard and Derivative (°C)
			Standard Curve		Derivative Curve				
	ThO_2 (mol-%)	O/U Ratio	Heating	Cooling	Heating	Cooling	Standard Curve	Derivative Curve	
4.3-1	2.50	1.68	[b]						[b]
4.5-1	2.50	1.75		2197	2377	2163	2197[b]	2270	2270[c]
4.7-1	2.38	1.83			2007	1901		1954	1954[c]
4.9-1	2.28	1.92	1846	1503	1826	1519	1675	1673	1674
4.11-1	2.41	1.98				1474		1474[d]	1474[c, d]
4.17-1	5.02	1.67	[b]						[b]
4.19-1	4.90	1.81			2285	2148		2217	2217[c]
4.21-1	4.92	1.85				1974		1974[d]	1974[c, d]
4.23-1	4.85	1.92			1884	1645		1765	1765[c]
4.25-1	4.88	1.95	[b]						[b]
4.29-1	9.91	1.58	[b]						[b]
4.31-1	10.00	1.69	[b]						[b]
4.33-2	9.89	1.76			2122	2078		2100	2100[c]
4.35-1	9.83	1.86			2017	1985		2001	2001[c]
4.37-1	9.98	1.92			1833	1563		1698	1698[c]
4.39-1	9.56	1.95	[b]						

[a] The temperatures listed are normally the average of two or more determinations.
[b] Liquidus and solidus temperatures only. See Table 25.
[c] From derivative curve only. No average standard curve data available.
[d] From cooling curve only. No heating curve data available.

Table 21

DECOMPOSITION TEMPERATURES IN THE URANIUM-CERIUM-OXYGEN SYSTEM

Exp. No.	Final Composition		Decomposition Temperatures[a] (°C)				Average of Heating and Cooling (°C)		Avg. of Standard and Derivative (°C)
			Standard Curve		Derivative Curve				
	CeO_2 (mol-%)	O/U Ratio	Heating	Cooling	Heating	Cooling	Standard Curve	Derivative Curve	
5.1-1	2.44	1.55	[b]						[b]
5.3-1	2.64	1.68			2328	2185		2257	2257[a]
5.5-1	2.42	1.75			2131	2092		2112	2112[c]
5.7-1	2.44	1.83			1994	1833		1914	1914[c]
5.11-1	2.31	1.92							
5.9-1	2.40	1.93			1503	1388		1446	1446[c]
5.15-1	5.06	1.53	[b]						[b]
5.17-1	4.65	1.71			2175	2225		2200	2200[c]
5.19-1	5.13	1.76			2142	1984		2063	2063[c]
5.21-1	5.07	1.82			2048	1817		1933	1933[c]
5.25-1	4.89	1.89							
5.23-1	5.13	1.91			1620	1275		1448	1448[c]
5.29-1	9.77	1.56	[b]						[b]
5.31-1	9.93	1.68			2243	2203		2223	2223[c]
5.33-1	10.14	1.76			2147	2013		2080	2080[c]
5.35-1	9.86	1.89			2041	1698		1870	1870[c]
5.39-1	9.95	1.94							
5.37-1	9.95	2.01				1050		1050[d]	1050[c, d]

[a] The temperatures listed are normally the average of two or more determinations.
[b] Liquidus and solidus temperatures only. See Table 26.
[c] From derivative curve only. No average standard curve data available.
[d] From cooling curve only. No heating curve data available.

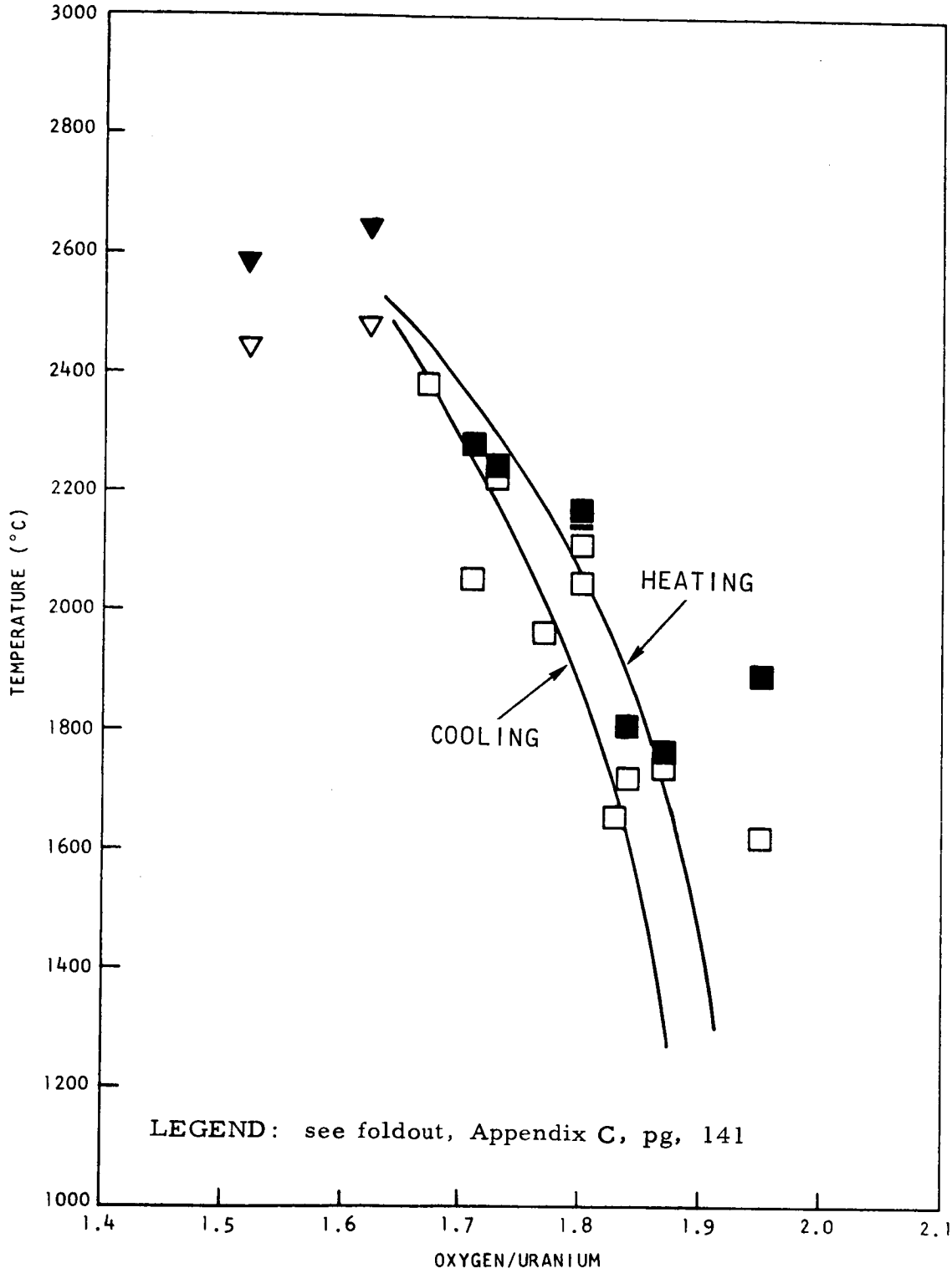

Fig. 17--Decomposition and monotectic temperatures of the uranium-oxygen system (standard curve)

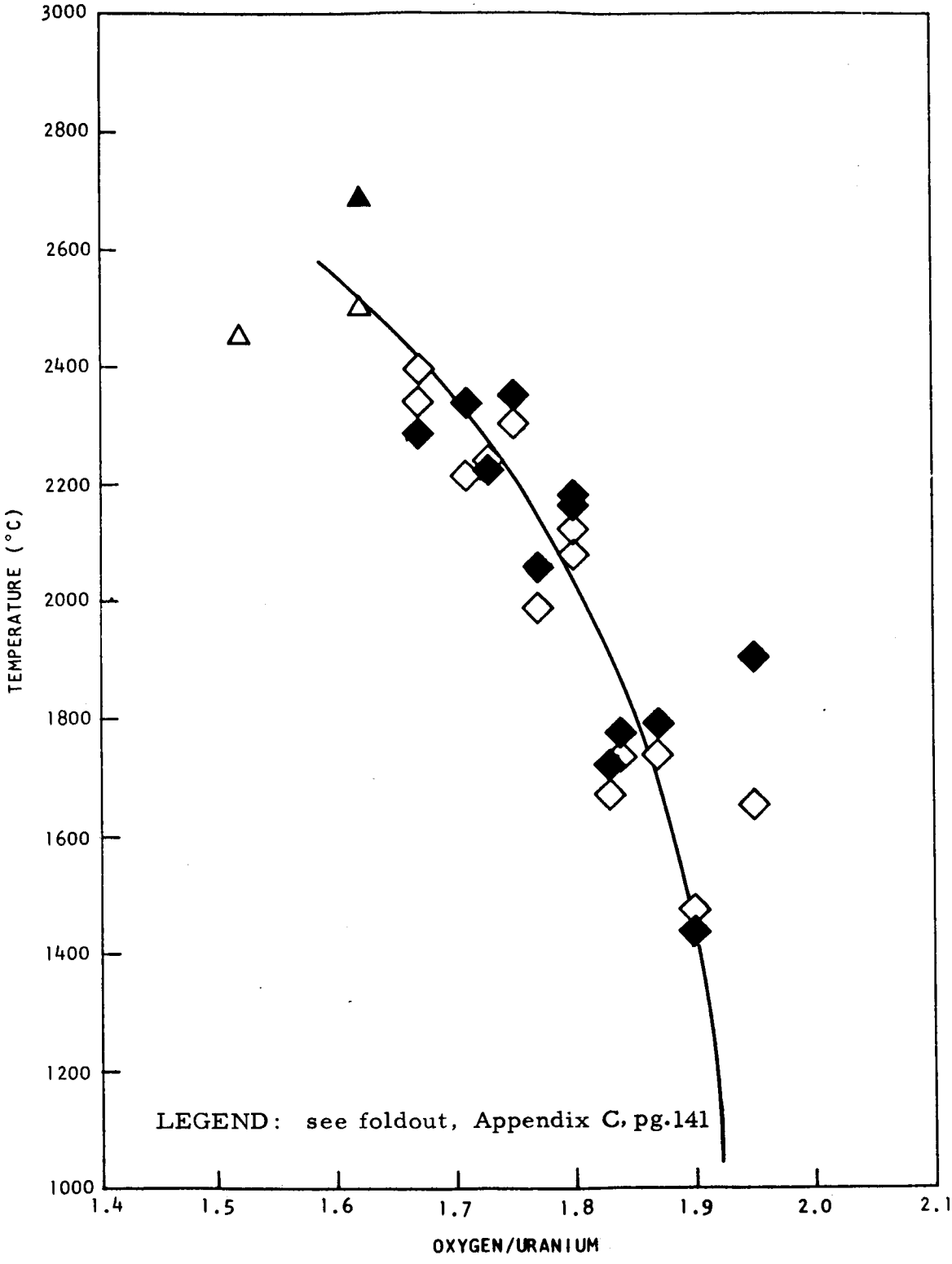

Fig. 18--Decomposition and monotectic temperatures of the uranium-oxygen system (derivative curve)

Table 22

LIQUIDUS AND SOLIDUS TEMPERATURES IN THE URANIUM-OXYGEN SYSTEM

Exp. No.	Final Composition O/U Ratio	Liquidus Temperatures (°C)							Monotectic or Solidus Temperatures (°C)						
		Standard Curve		Derivative Curve		Avg. of Heating and Cooling		Avg. of Standard and Derivative	Standard Curve		Derivative Curve		Avg. of Heating and Cooling		Avg. of Standard and Derivative
		Heating	Cooling	Heating	Cooling	Standard Curve	Derivative Curve		Heating	Cooling	Heating	Cooling	Standard Curve	Derivative Curve	
1.1-1	1.52	2696	2634	----	2667	2665	2667[a]	2665[b]	2588[c]	2446[c]	----	2450[c]	2517[c]	2450[a,c]	2517[b,c]
1.15-1	1.62	2759	2717	----	2740	2738	2740[a]	2738[b]	2646[c]	2486[c]	2691[c]	2498[c]	2566[c]	2595[c]	2581[c]
1.3-2	1.67	----	2690	----	----	2690[a]	----	2690[a,b]	----	2496	----	2505	2496[a]	2505[a]	2500[a]
1.3-3	1.67	2524	2620	----	----	2572	----	2572[b]	----	2443	----	----	2443[a]	----	2443[a,b]
1.5-1	1.71	----	2801	----	2839	2801[a]	2839[a]	2820[a]	----	2485	----	----	2485[a]	----	2485[a,b]
1.5-5	1.73	----	2740	----	2783	2740[a]	2783[a]	2761[a]	----	2519	----	2488	2519[a]	2488[a]	2504[a]
1.5-4	1.75	----	----	----	----	----	----	----	----	----	----	----	----	----	----
1.7-3	1.77	2696	2696	----	----	2696	----	2696[b]	----	----	----	----	----	----	----
1.7-2	1.80	----	----	----	----	----	----	----	----	2631	----	2636	2631	2636[a]	2634[a]
1.17-1	1.80	2890	2849	2888	2910	2870	2899	2885	----	2596	2881	2634	2596[a]	2758	2758[d]
1.9-3	1.83	----	----	----	----	----	----	----	----	----	----	----	----	----	----
1.9-4	1.84	----	2668	----	2605	2668[a]	2605[a]	2637[a]	----	----	----	2424	----	2424[a]	2424[a,d]
1.9-4'	1.87	3009	2874	2896	2907	2942	2902	2922	----	2618	----	2588	2618[a]	2588[a]	2603[a]
1.9-5	1.90	2861	2781	2859	2787	2821	2823	2822	----	2548	----	2505	2548[a]	2505[a]	2527[a]
1.11-3	1.92	----	2802	----	2810	2802[a]	2810[a]	2806[a]	----	2632	----	2610	2632[a]	2610[a]	2621[a]
1.9-2	1.95	----	----	----	----	----	----	----	----	----	----	----	----	----	----
1.11-2	2.02	3016	2892	----	2900	2954	2900[a]	2954[b]	----	2392	----	2385	2392[a]	2385[a]	2388[a]
1.11-2'	2.02	3030	2884	3014	2908	2957	2961	2959	----	2424	----	2391	2424[a]	2391[a]	2408[a]
1.13-1	2.06	2846	2776	2874	2795	2811	2835	2823	----	2418	----	2421	2418[a]	2421[a]	2420[a]

[a] From cooling curve only. No heating curve data available.
[b] From standard curve average only. No average derivative curve data available.
[c] Monotectic temperature.
[d] From derivative curve average only. No average standard curve data available.

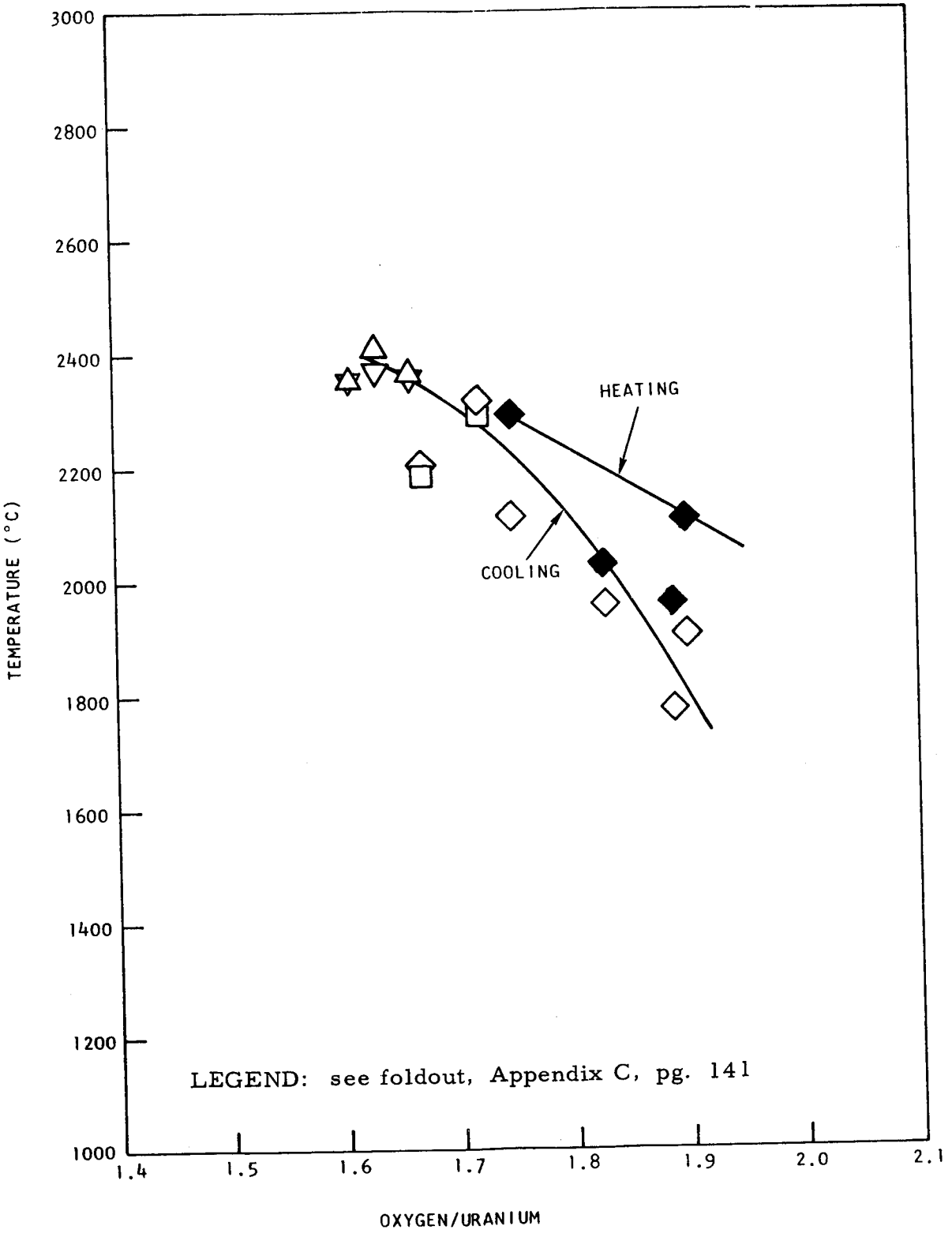

Fig. 19--Decomposition temperatures in the uranium-calcium-oxygen system (2.5 mol-% calcia)

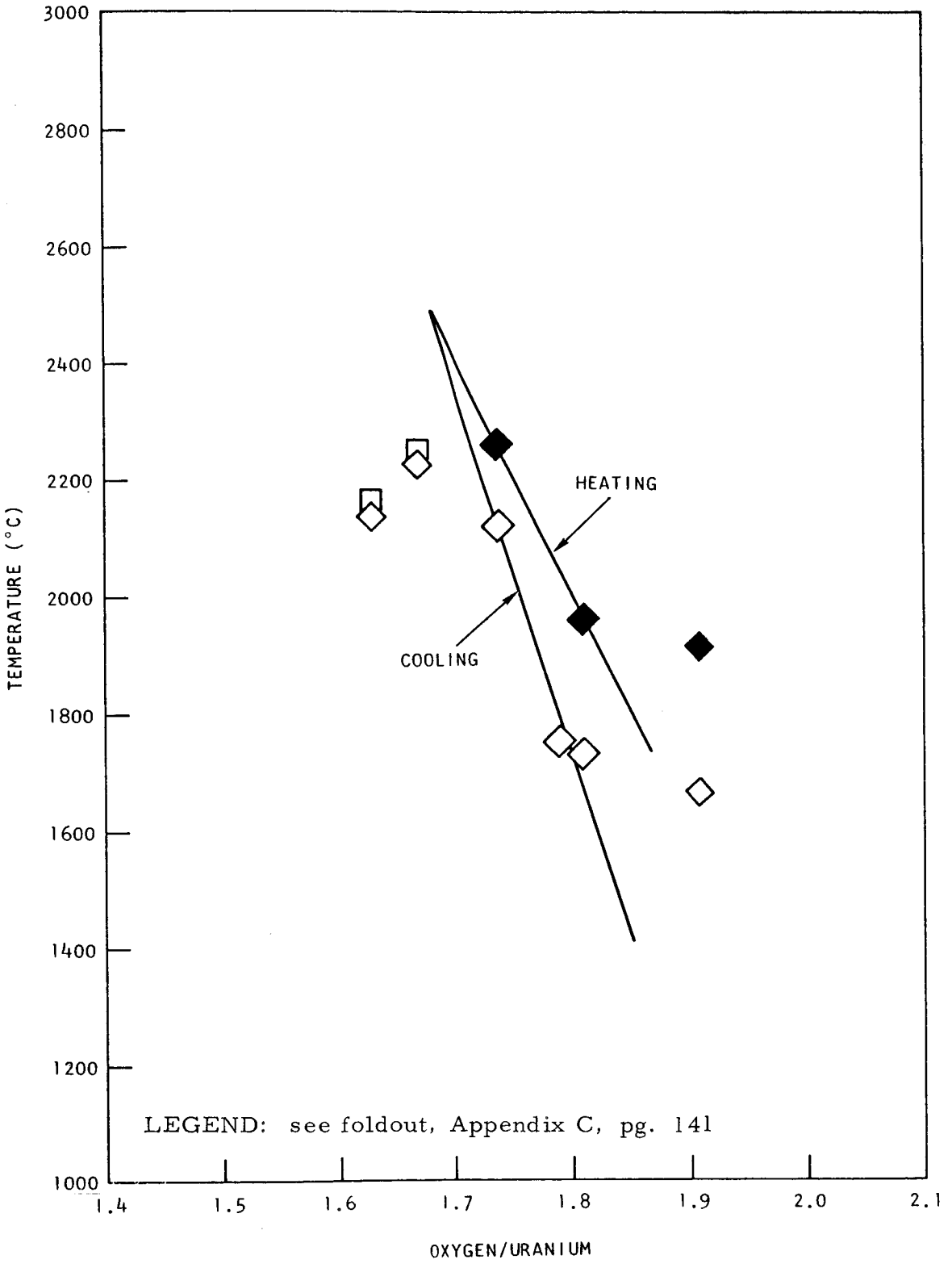

Fig. 20--Decomposition temperatures in the uranium-calcium-oxygen system (5.0 mol-% calcia)

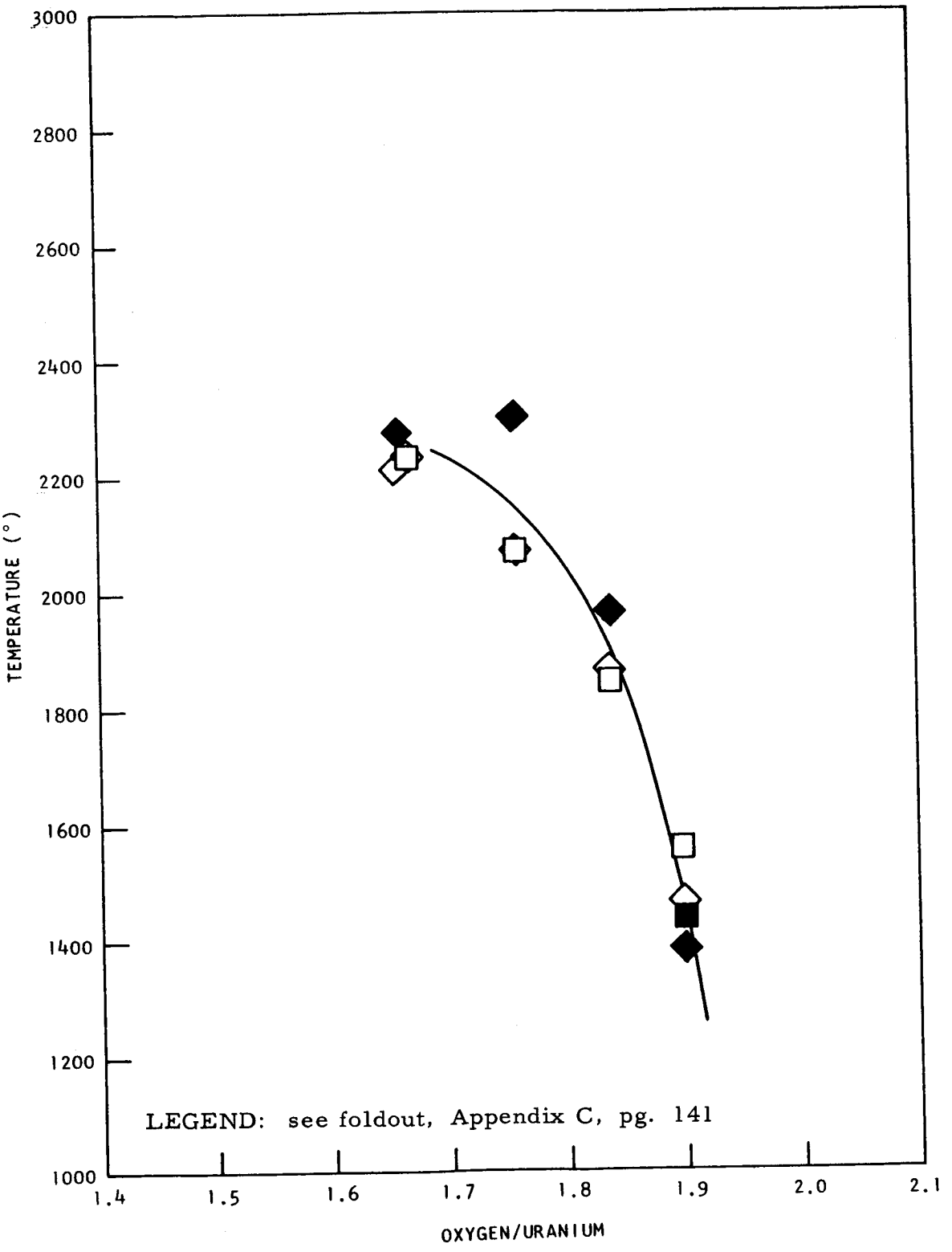

Fig. 21--Decomposition temperatures in the uranium-calcium-oxygen system (10 mol-% calcia)

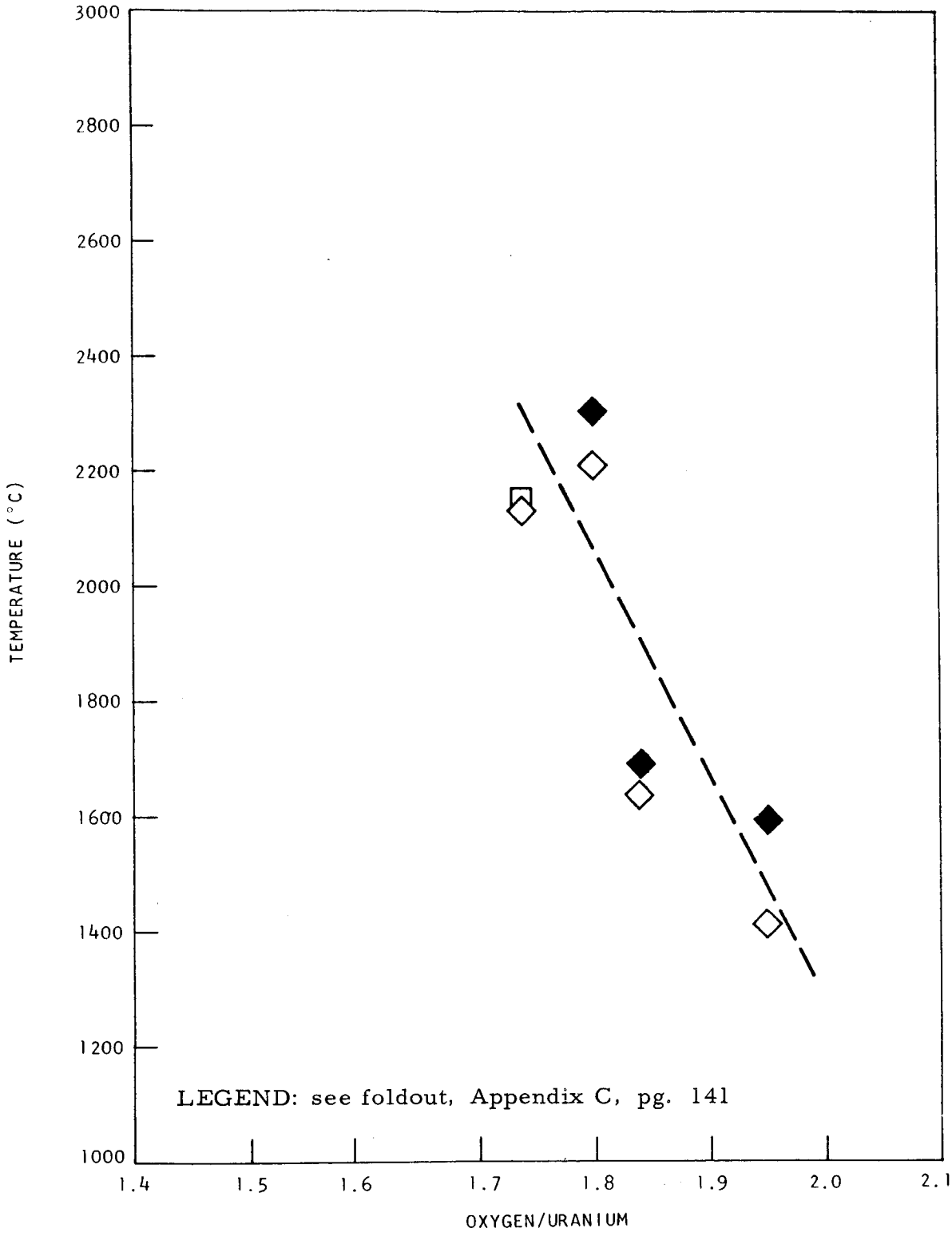

Fig. 22--Decomposition temperatures in the uranium-calcium-oxygen system (15 mol-% calcia)

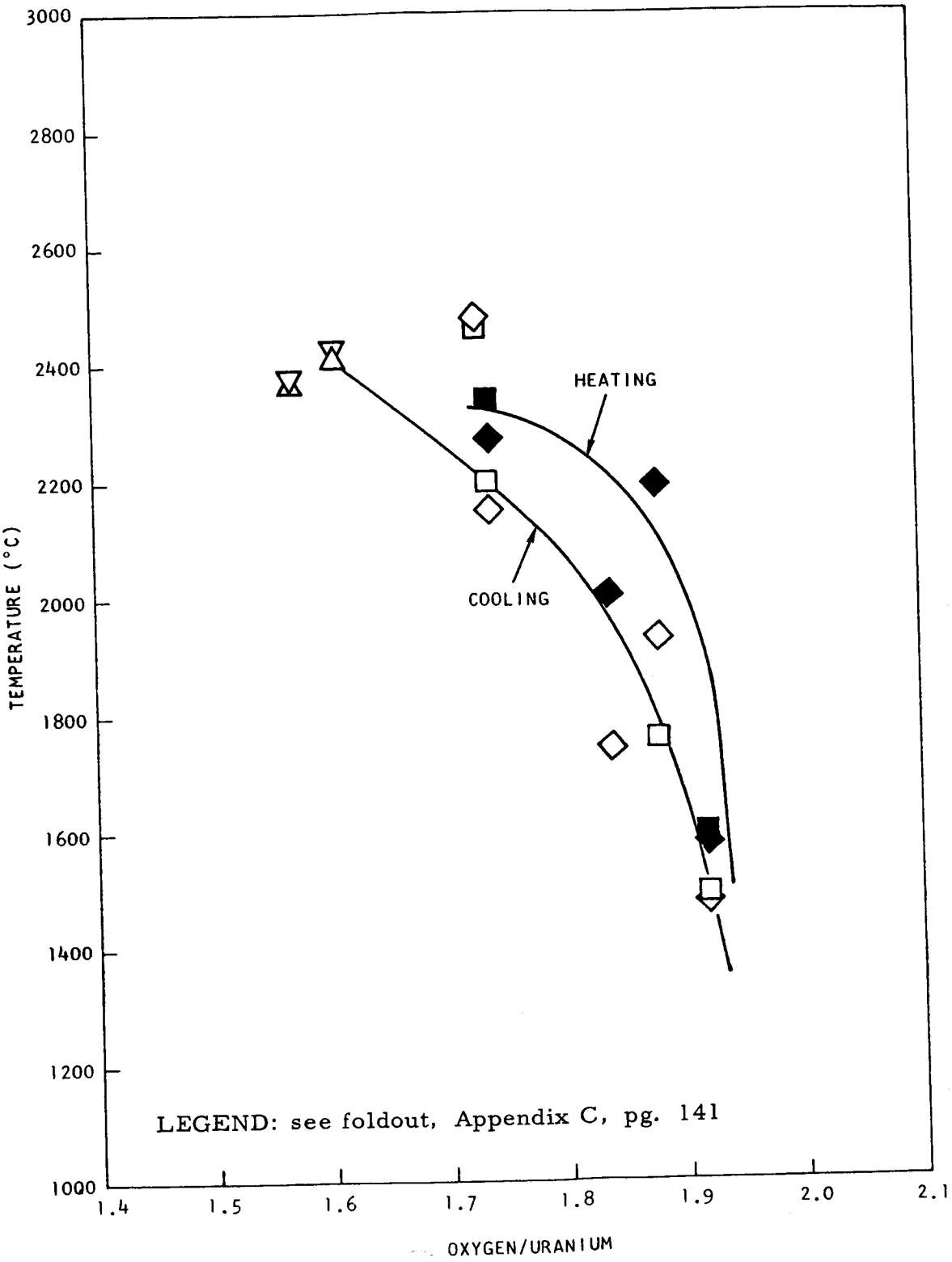

Fig. 23--Decomposition temperatures in the uranium-yttrium-oxygen system (2.5 mol-% yttria)

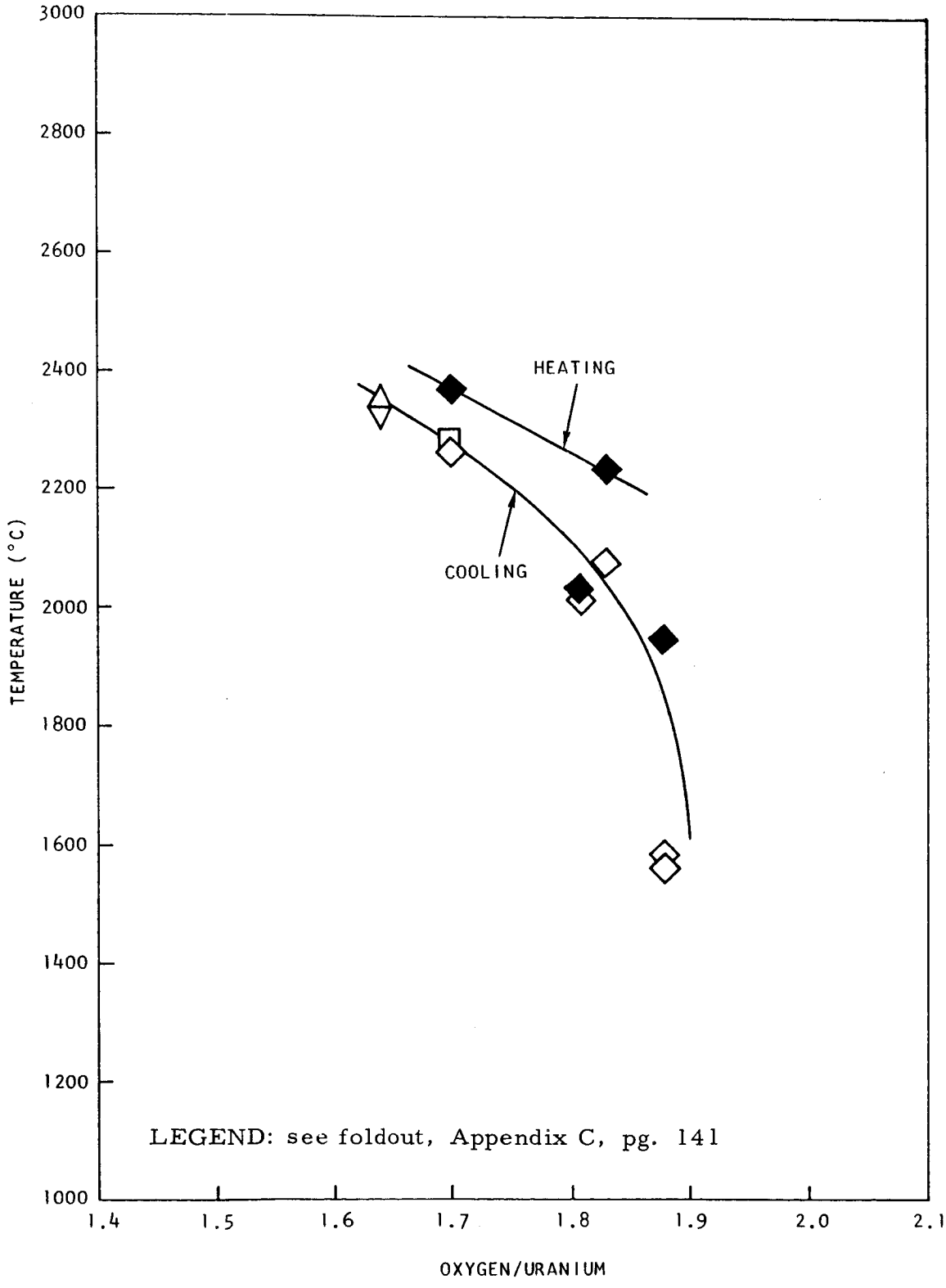

Fig. 24--Decomposition temperatures in the uranium-yttrium-oxygen system (5.0 mol-% yttria)

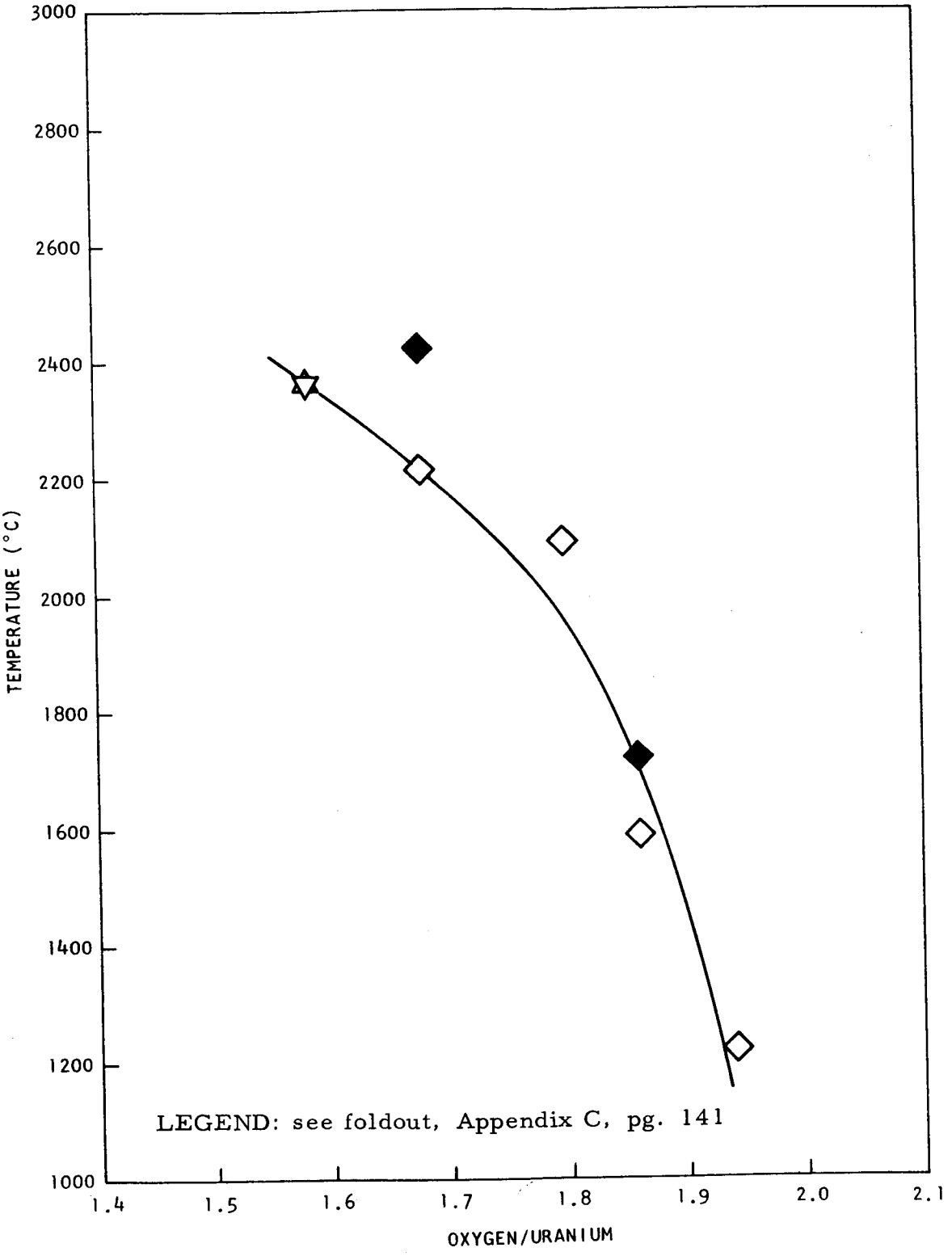

Fig. 25--Decomposition temperatures in the uranium-yttrium-oxygen system (10.0 mol-% yttria)

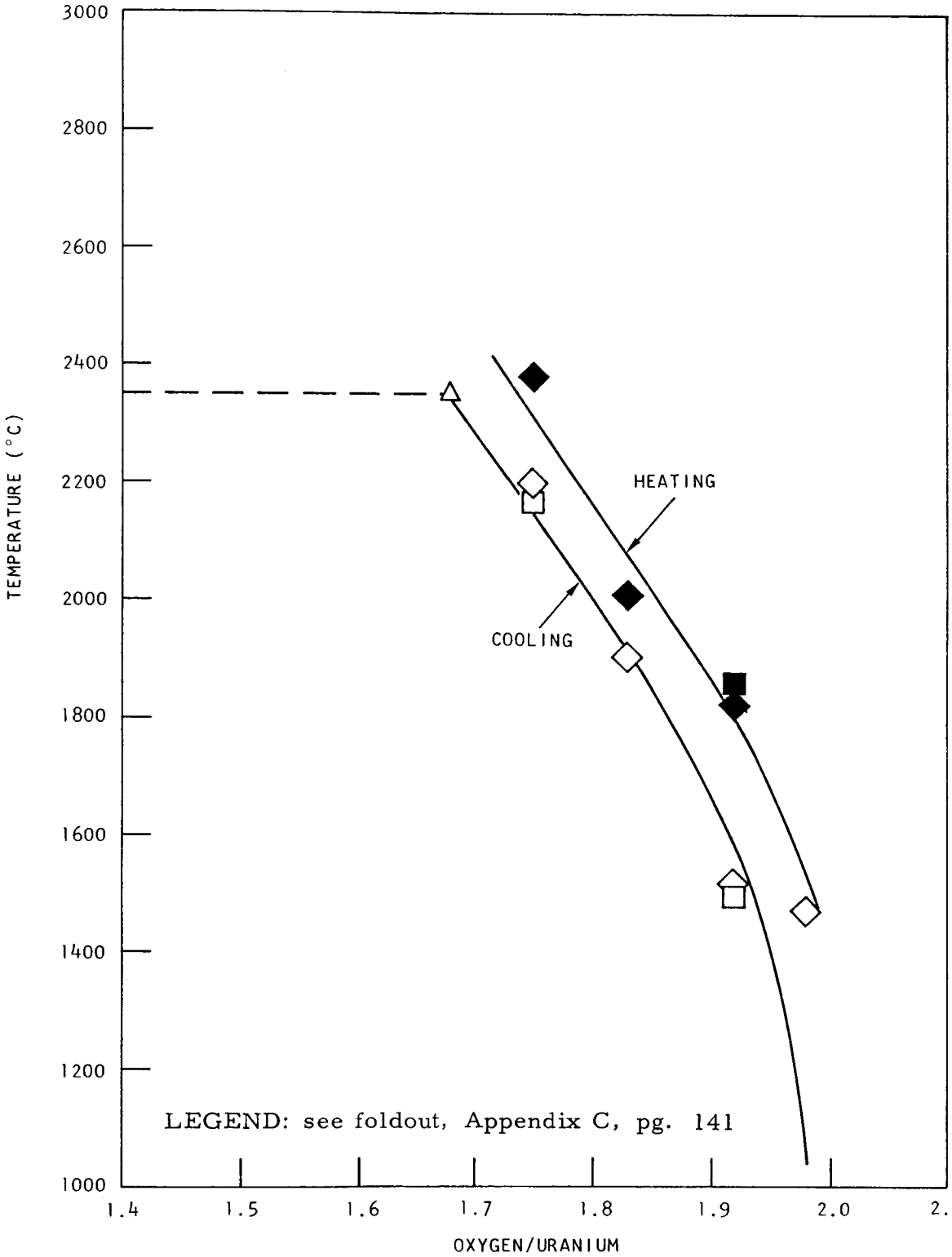

Fig. 26--Decomposition temperatures in the uranium-thorium-oxygen system (2.5 mol-% thoria)

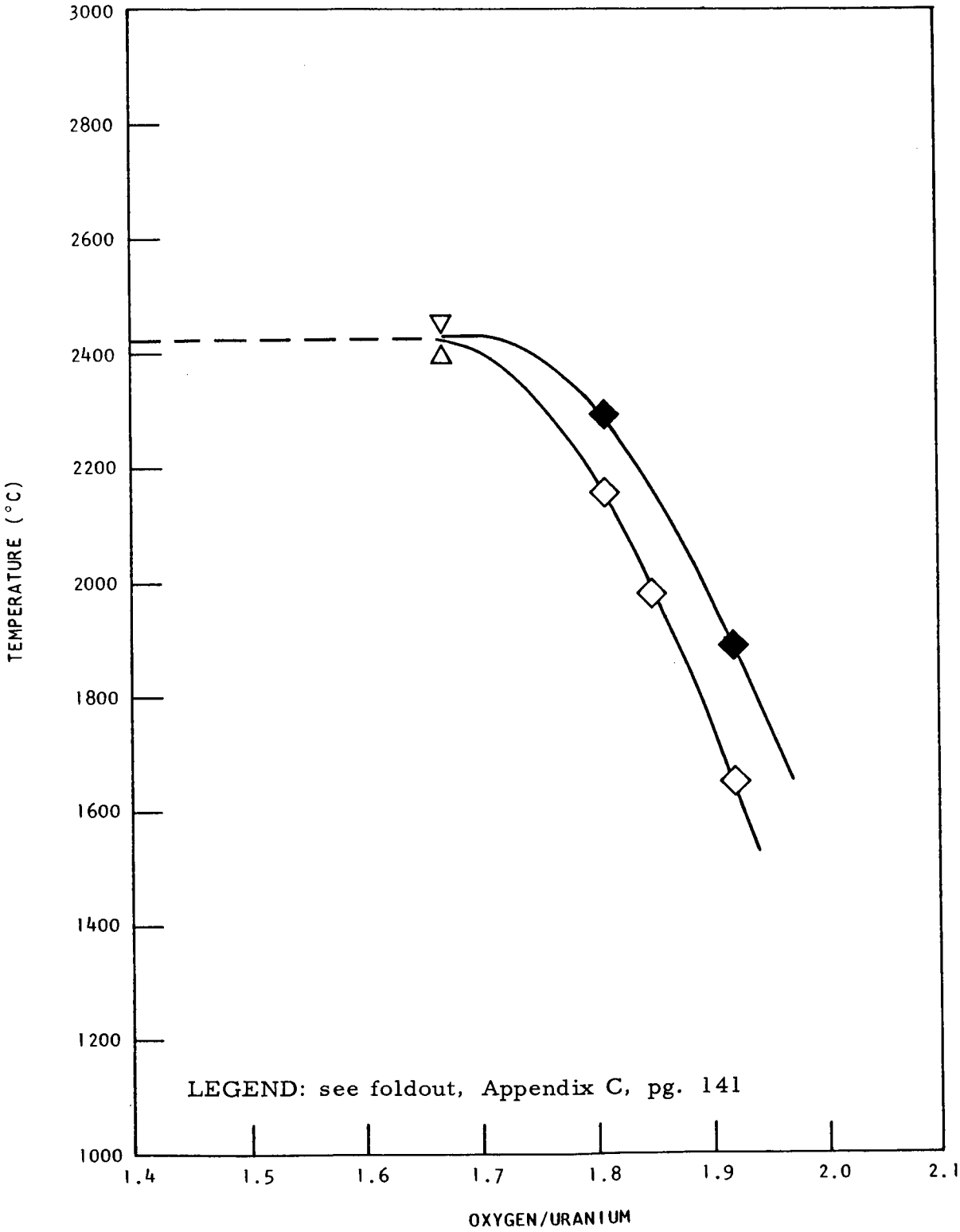

Fig. 27--Decomposition temperatures in the uranium-thorium-oxygen system (5.0 mol-% thoria)

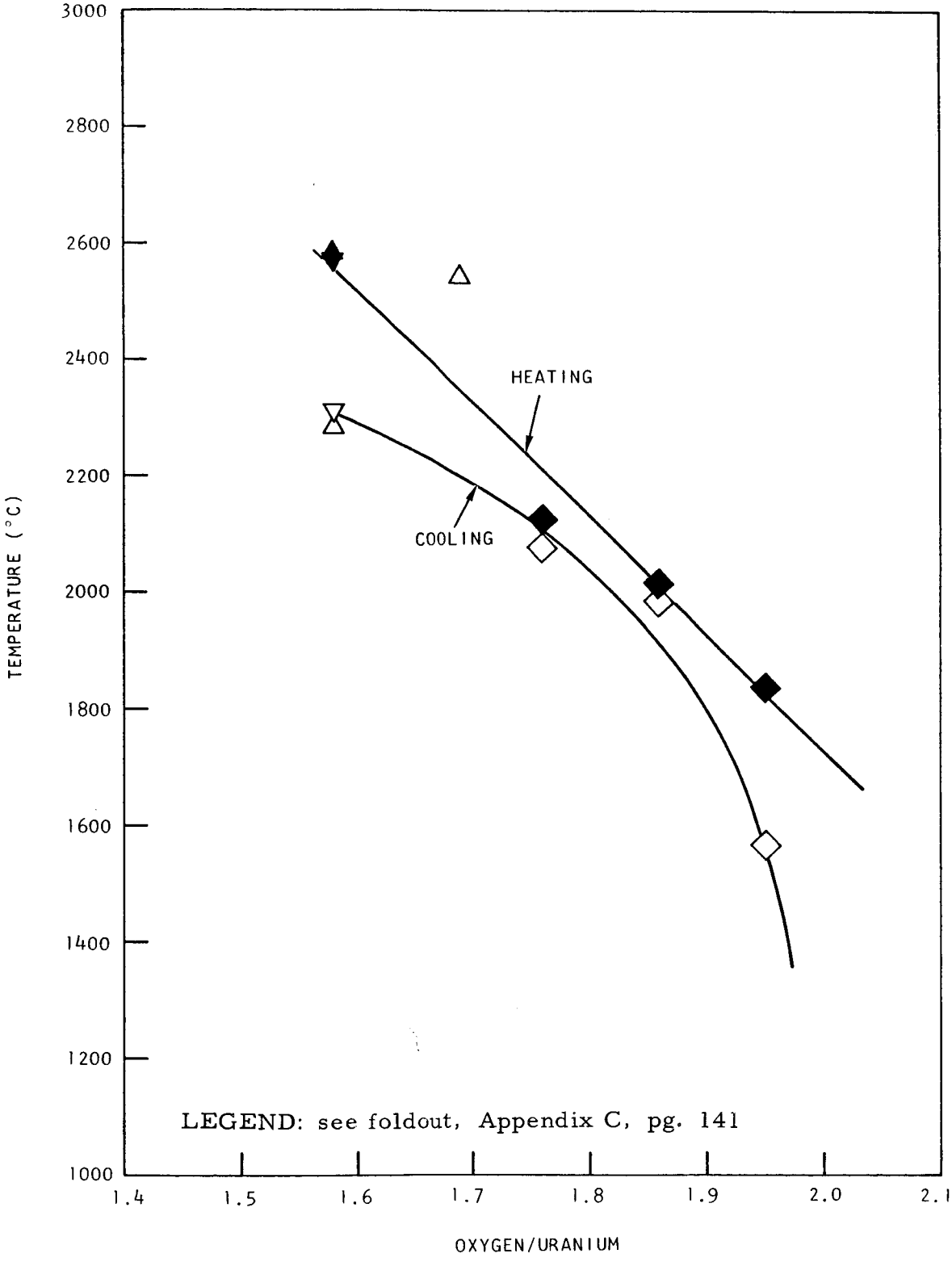

Fig. 28--Decomposition temperatures in the uranium-thorium-oxygen system (10.0 mol-% thoria)

ceria-stabilized series for the same compositions are shown in Figs. 29 through 31.

7.2.2. Liquidus and Solidus Temperatures

The sensitivity of the infrared detectors utilized for determining the thermal analysis curves to the emissivity changes accompanying phase transformations has made it possible to determine the liquidus temperatures of samples studied in this program. Although not originally considered a part of this program and of lesser precision, these data are presented in this section in the interests of obtaining a more complete phase diagram of substoichiometric UO_2. Solidus temperatures were also measured, when possible, and are included. As noted earlier, their precision is considerably lower than even that of the liquidus temperatures and in most cases the solidus has only been dashed in over a short region.

The liquidus and solidus (or monotectic) temperatures of the five series of samples are given in Tables 22 through 26. Where possible, these temperatures were measured on both the heating and cooling parts of the cycle and data are presented from both standard and derivative curves. In a number of cases, the liquidus temperatures could not be determined on cooling from the derivative curves. In a large number of cases the liquidus temperature could not be determined from either curve, on heating. Only in rare instances was it possible to determine the solidus temperature during the heating portion of the curve. Thus, the solidus temperatures are distorted relative to the liquidus temperatures by not being averaged with a point determined on the heating cycle. The results are therefore likely to be low. With this caution, the data have been included in the figures.*

The liquidus and solidus temperatures for the unstabilized U-UO_2 system are plotted in Figs. 32 and 33. The data in Fig. 32 were obtained from the standard curve while the data in Fig. 33 were obtained from the derivative curve. The agreement between the data on the liquidus temperatures in the two figures is quite good, considering the extreme temperatures involved.

The liquidus and solidus temperatures for the 13 stabilized samples are plotted in Figs. 34 through 46. The calcia-stabilized series, at 2.5, 5.0, 10.0, and 15.0 mol-% CaO are shown in Figs. 34 through 37. The

*The liquidus data which are plotted in the above figures are taken from columns 3, 4, 5, and 6 of Tables 22 through 26. These are the basic data obtained from measurement of both the standard and derivative thermal analysis curves on the heating and cooling cycles. The solidus data are taken from columns 10, 11, 12, and 13 of the same tables.

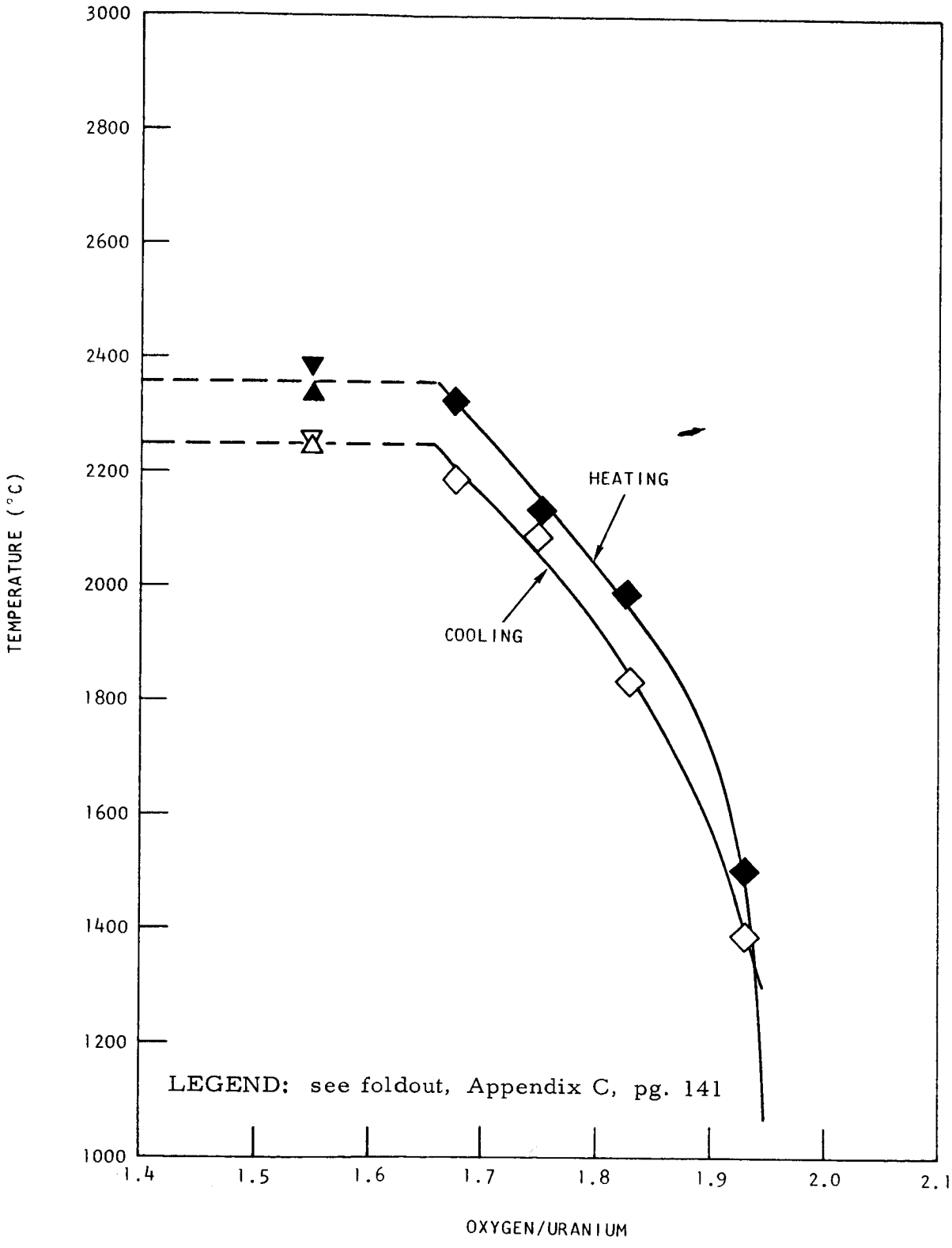

Fig. 29--Decomposition temperatures in the uranium-cerium-oxygen system (2.5 mol-% ceria)

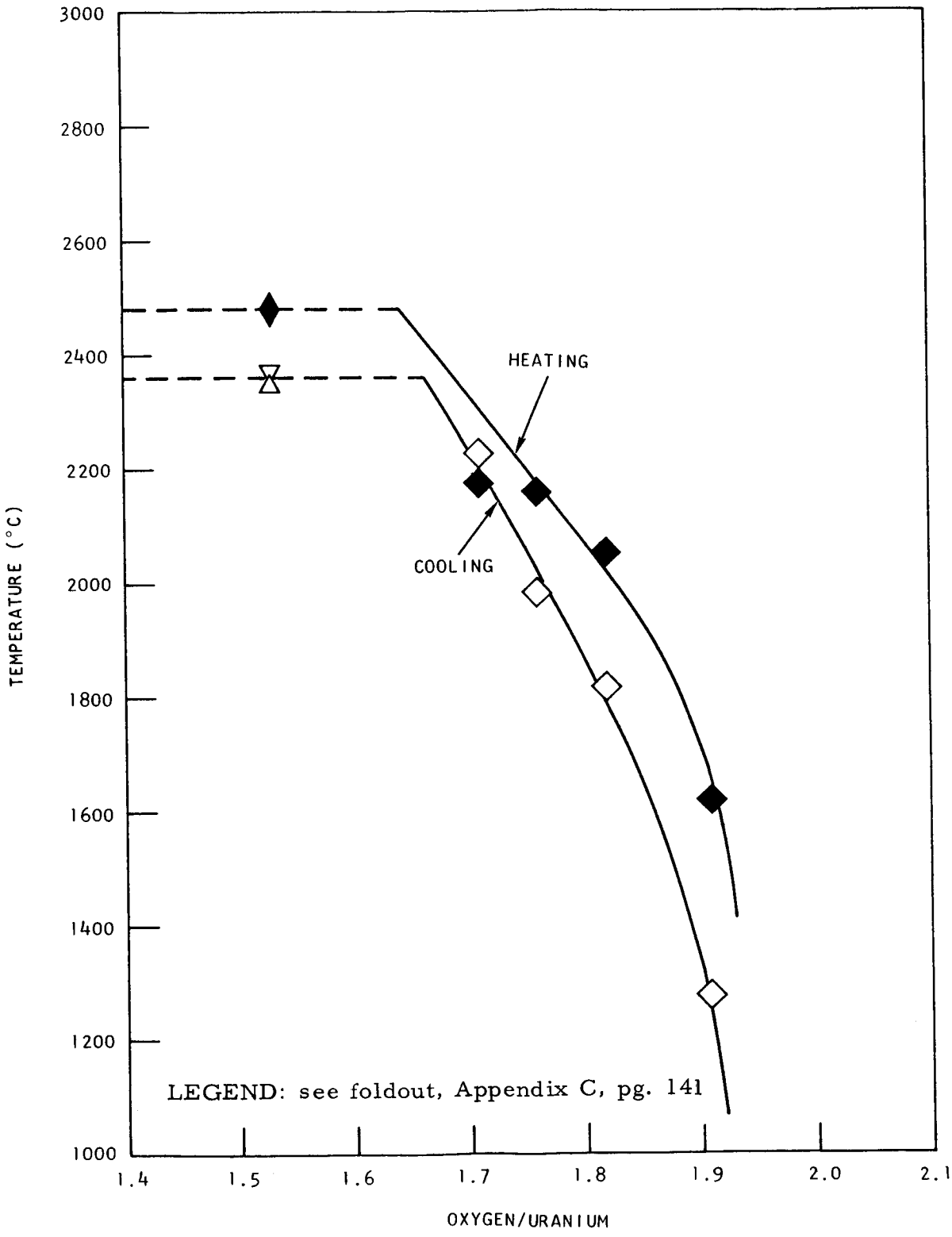

Fig. 30--Decomposition temperatures in the uranium-cerium-oxygen system (5.0 mol-% ceria)

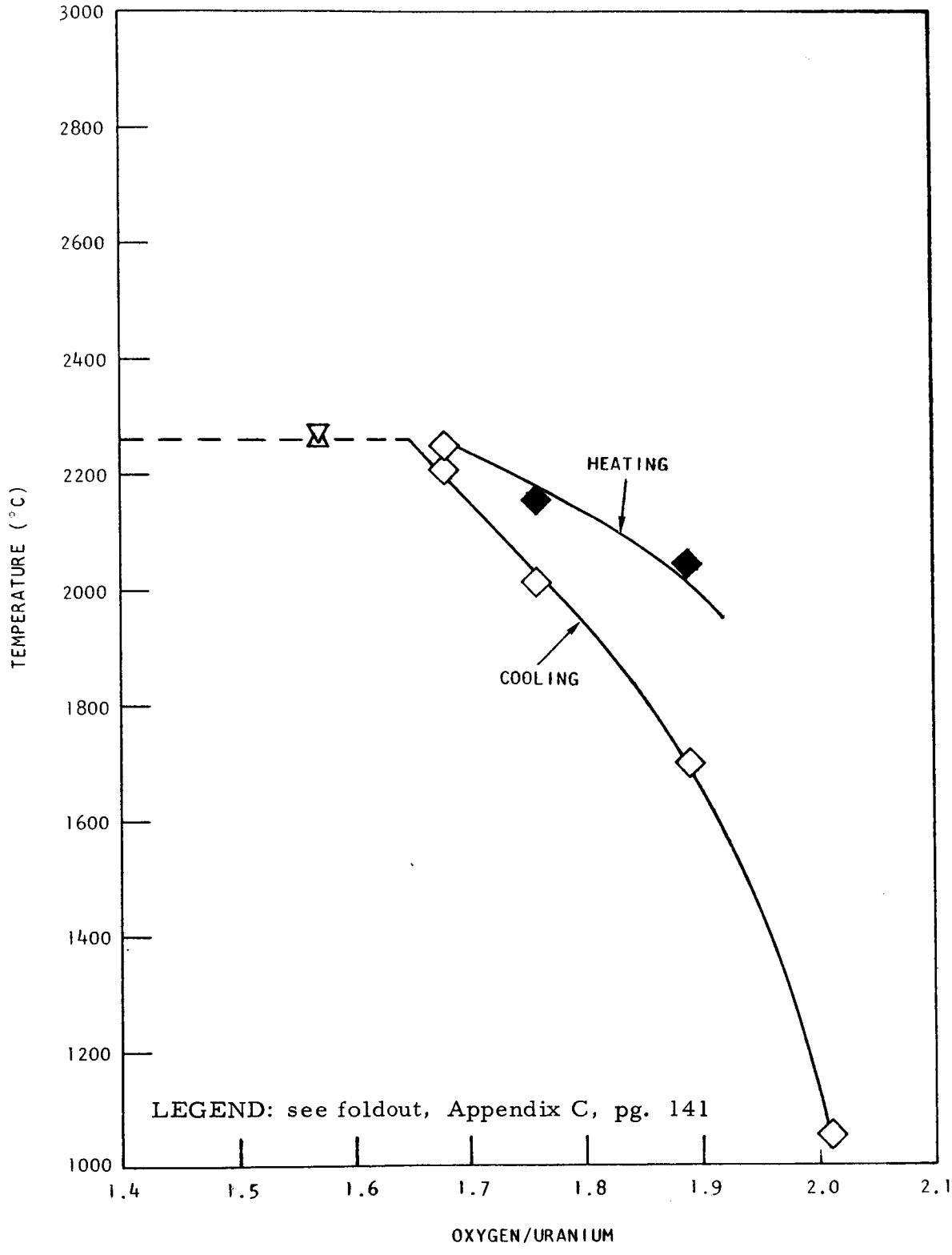

Fig. 31--Decomposition temperatures in the uranium-cerium-oxygen system (10.0 mol-% ceria)

Table 23

LIQUIDUS AND SOLIDUS TEMPERATURES IN THE URANIUM-CALCIUM-OXYGEN SYSTEM

Exp. No.	Final Composition CaO (mol-%)	Final Composition O/U Ratio	Liquidus Temperatures (°C) Standard Curve Heating	Liquidus Temperatures (°C) Standard Curve Cooling	Liquidus Temperatures (°C) Derivative Curve Heating	Liquidus Temperatures (°C) Derivative Curve Cooling	Liquidus Temperatures (°C) Avg. of Heating and Cooling Standard Curve	Liquidus Temperatures (°C) Avg. of Heating and Cooling Derivative Curve	Liquidus Temperatures (°C) Avg. of Standard and Derivative	Monotectic or Solidus Temperatures (°C) Standard Curve Heating	Monotectic or Solidus Temperatures (°C) Standard Curve Cooling	Monotectic or Solidus Temperatures (°C) Derivative Curve Heating	Monotectic or Solidus Temperatures (°C) Derivative Curve Cooling	Monotectic or Solidus Temperatures (°C) Avg. of Heating and Cooling Standard Curve	Monotectic or Solidus Temperatures (°C) Avg. of Heating and Cooling Derivative Curve	Monotectic or Solidus Temperatures (°C) Avg. of Standard and Derivative
2.0-1	1.30	1.61	2581	2500	2616	2536	2542	2576	2559		2348[a]		2350[a]	2348[b]	2350[b]	2349[b]
2.15-1	1.94	1.63	2726	2569	2736	2588	2648	2662	2655		2409[a]		2362[a]	2409[b]	2362[b]	2386[b]
2.1-1	1.30	1.66	2664	2602	2704	2642	2633	2673	2653							
2.17-1	2.60	1.67	2675	2657	2706	2692	2666	2699	2683		2469		2486	2469[b]	2486[b]	2478[b]
2.3-1	1.95	1.72	2708	2676	2721	2699	2692	2710	2701		2484		2478	2484[b]	2478[b]	2481[b]
2.5-1	1.97	1.75	2748	2723	2772	2745	2746[b]	2759[b]	2753		2555		2596	2555[b]	2596[b]	2576[b]
2.5-2	1.33	1.83		2608		2627	2608[b]	2627[b]	2618[b]		2426		2406	2426[b]	2406[b]	2416[b]
2.7-2	1.32	1.89	2713	2648	2720	2657	2681	2689	2685		2394		2421	2394[b]	2421[b]	2408[b]
2.7-1	1.99	1.90	2909	2773	2893	2807	2841	2850	2846		2605		2546	2605[b]	2546[b]	2576[b]
2.9-1	2.00	1.92	No Data - Excessive Volatilization													
2.11-1	1.99	1.95	No Data - Excessive Volatilization													
2.13-1	2.04	2.04	No Data - Excessive Volatilization													
2.14-1	3.51	1.63	2413	2309	2404	2339	2361	2372	2367		2285		2262	2285[b]	2262[b]	2274[b]
2.15-2	3.86	1.67	2555	2533	2561	2555	2544	2558	2551		2452		2419	2452[b]	2419[b]	2436[b]
2.19-1	3.23	1.74	2750	2685	2754	2708	2718	2731	2725		2486		2490	2486[b]	2490[b]	2488[b]
2.23-1	3.26	1.79	2850	2680	2850	2707	2745	2779	2762		2402		2387	2402[b]	2387[b]	2395[b]
2.21-1	3.25	1.81		2628	2782	2641	2628[b]	2711	2711[c]		2478		2478	2478[b]	2478[b]	2478[b]
2.21-2	3.91	1.91									2349		2332	2349[b]	2332[b]	2341[b]
2.25-1	3.89	1.99		2719		2729	2719[b]	2729[b]	2724[b]		2398		2385	2398[b]	2385[b]	2392[b]
2.27-1	3.38	2.03		2660		2623	2660[b]	2623[b]	2642[b]		2379		2369	2379[b]	2369[b]	2374[b]
2.28-1	7.98	1.66	2520	2447	2542	2463	2484	2503	2494		2408		2393	2408[b]	2393[b]	2401[b]
2.29-1	5.37	1.67	2630	2473	2608	2558	2552	2583	2568							
2.31-1	6.35	1.76	2732	2668	2737	2658	2700	2698	2699		2459		2439	2459[b]	2439[b]	2449[b]
2.33-1	6.98	1.84	2852	2725	2851	2735	2789	2793	2791		2515		2499	2515[b]	2499[b]	2507[b]
2.35-1	7.01	1.90		2770	2857	2801	2770[b]	2829[b]	2829[c]		2452		2440	2452[b]	2440[b]	2446[b]
2.39-1	7.42	1.96		2744		2816	2744[b]	2816[b]	2780[b]		2351		2275	2351[b]	2275[b]	2313[b]
2.37-1	7.09	1.97	2911	2766	2885	2795	2839	2840	2840		2319		2315	2319[b]	2315[b]	2317[b]
2.41-1	7.24	2.02		2681	2903	2690	2681[b]	2797	2797[c]				2341		2341[b]	2341[b, c]
2.43-1	9.22	1.74	2682	2626	2686	2652	2654	2648[b]	2662		2569		2546	2569[b]	2546[b]	2558[b]
2.45-1	10.15	1.80		2591		2594	2591[b]	2594[b]	2593[b]		2537		2537	2537[b]	2537[b]	2537[b]
2.47-1	11.35	1.84		2487		2498	2487[b]	2498[b]	2493[b]				2295		2295[b]	2295[b, c]
2.49-1	11.65	1.95	2762	2682	2749	2729	2722	2739	2731				2373		2373[b]	2373[b, c]
2.55-1	12.24	1.97		2684		2687	2684[b]	2687[b]	2686[b]							
2.53-1	12.05	1.98	2826	2826	2827	2807	2826	2817	2822		2429		2321	2429[b]	2321[b]	2375[b]
2.51-1	12.01	1.99	2825	2710	2812	2727	2768	2770	2769				2247		2247[b]	2247[b, c]

[a] Monotectic temperature.

[b] From cooling curve only. No heating curve data available.

[c] From derivative curve average only. No average standard curve data available.

Table 24

LIQUIDUS AND SOLIDUS TEMPERATURES IN THE URANIUM-YTTRIUM-OXYGEN SYSTEM

Exp. No.	Final Composition		Liquidus Temperatures (°C)							Monotectic or Solidus Temperatures (°C)						
			Standard Curve		Derivative Curve		Avg. of Heating and Cooling		Avg. of Standard and Derivative	Standard Curve		Derivative Curve		Avg. of Heating and Cooling		Avg. of Standard and Derivative
	Y_2O_3 (mol-%)	O/U Ratio	Heating	Cooling	Heating	Cooling	Standard Curve	Derivative Curve		Heating	Cooling	Heating	Cooling	Standard Curve	Derivative Curve	
3.1-1	2.09	1.61	2730	2621	2804	----	2676	2804[a]	2676[b]	----	2418[c]	----	2414[c]	2418[c,d]	2414[c,d]	2416[c,d]
3.3-1	2.61	1.73	2710	2674	----	2696	2692	2696[c]	2692[b]	----	2553	----	2597	2553[d]	2597[d]	2575[a]
3.5-1	2.62	1.74	----	2695	----	----	2695[c]	----	2695[b,c]	----	2427	----	2459	2427[d]	2459[d]	2443[d]
3.7-1	1.96	1.88	2831	2757	2845	2778	2794	2812	2803	----	2553	----	2534	2553[d]	2594[d]	2524[d]
3.9-1	2.62	1.92	2953	2787	----	----	2870	----	2870[b]	----	----	----	----	----	----	----
3.11-1	2.64	2.03	3007	2861	----	2870	2934	2870[c]	2934[b]	----	2518	----	2546	2518[d]	2546[d]	2532[d]
3.13-1	2.27	2.04	2992	2848	2996	2886	2920	2941	2931	----	2630	----	2510	2630[d]	2510[d]	2570[d]
3.15-2	4.89	1.64	2613	2631	2644	2652	2622	2648	2635	----	2335[c]	----	2346[c]	2335[c,d]	2346[c,d]	2341[c,d]
3.17-2	4.51	1.70	2758	2674	2791	2688	2716	2740	2728	----	2479	----	2412	2479[d]	2412[d]	2446[d]
3.19-2	4.59	1.83	2865	2789	2875	2787	2827	2831	2829	----	2503	----	2505	2503[d]	2505[d]	2504[d]
3.19-3	4.79	1.81	2796	2732	2812	2751	2764	2782	2773	----	2476	----	2457	2476[d]	2457[d]	2467[d]
3.21-2	4.59	1.88	2918	2803	2890	2812	2861	2851	2856	----	2491	----	2481	2491[d]	2481[d]	2486[d]
3.21-3	4.83	1.88	2832	2762	2843	2757	2797	2800	2799	----	2385	----	2385	2385[d]	2385[d]	2385[d]
3.23-2	4.58	1.93	3003	2871	3000	2885	2937	2943	2940	----	----	----	2447	----	2447[d]	2447[d,e]
3.25-1	4.89	2.02	2970	2808	2973	2809	2889	2891	2890	----	2524	----	2376	2524[d]	2376[d]	2450[d]
3.27-1	4.86	2.10	2985	2793	2983	2805	2889	2894	2892	----	----	----	2372	----	2372[d]	2372[d,e]
3.29-2	8.79	1.58	2671	2565	2692	2577	2618	2635	2627	----	----	----	----	----	----	----
3.31-2	8.81	1.68	2761	2645	2761	2681	2703	2721	2712	----	2423	----	2409	2423[d]	2409[d]	2416[d]
3.33-2	8.78	1.80	2836	2724	2849	2735	2780	2792	2786	----	2468	----	2445	2468[d]	2445[d]	2457[d]
3.35-2	8.78	1.86	2756	2726	2754	2732	2741	2743	2742	----	----	----	2270	----	2270[d]	2270[d,e]
3.37-2	8.82	1.94	2954	2819	2948	2811	2887	2880	2884	----	----	----	2422	----	2422[d]	2422[d,e]
3.39-1	8.58	2.08	3122	2842	3086	2845	2982	2966	2974	----	2511	----	2450	2511[d]	2450[d]	2481[d]
3.41-1	9.06	2.14	3011	2768	2993	2754	2890	2874	2882	----	----	----	2333	----	2333[d]	2333[d,e]

[a] From heating curve only. No cooling curve data available.
[b] From standard curve average only. No average derivative curve data available.
[c] Monotectic temperature.
[d] From cooling curve only. No heating curve data available.
[e] From derivative curve average only. No average standard curve data available.

Table 25

LIQUIDUS AND SOLIDUS TEMPERATURES IN URANIUM-THORIUM-OXYGEN SYSTEM

Exp. No.	Final Composition		Liquidus Temperatures (°C)							Monotectic or Solidus Temperatures (°C)						
			Standard Curve		Derivative Curve		Heating/Cooling (Avg.)		Standard/ Derivative (Avg.)	Standard Curve		Derivative Curve		Heating/Cooling (Avg.)		Standard/ Derivative (Avg.)
	ThO_2 (mol-%)	O/U Ratio	Heating	Cooling	Heating	Cooling	Standard Curve	Derivative Curve		Heating	Cooling	Heating	Cooling	Standard Curve	Derivative Curve	
4.3-1	2.50	1.68	2749	2640	2736	2663	2695	2700	2698		2351[c]		2348[c]	2351[a, c]	2348[a, c]	2350[a, c]
4.5-1	2.50	1.75	2734	2704	2753	2720	2719	2737	2728		2468		2479	2468[a]	2479[a]	2474[a]
4.7-1	2.38	1.83	2809	2665	2810	2691	2737	2750	2744		2490		2459	2490[a]	2459[a]	2475[a]
4.9-1	2.28	1.92		2814	2977	2811	2814[a]	2894	2894[b]				2518		2518[a]	2518[a, b]
4.11-1	2.41	1.98		2841	2939	2834	2841[a]	2887	2887[b]		2392		2402	2392[a]	2402[a]	2397[a]
4.17-1	5.02	1.67	2699	2656	2720	2659	2678	2690	2684		2456[c]		2395[c]	2456[a, c]	2395[a, c]	2425[a, c]
4.19-1	4.90	1.81	2795	2721	2791	2736	2758	2764	2761				2457		2457[a]	2457[a, b]
4.21-1	4.92	1.85	2938	2878	2937	2902	2908	2920	2914		2564		2528	2564[a]	2528[a]	2546[a]
4.23-1	4.85	1.92	2870	2760	2888	2765	2815	2827	2821		2393		2461	2393[a]	2461[a]	2427[a]
4.25-1	4.88	1.95		2751		2741	2751[a]	2741[a]	2746[a]				2354		2354[a]	2354[a, b]
4.29-1	9.91	1.58								2570	2303	2585	2281	2437	2433	2435
4.31-1	10.00	1.69	2810	2698	2817	2720	2754	2770	2762		2551[c]		2540[c]	2551[a, c]	2540[a, c]	2546[a, c]
4.33-1	9.89	1.76	2923	2789	2946	2790	2856	2868	2862		2549		2568	2549[a]	2568[a]	2558[a]
4.35-1	9.83	1.86	2952	2828	2910	2842	2890	2876	2883		2477		2481	2477[a]	2481[a]	2479[a]
4.37-1	9.98	1.90	2976	2940	2974	2940	2958	2957	2958				2454		2454[a]	2454[a, b]
4.39-1	9.56	1.96	2879	2847	2884	2833	2863	2859	2861				2498		2498[a]	2498[a, b]

[a] From cooling curve only. No heating curve data available.
[b] From derivative curve only. No average standard curve data available.
[c] Monotectic temperature.

Table 26

LIQUIDUS AND SOLIDUS TEMPERATURES IN THE URANIUM-CERIUM-OXYGEN SYSTEM

Exp. No.	Final Composition		Liquidus Temperatures (°C)							Monotectic or Solidus Temperatures (°C)						
			Standard Curve		Derivative Curve		Heating/Cooling (Avg.)		Standard/ Derivative (Avg.)	Standard Curve		Derivative Curve		Heating/Cooling (Avg.)		Standard/ Derivative (Avg.)
	CeO_2 (mol-%)	O/U Ratio	Heating	Cooling	Heating	Cooling	Standard Curve	Derivative Curve		Heating	Cooling	Heating	Cooling	Standard Curve	Derivative Curve	
5.1-1	2.44	1.55	2493	2518	2508	2488	2505	2498	2502	2390[a]	2255[a]	2323[a]	2237[a]	2322[a]	2280[a]	2301[a]
5.3-1	2.64	1.68	2629	2576	2635	2565	2603	2600	2602	----	2383	----	2388	2383[b]	2388[b]	2386[b]
5.5-1	2.42	1.75	2828	2703	2831	2715	2768	2773	2771	----	2469	----	2464	2469[b]	2464[b]	2467[b]
5.7-1	2.44	1.83	2823	2738	2821	2743	2781	2782	2782	----	2497	----	2523	2497[b]	2523[b]	2510[b]
5.11-1	2.31	1.92	2927	2850	2939	2843	2889	2891	2890	----	2345	----	2355	2345[b]	2355[b]	2350[b]
5.9-1	2.40	1.93	2843	2751	2842	2741	2797	2792	2795	----	2300	----	2371	2300[b]	2371[b]	2336[b]
5.15-1	5.06	1.53	2634	2548	2650	2552	2591	2601	2596	2469[a]	2368[a]	2489[a]	2345[a]	2439[a]	2417[a]	2428[a]
5.17.1	4.65	1.71	2774	2656	2801	2654	2715	2728	2722	----	2431	2644	2441	2431[b]	2543	2543[c]
5.19-1	5.13	1.76	2722	2714	2726	2744	2718	2735	2727	----	2491	----	2499	2491[b]	2499[b]	2495[b]
5.21-1	5.07	1.82	2922	2766	2924	2772	2844	2848	2846	----	2458	----	2491	2458[b]	2491[b]	2475[b]
5.25-1	4.89	1.89	2982	2819	3002	2817	2901	2910	2906	----	----	----	2415	----	2415[b]	2415[b, c]
5.23-1	5.13	1.91	2959	2801	2954	2805	2880	2880	2880	----	2369	----	2427	2369[b]	2427[b]	2398[b]
5.29-1	9.77	1.56	2561	2518	2577	2518	2540	2548	2544	----	2268[a]	----	2256[a]	2268[a, b]	2256[a, b]	2262[a, b]
5.31-1	9.93	1.68	----	2719	2867	2720	2719[a]	2794	2794[b]	----	2463	----	2500	2463[b]	2500[b]	2482[b]
5.33-1	10.14	1.76	2822	2726	2856	2742	2774	2799	2787	----	2485	----	2501	2485[b]	2501[b]	2493[b]
5.35-1	9.86	1.89	2894	2793	2902	2820	2844	2861	2853	----	2410	----	2447	2410[b]	2447[b]	2429[b]
5.39-1	9.95	1.94	2945	2819	2946	2843	2882	2895	2889	----	2440	----	2434	2440[b]	2434[b]	2437[b]
5.37-1	9.95	2.01	2933	2775	2928	2796	2854	2862	2858	----	2436	----	2444	2436[b]	2444[b]	2440[b]

[a] Monotectic temperature.
[b] From cooling curve only. No heating curve data available.
[c] From derivative curve only. No average standard curve data available.

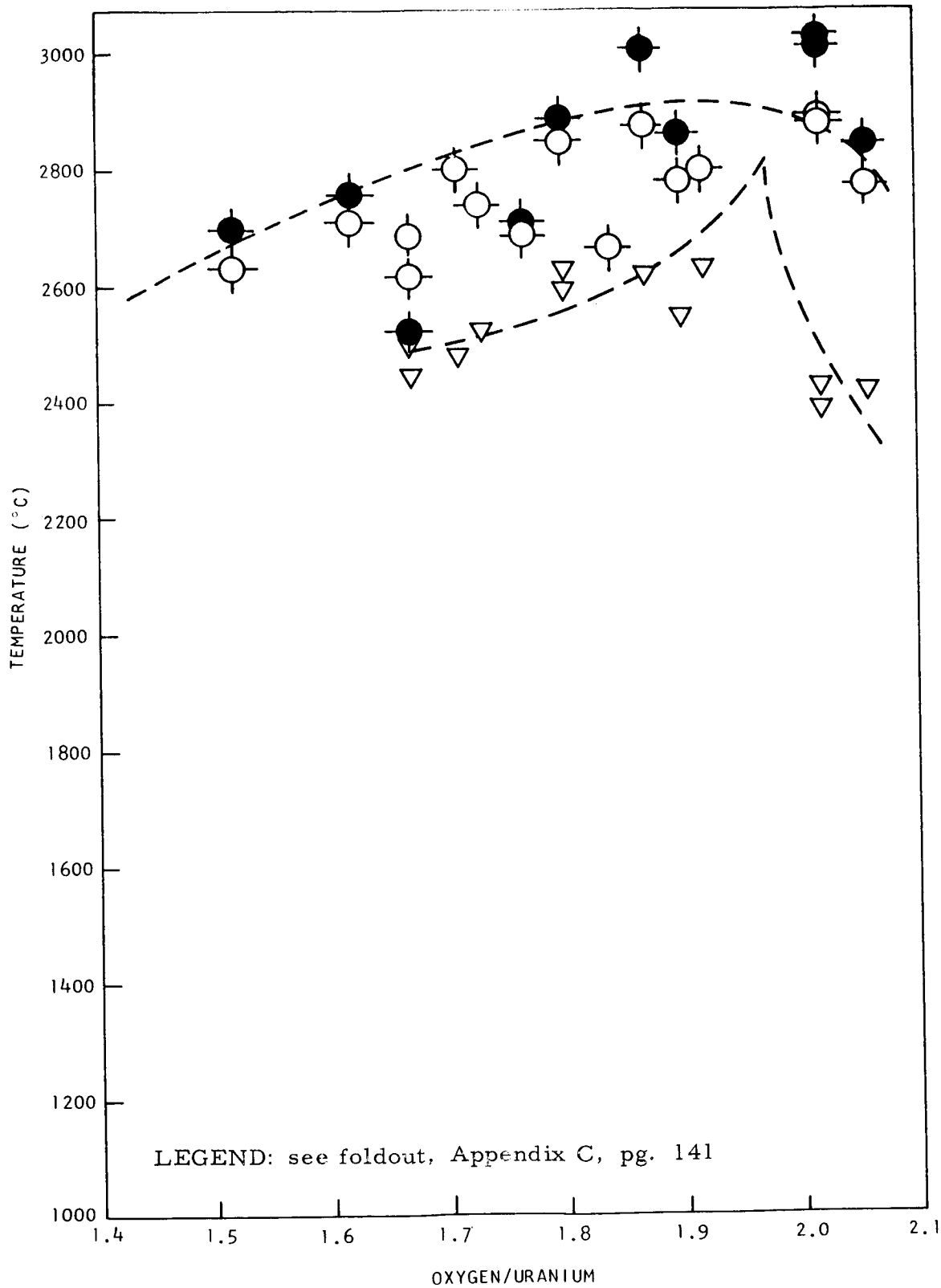

Fig. 32--Liquidus and solidus temperatures in the unstabilized U-O system (standard curve)

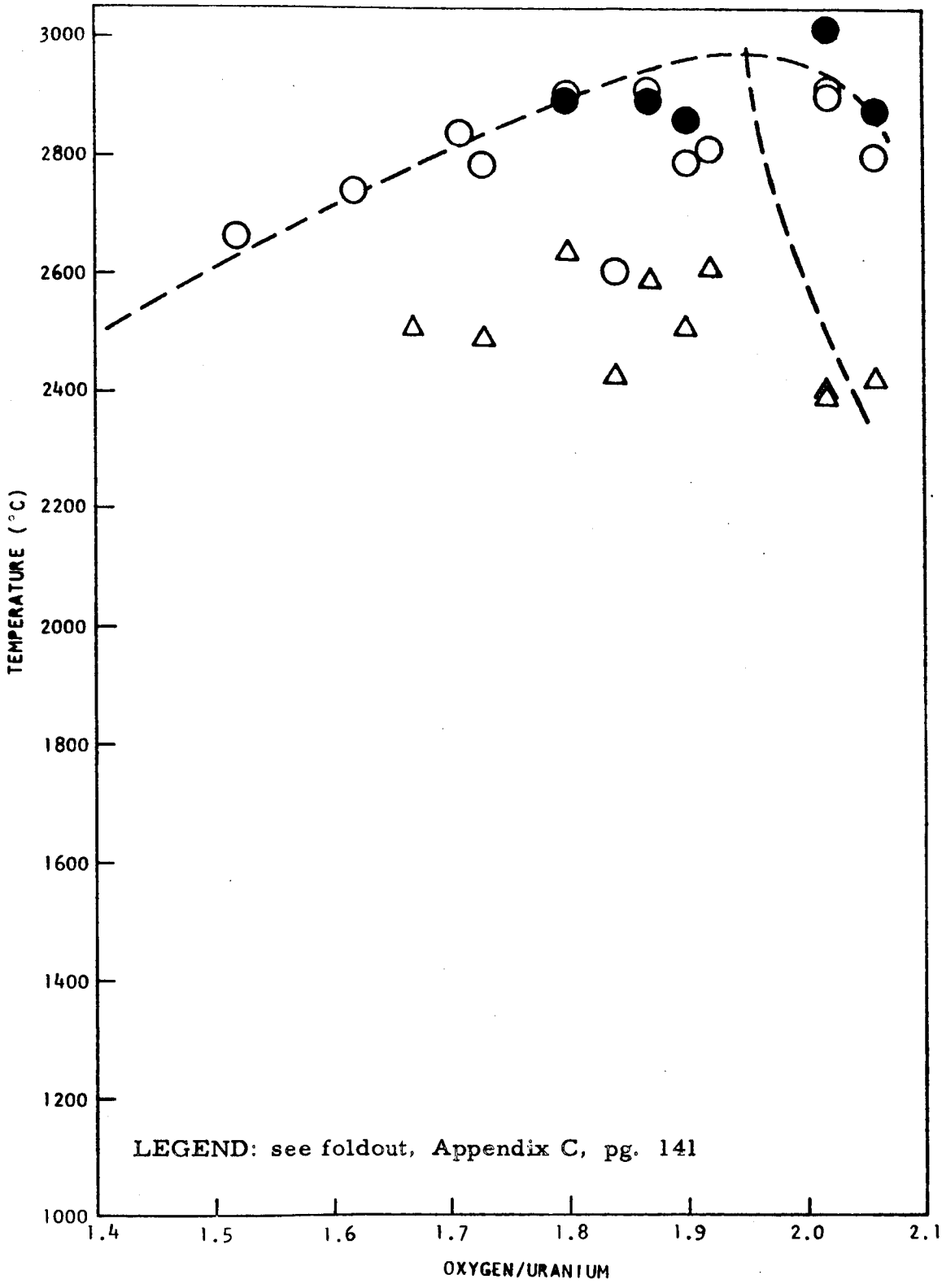

Fig. 33--Liquidus and solidus temperatures in the unstabilized U-O system (derivative curve)

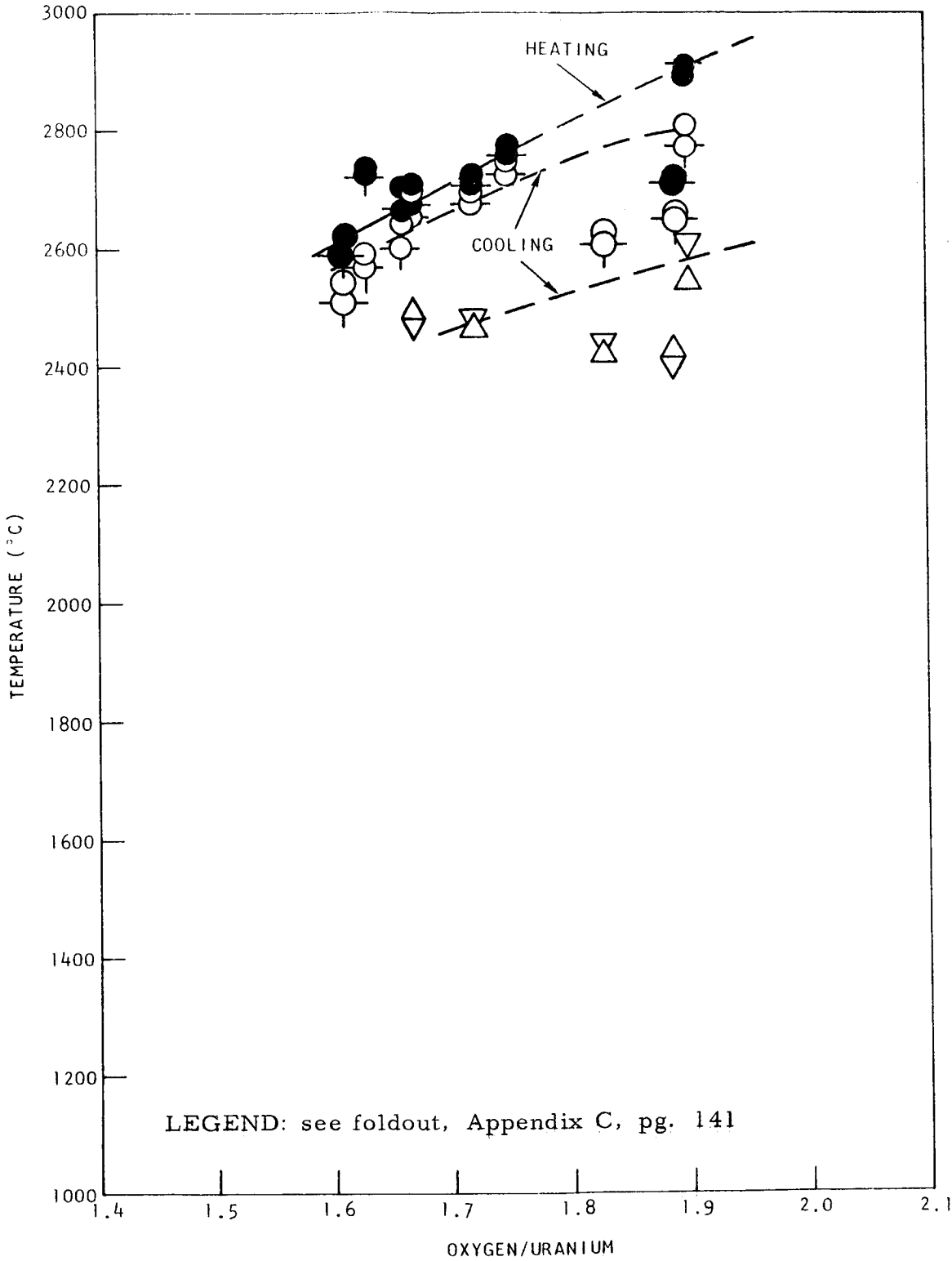

Fig. 34--Liquidus and solidus temperatures in the uranium-calcium-oxygen system (2.5 mol-% calcia)

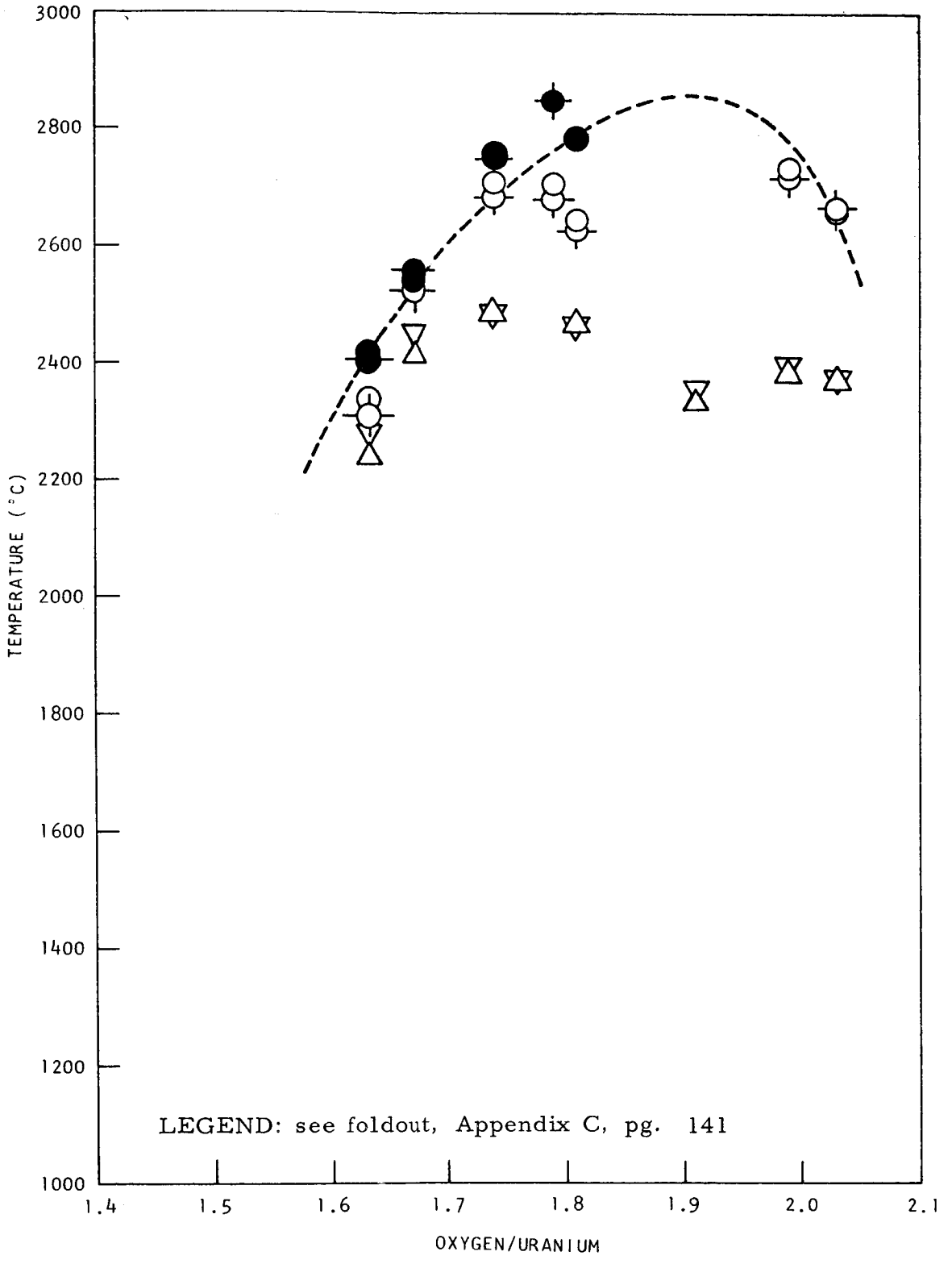

Fig. 35--Liquidus and solidus temperatures in the uranium-calcium-oxygen system (5.0 mol-% calcia)

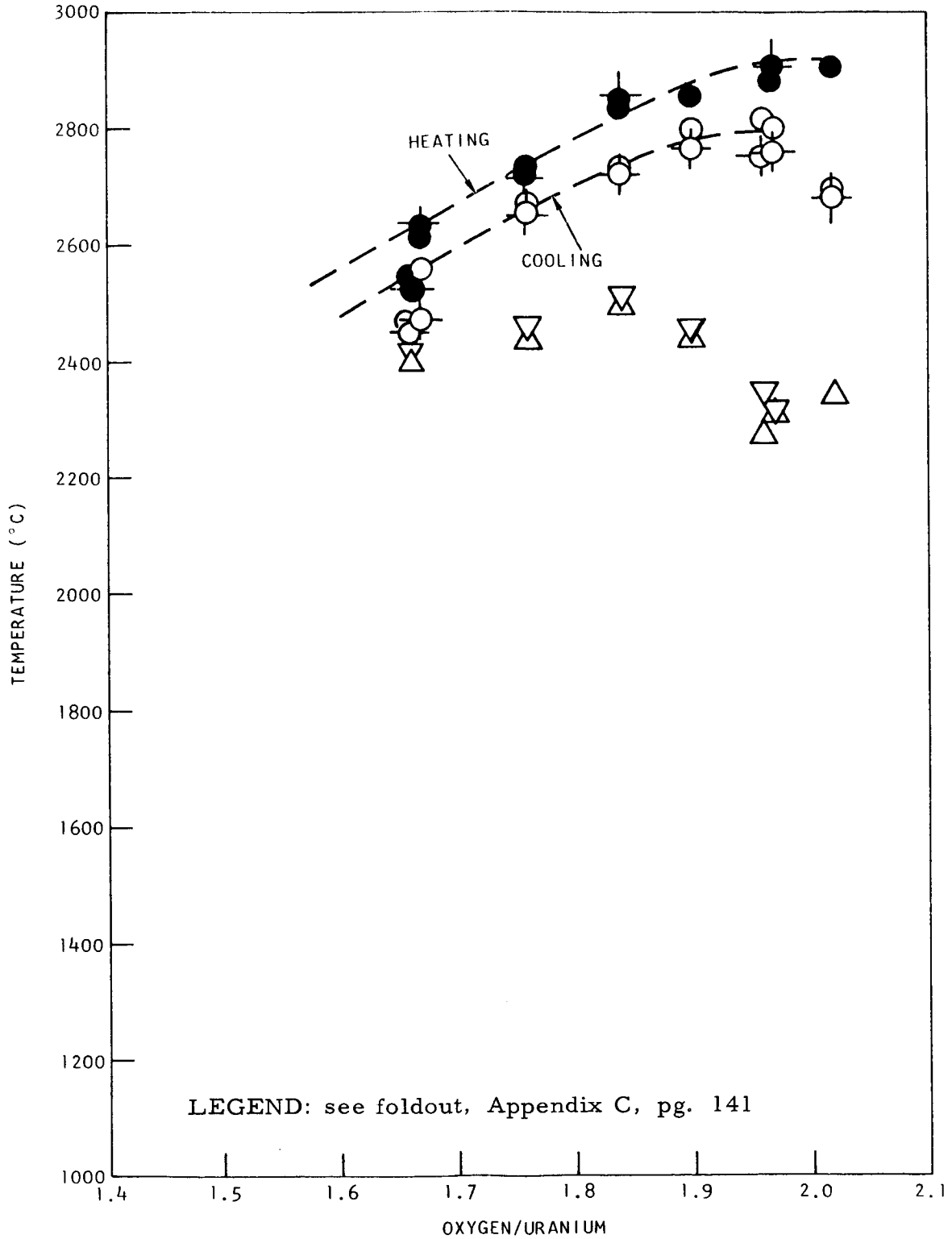

Fig. 36--Liquidus and solidus temperatures in the uranium-calcium-oxygen system (10.0 mol-% calcia)

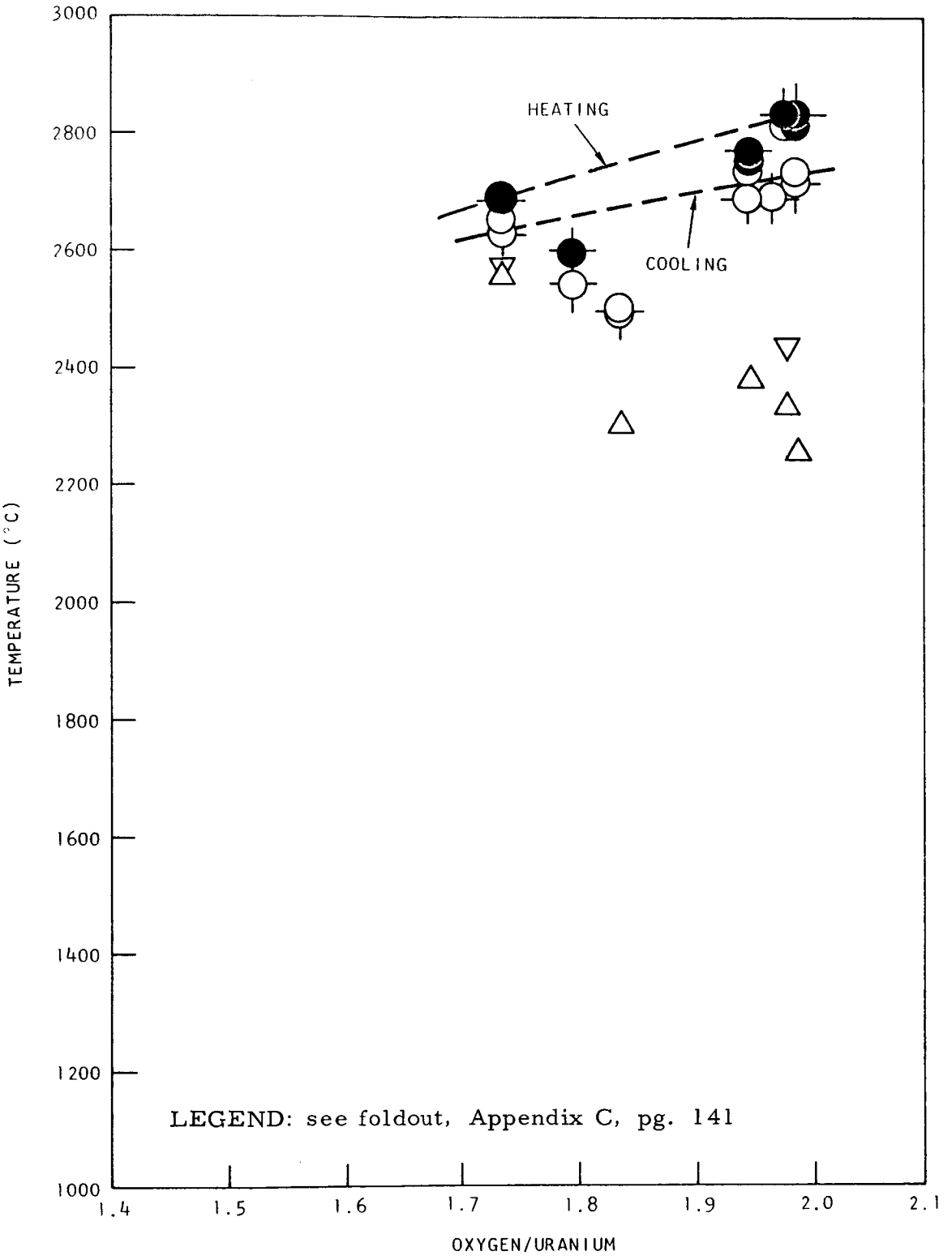

Fig. 37--Liquidus and solidus temperatures in the uranium-calcium-oxygen system (15.0 mol-% calcia)

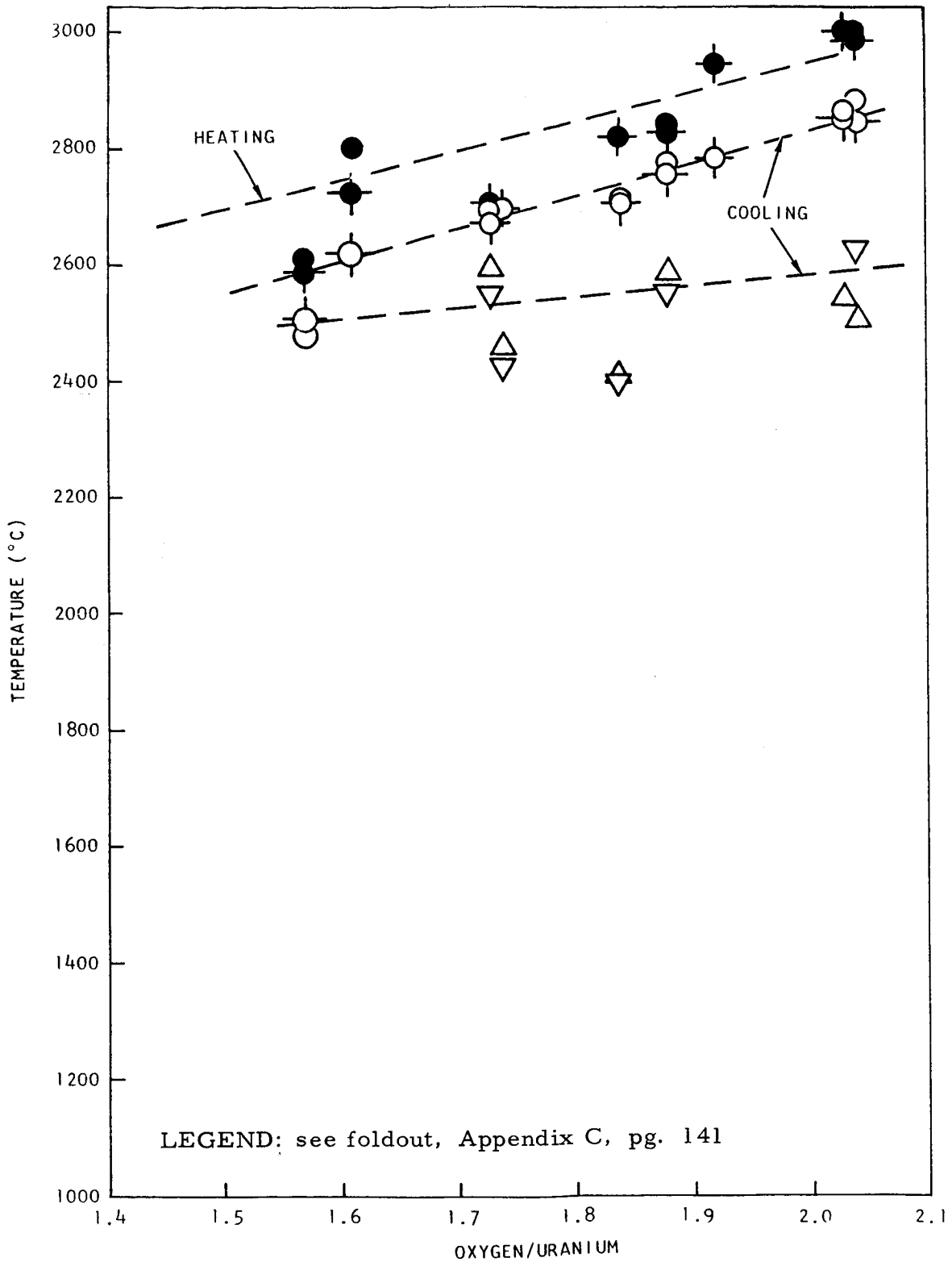

Fig. 38--Liquidus and solidus temperatures in the uranium-yttrium-oxygen system (2.5 mol-% yttria)

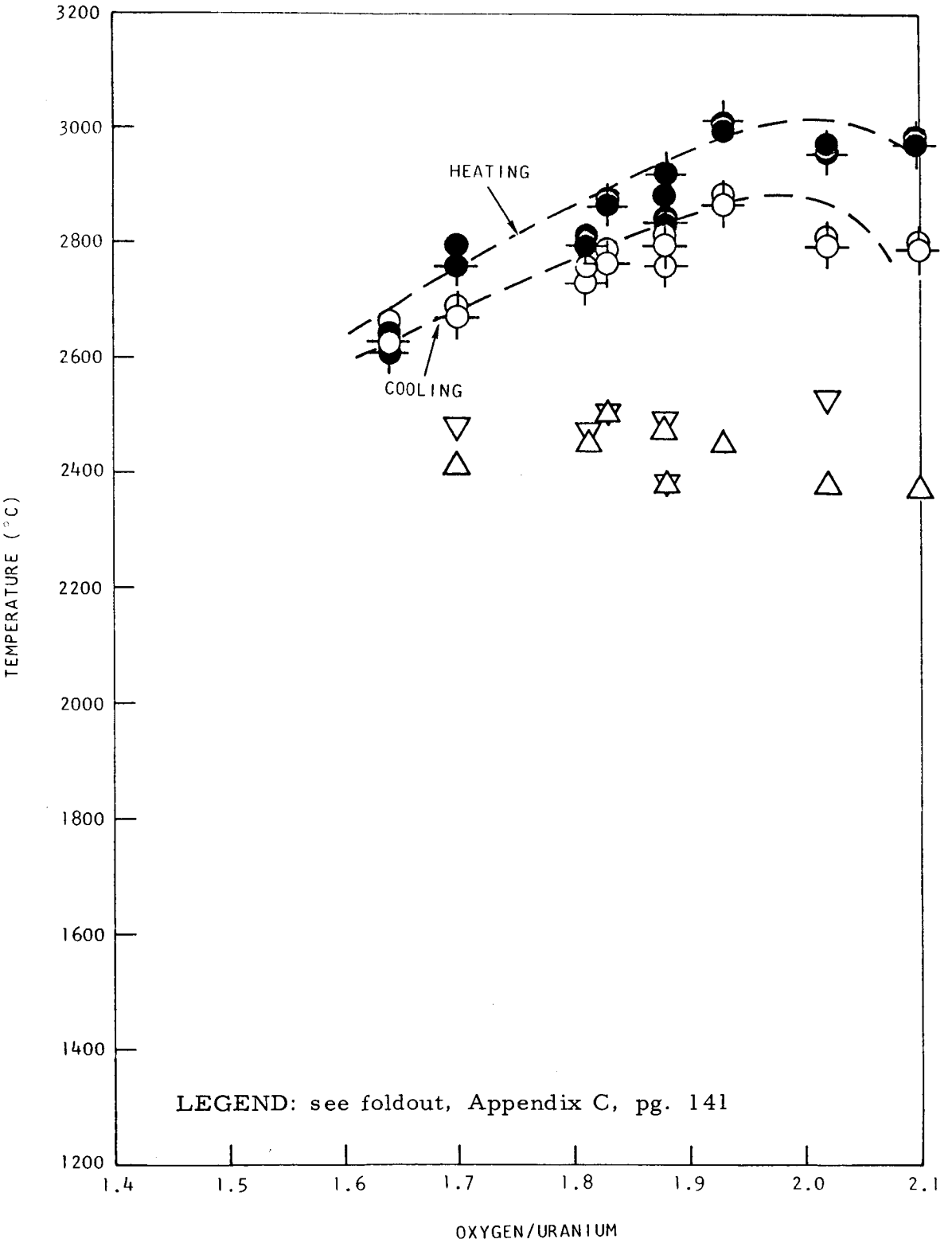

Fig. 39--Liquidus and solidus temperatures in the uranium-yttrium-oxygen system (5.0 mol-% yttria)

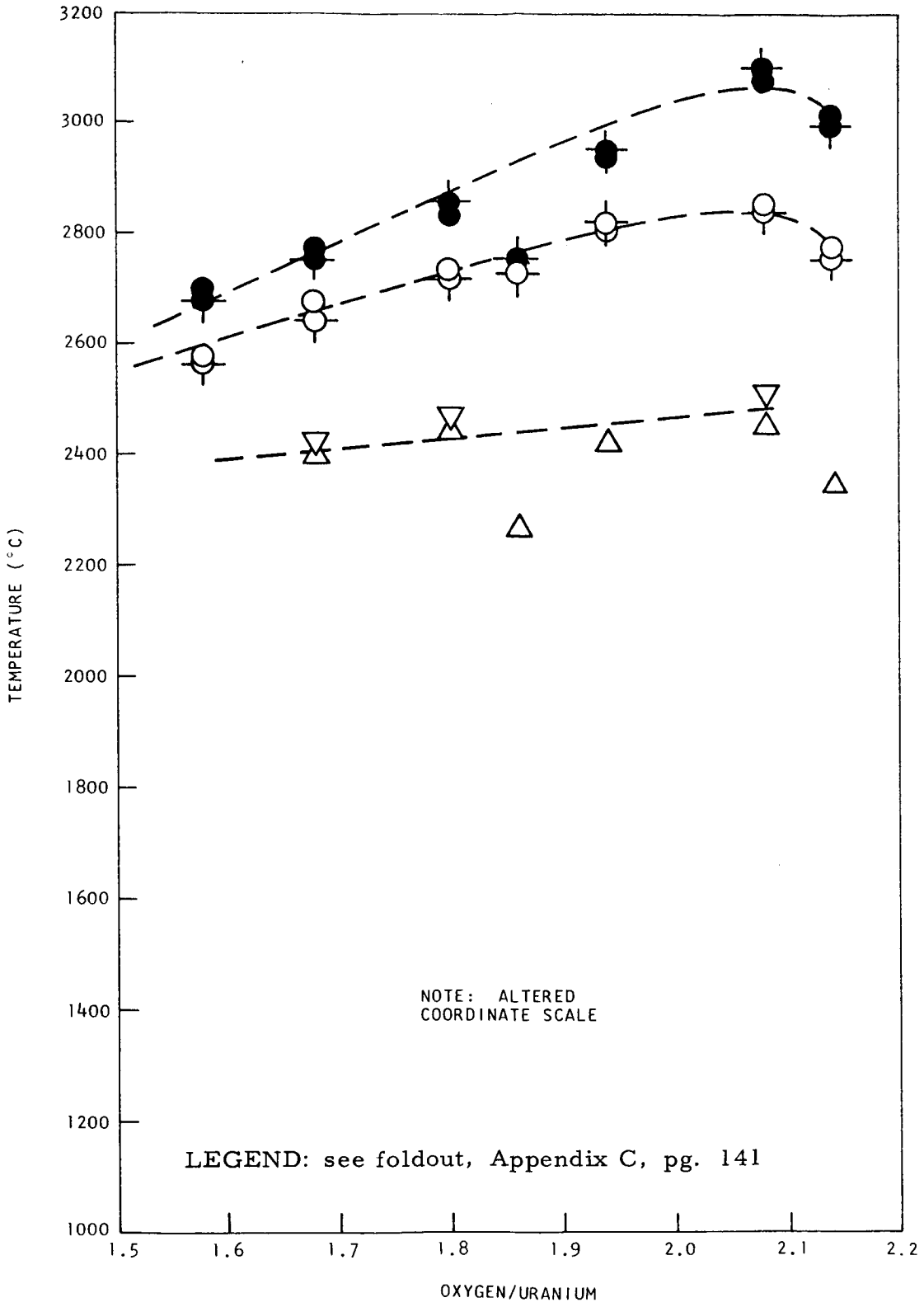

Fig. 40--Liquidus and solidus temperatures in the uranium-yttrium-oxygen system (10.0 mol-% yttria)

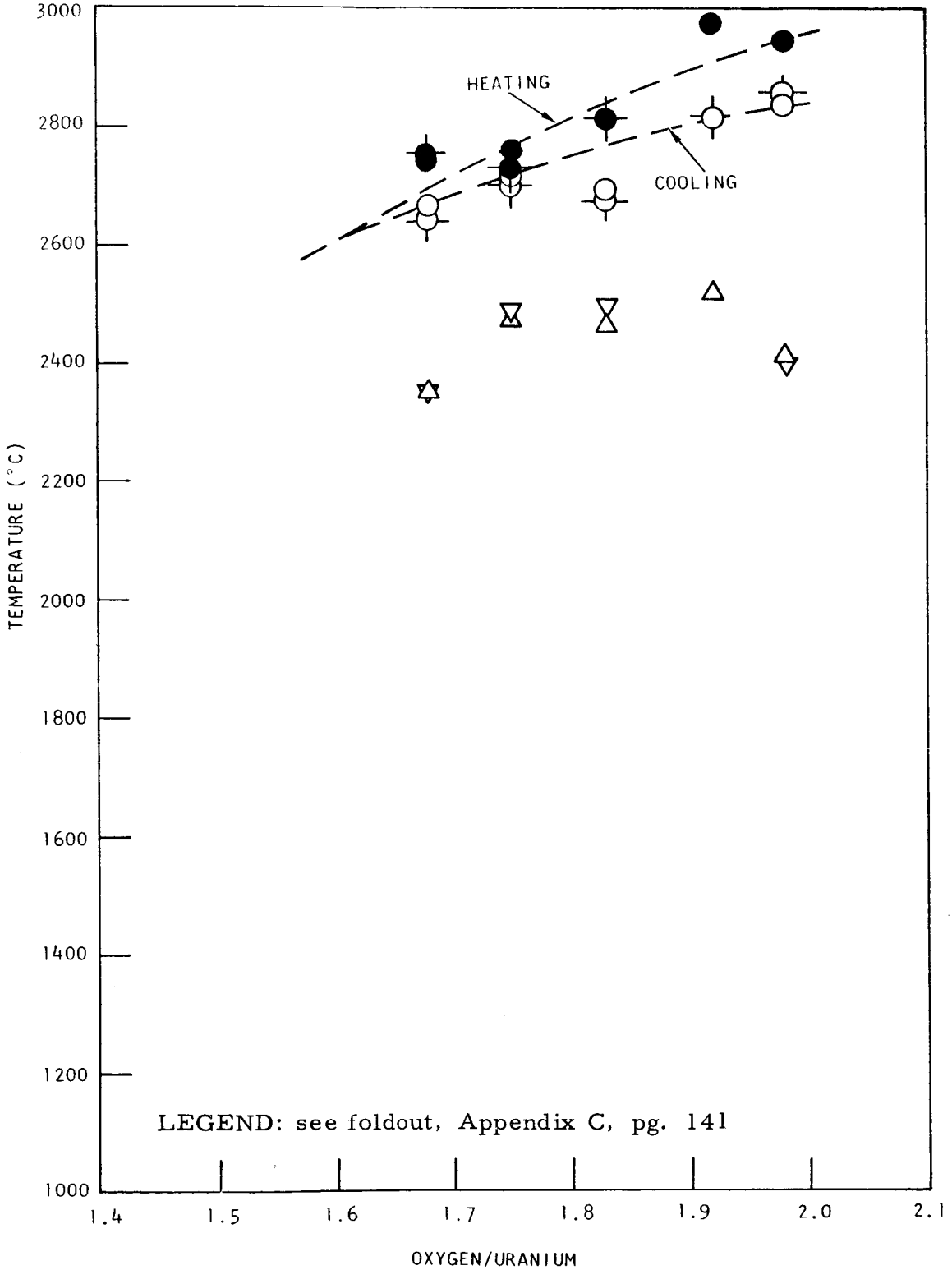

Fig. 41--Liquidus and solidus temperatures in the uranium-thorium-oxygen system (2.5 mol-% thoria)

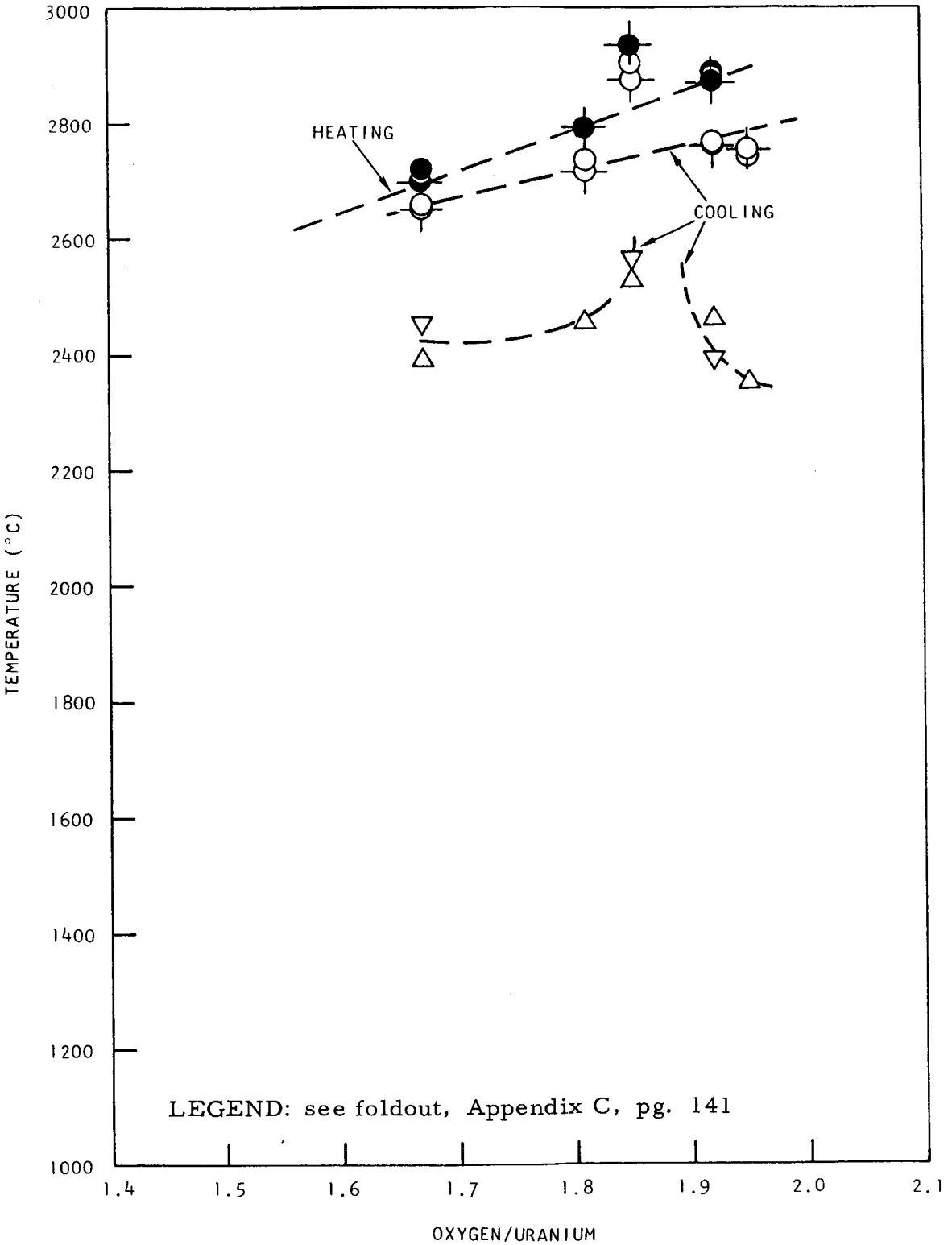

Fig. 42--Liquidus and solidus temperatures in the uranium-thorium-oxygen system (5.0 mol-% thoria)

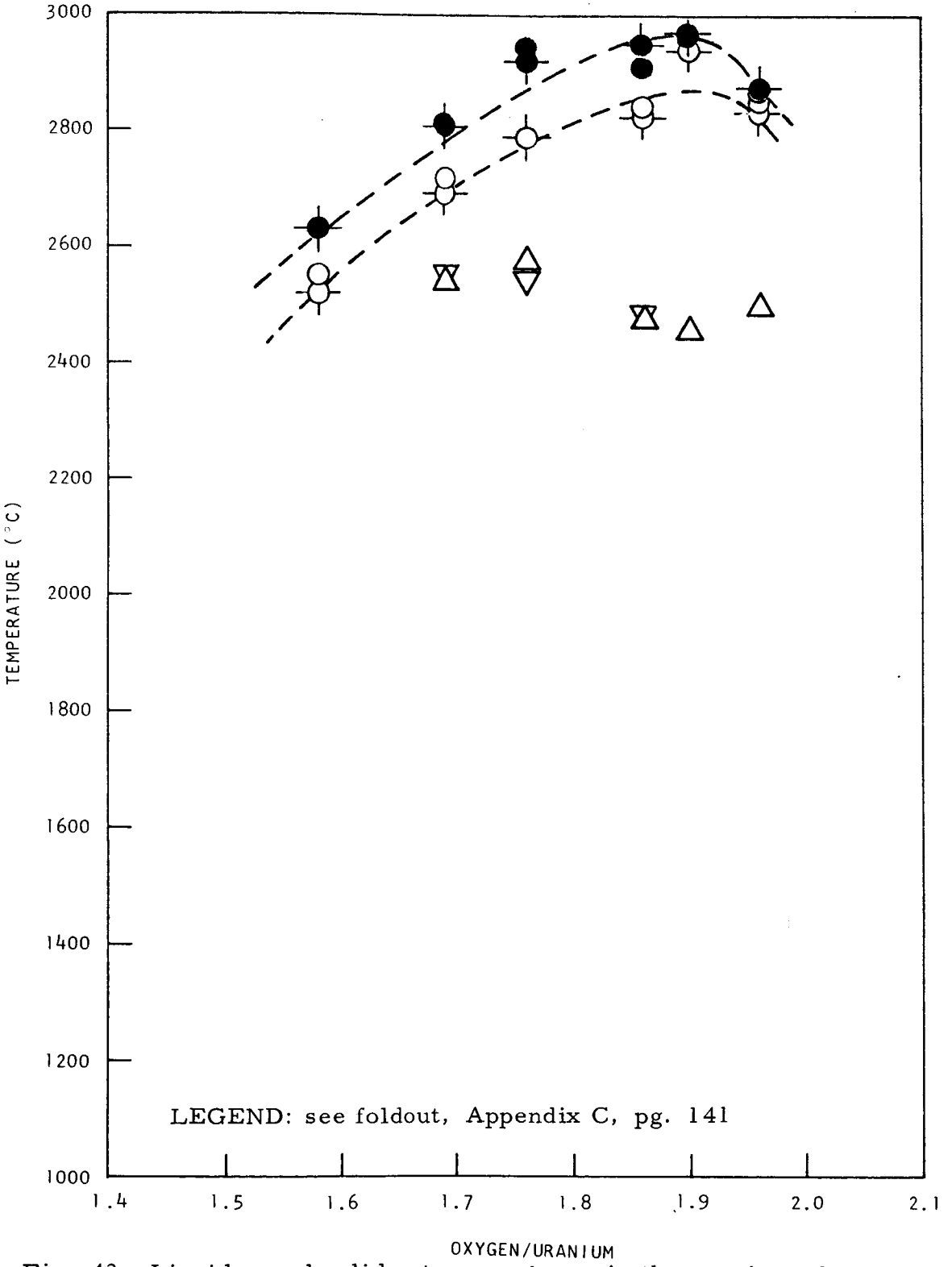

Fig. 43--Liquidus and solidus temperatures in the uranium-thorium-oxygen system (10.0 mol-% thoria)

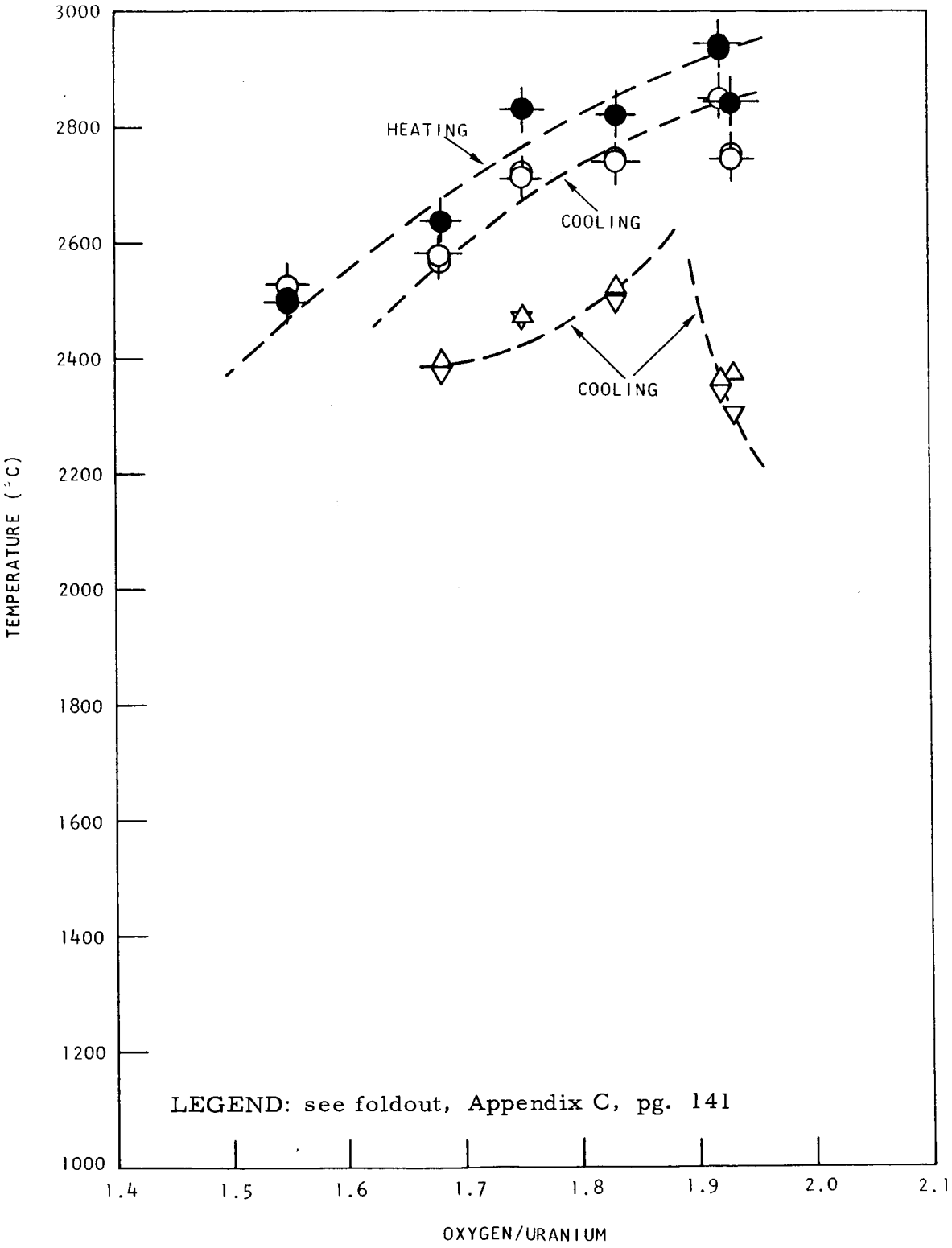

Fig. 44--Liquidus and solidus temperatures in the uranium-cerium-oxygen system (2.5 mol-% ceria)

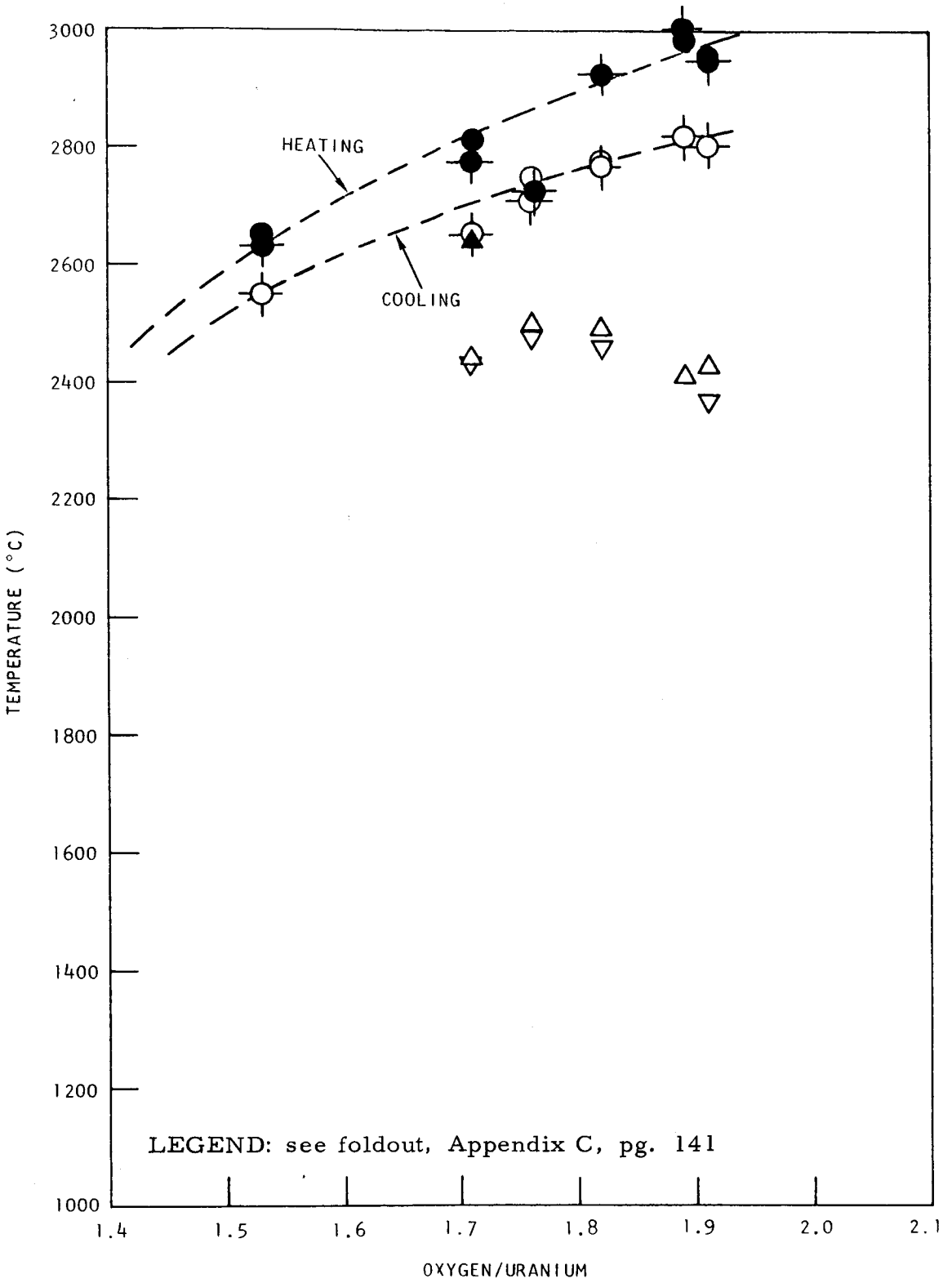

Fig. 45--Liquidus and solidus temperatures in the uranium-cerium-oxygen system (5.0 mol-% ceria)

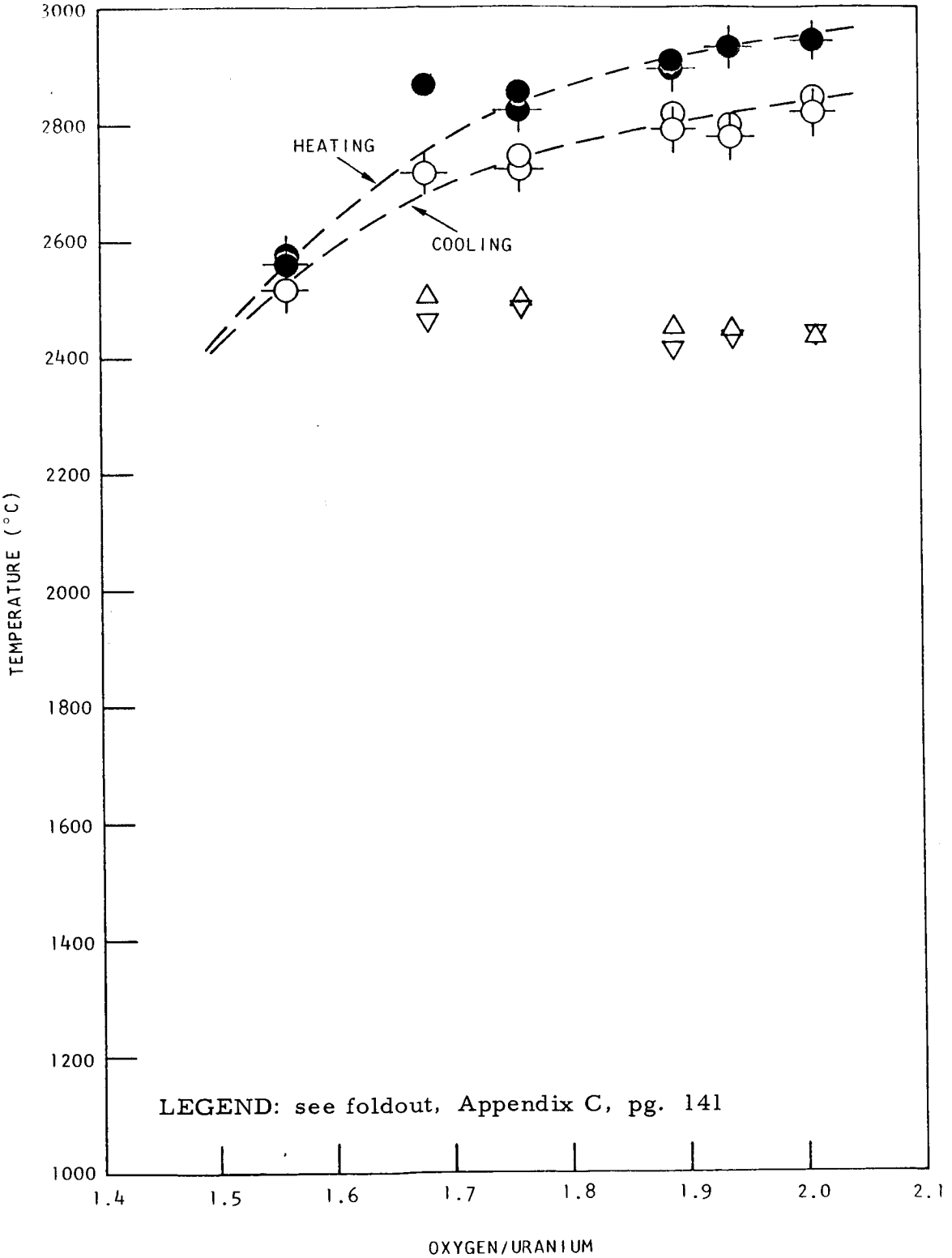

Fig. 46--Liquidus and solidus temperatures in the uranium-cerium-oxygen system (10.0 mol-% ceria)

yttria-, thoria-, and ceria-stabilized series, at 2.5, 5.0, and 10.0 mol-% of stabilizing oxide are shown in Figs. 38 through 46.

The data presented above are reduced, analyzed, discussed, and compared with the results of other workers in the following section.

7.3. Phase Boundaries

The data presented in the tables and curves in the previous section were reduced by averaging as described in Section 5.3, and these values were used to plot the phase boundaries in this section.

7.3.1. Phase Boundaries in the Unstabilized U-O System

The averaged values of the decomposition, liquidus, and solidus temperatures for the unstabilized U-UO_2 system are plotted in Fig. 47* and the best curves have been drawn through the data. These are the resulting phase boundaries for the binary system. In Figure 48 the decomposition curve, as determined in the present study, is compared with the data reported by others. The curve of Edwards and Martin is calculated from the equation (5)

$$\log X_U = 1.404 - 6759/T \,, \qquad (7)$$

where X_U is the mole fraction of uranium in UO_2 and T is the absolute temperature. The curve of Bates and Daniel (7) is a smooth curve passed through the points in Fig. 2. The original data reported by GE-NMPO (4) obtained by equilibration in rhenium capsules are plotted. In addition, these data are corrected using the ratio of the vapor pressure of uranium, P_U, over URe_2 as reported by GE-NMPO (8)to the vapor pressure of pure uranium ($\overset{o}{p}$). The factor of $p/p^o = 30$ is assumed to apply over the entire temperature range of the measurements rather than just at the temperature of measurement (1450°C). This is equivalent to assuming that the heat of formation of URe_2 is not temperature dependent over the range 1350° to 1800°C. It is clear, however, that both sets of data from GE-NMPO are in fair agreement with the data of Edwards and Martin extrapolated to lower temperatures within the present range of precision of the data. The data of Bates and Daniel agree with the other equilibrium data at lower temperatures, but diverge from the Edwards and Martin data at higher temperatures. The data from the present study is widely scattered compared to the equilibrium data. This is not surprising, however, in view of the steepness of the decomposition curve. The decomposition curve, as determined by thermal analysis, crosses the Edwards and Martin curve at about 2250°C, and at lower temperatures differs from the latter by ~0.08 units of O/U ratio.

*Fig. 47 is provided in foldout form to facilitate comparison of the stabilized systems with the unstabilized U-O system.

This page intentionally left blank.

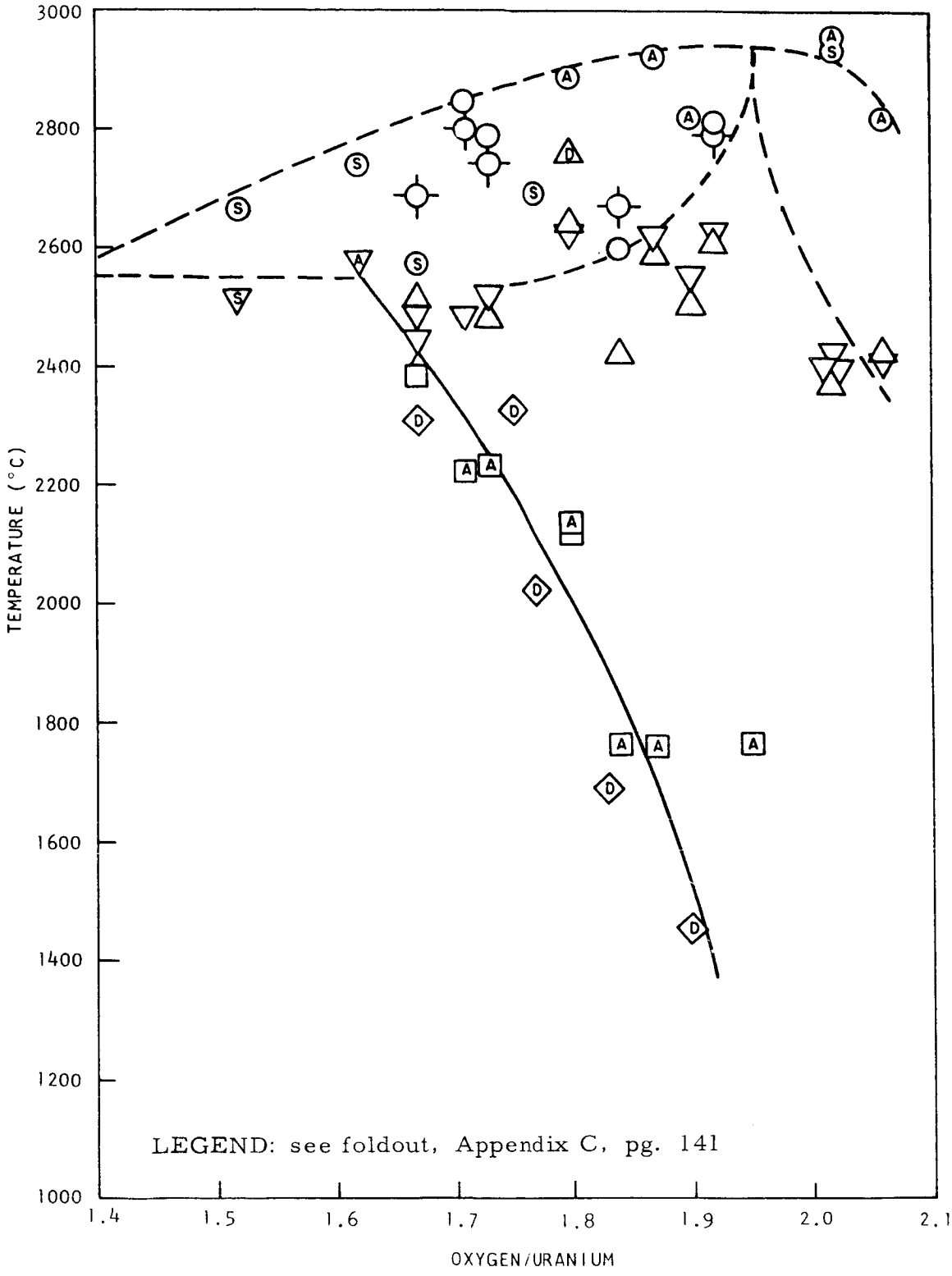

Fig. 47--Phase boundaries in the uranium-oxygen system from thermal analysis experiments

Fig. 47.--Phase boundaries in the uranium-oxygen system from thermal analysis experiments

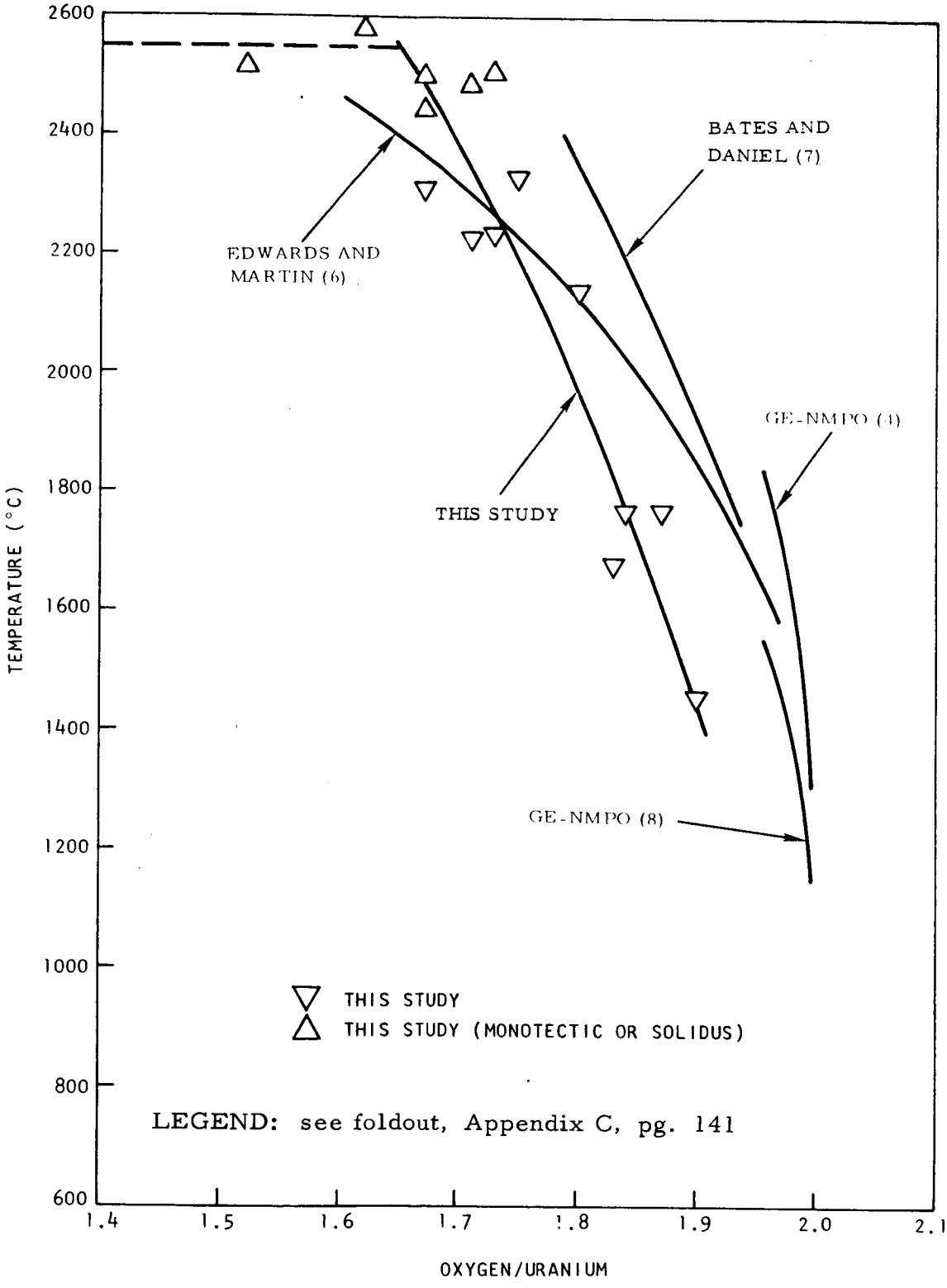

Fig. 48--Decomposition temperatures of hypostoichiometric UO_2

PRECEDING PAGE BLANK NOT FILMED.

The liquidus temperatures of the binary U-UO_2 system are shown in Fig. 49. The straight line data were calculated from the equation given by GE-NMPO (22), while the five points of Bates and Daniel (7) are indicated by circles. The present study has determined the liquidus data shown as triangles and a smooth curve has been drawn through the data.*

There is good agreement between the data of Bates and Daniel and GE-NMPO. The problem that arises in accepting their data as the liquidus curve is that it is very difficult to extrapolate their reported curves to the monotectic temperature at anywhere near the monotectic composition. This is true whether one assumes the monotectic temperature 2470°C, as reported by Edwards and Martin (6) or the value of 2550°C, as determined in this study. The data of both investigators appear to extrapolate to the monotectic temperature at the p-tristeric point at ~$UO_{1.60}$.

Bates and Daniel carried out their studies in "V-shaped" filament strip and were, therefore, subject to similar changes in O/U ratio, as were observed in the present study. The investigators at GE-NMPO used closed (welded) crucibles with black-body wells. Under these circumstances, however, it may be difficult to distinguish the liquidus from the solidus temperature. The situation clearly has not been fully resolved.

7.3.2. Phase Boundaries in the Calcia-stabilized U-O System

The averaged values of the liquidus, solidus, and decomposition temperatures for calcia-stabilized U-O samples containing nominally 2.5, 5.0, 10.0, and 15.0 mol-% calcia are plotted in Figs. 50, 51, 52, and 53, respectively. The best curves are drawn through the liquidus and decomposition data, giving added weight to those points which are averages of heating and cooling determinations. Heating or cooling points are shown on the plots when an average value is not available.

The data in the calcia systems are widely scattered as a result of the varying calcia contents which resulted from vaporization of the samples. In fact, the series initially containing 15 mol-% calcia (final content ~11 mol-%) yielded no data on the decomposition or liquidus temperatures on the heating part of the cycle. All the data in Fig. 53 are from cooling curves. The phase boundaries shown by the dotted lines are therefore low. The other calcia series yielded good data on the liquidus temperatures, but the decomposition temperatures were difficult to determine. The estimated monotectic temperature in Fig. 50 may be somewhat low. The data clearly indicate a depression of about 100 plus degrees in the liquidus temperatures. This behavior has also been observed by NMPO (13).

*Only the averages of heating and cooling curves are shown in this figure.

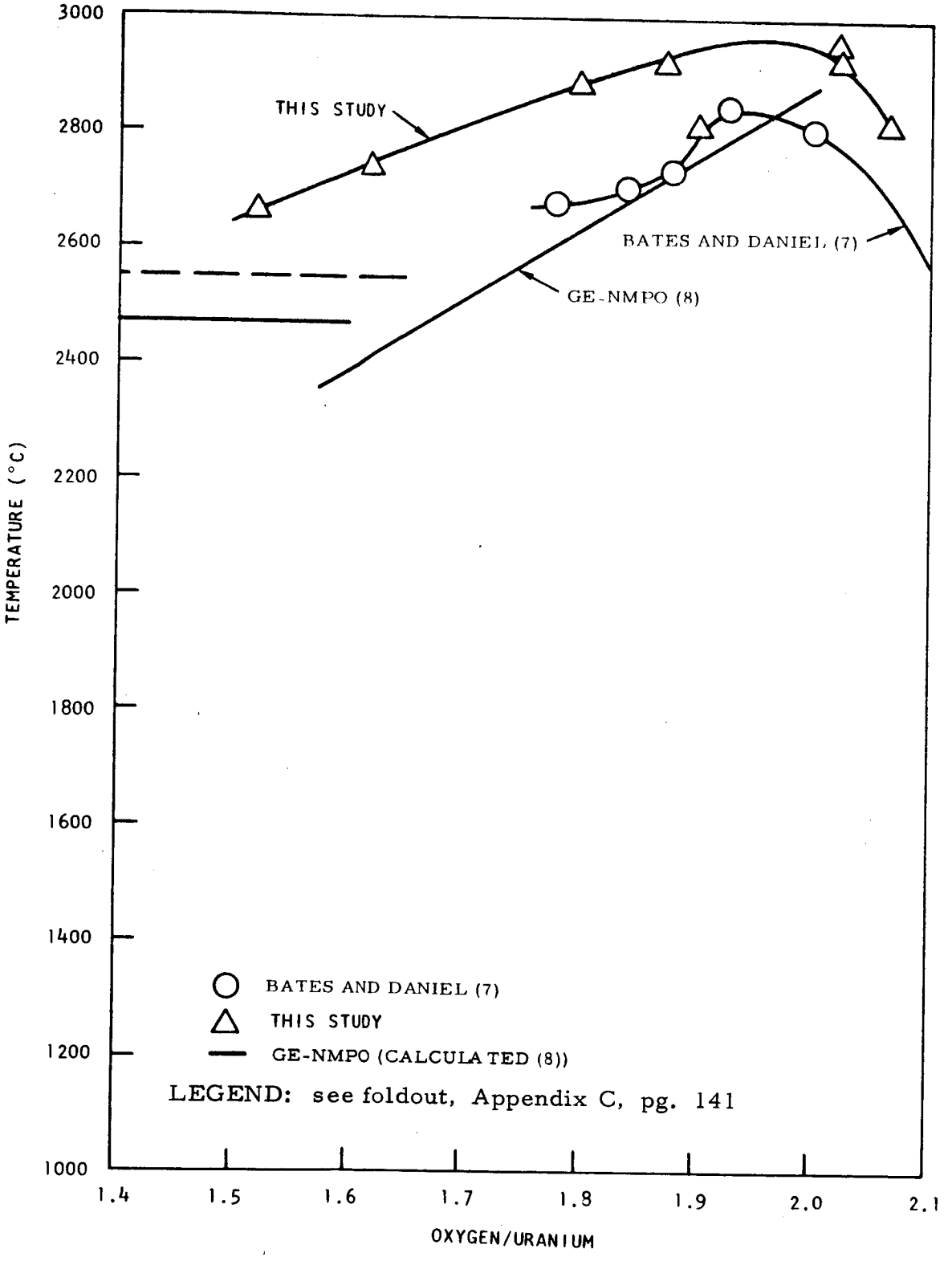

Fig. 49--Liquidus temperatures of hypostoichiometric UO_2

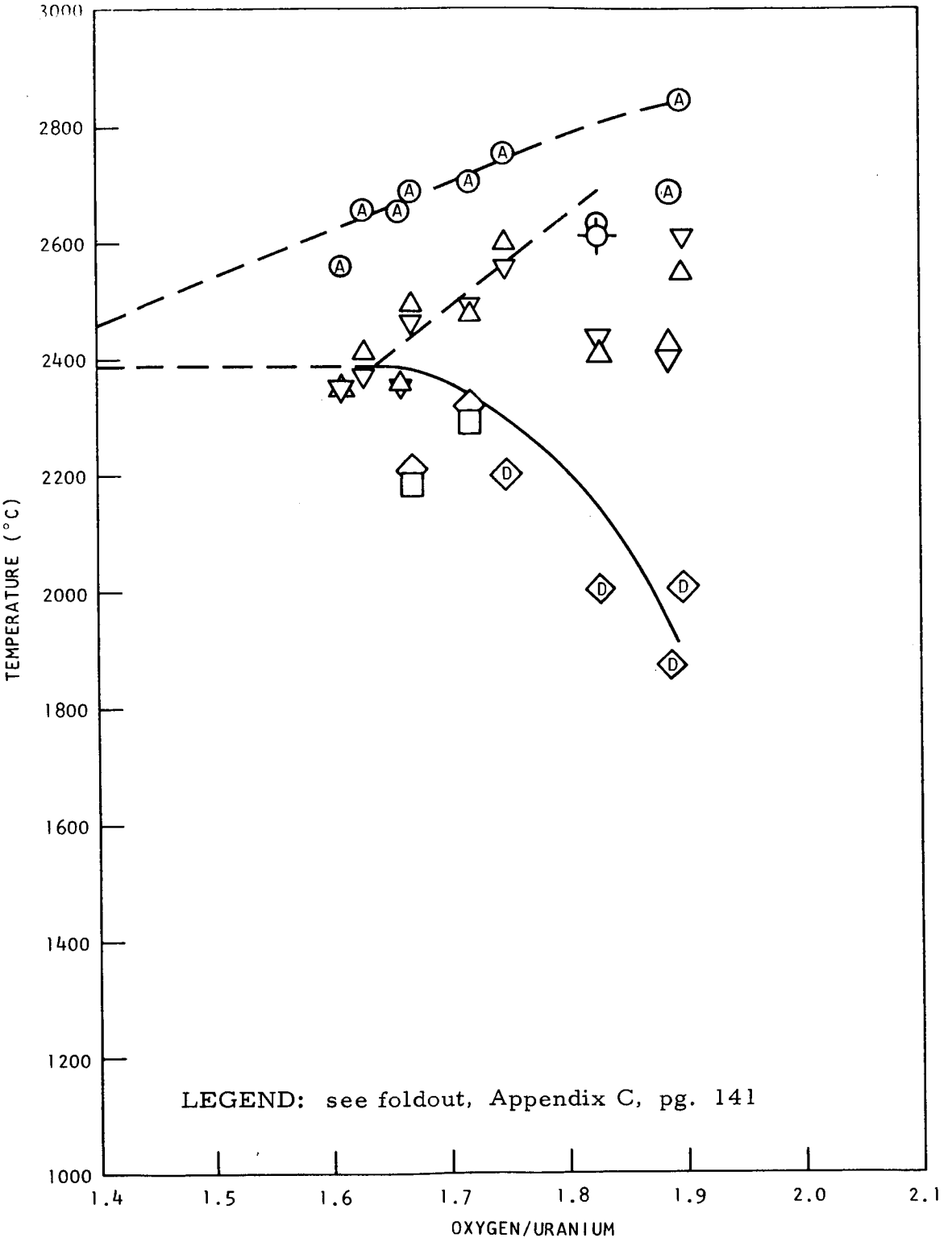

Fig. 50--Phase boundaries in the uranium-calcium-oxygen system (2.5 mol-% calcia)

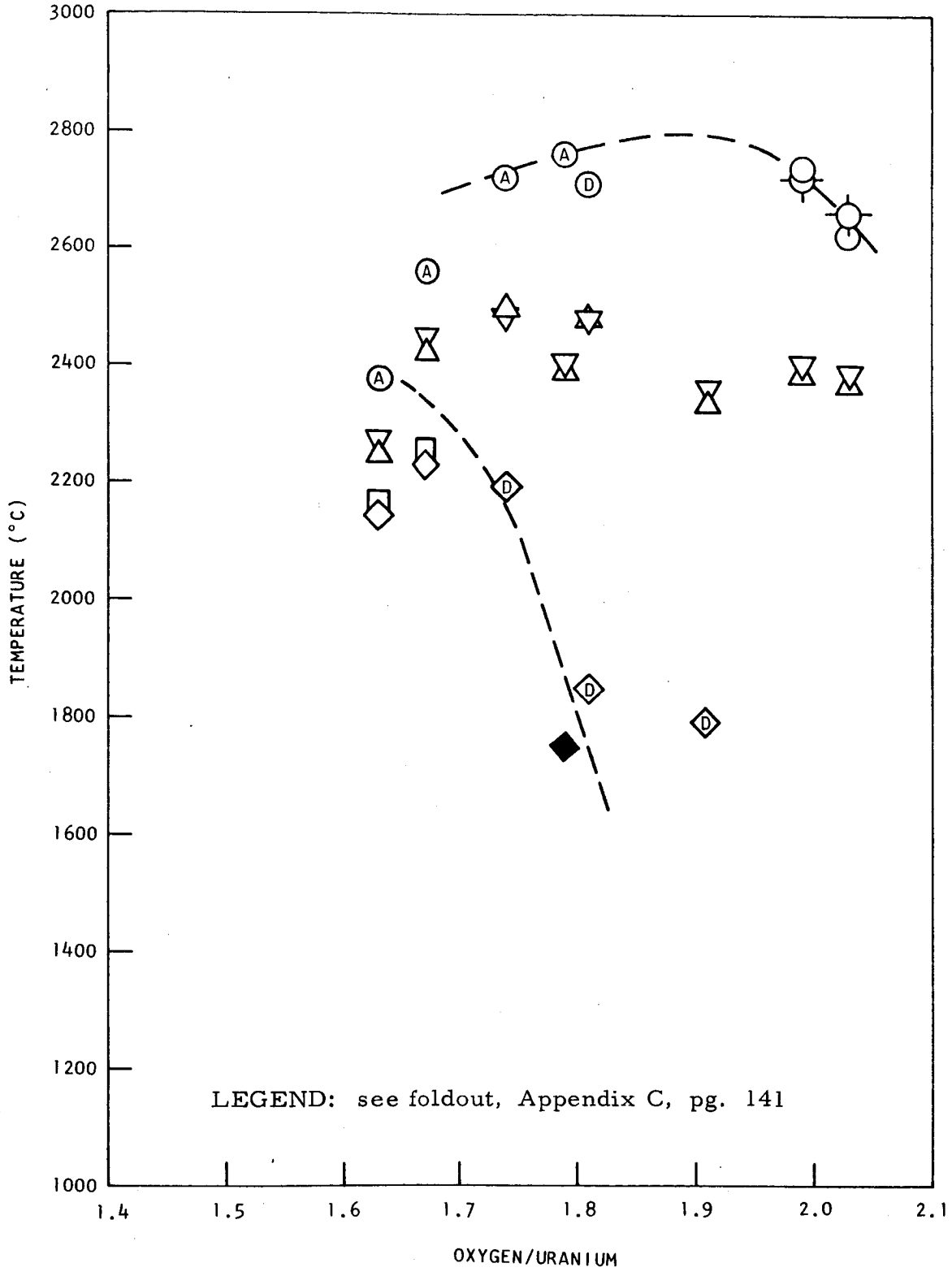

Fig. 51--Phase boundaries in the uranium-calcium-oxygen system (5.0 mol-% calcia)

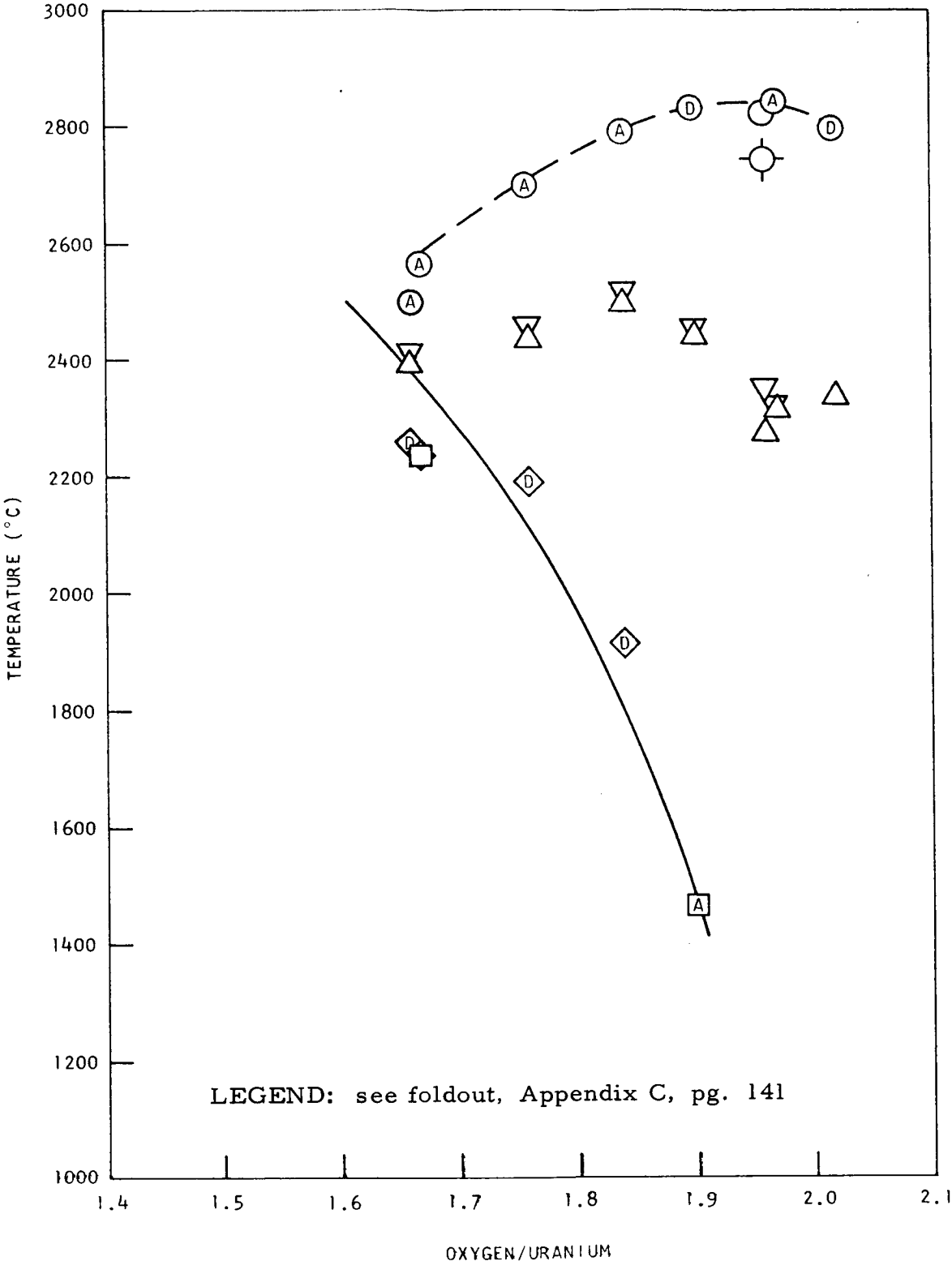

Fig. 52--Phase boundaries in the uranium-calcium-oxygen system (10.0 mol-% calcia)

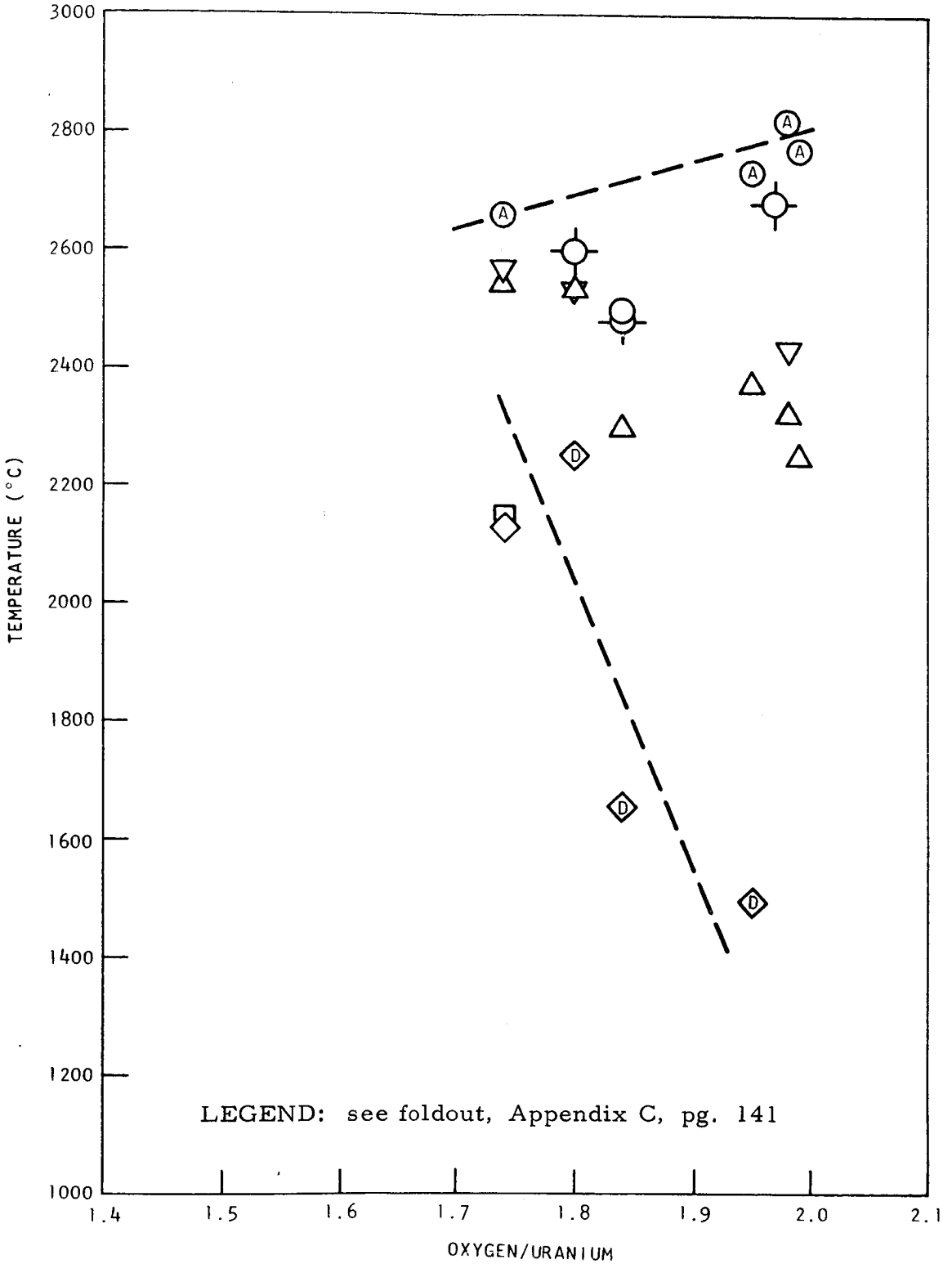

Fig. 53--Phase boundaries in the uranium-calcium-oxygen system (15.0 mol-% calcia)

The data on the 15.0 mol-% calcia series show sufficient scatter to obviate any gains to be realized from having data over a wider range of CaO content. The monotectic temperature is estimated to be 2380° ±100°C and the p-tristeric point at O/U = 1.63 ±0.05 for the series containing 2.5 mol-% calcia. It was not possible to estimate these data for the other calcia series.

7.3.3. Phase-Boundaries in the Yttria-stabilized U-O System

The averaged values for liquidus, solidus, and decomposition temperatures for yttria-stabilized uranium-oxygen samples with 2.5, 5.0, and 10.0 mol-% yttria are plotted in Figs. 54, 55, and 56, respectively. The best curves are drawn through the data for the liquidus and decomposition temperatures, yielding the phase boundaries shown in the respective figures. Once again it should be noted that the decomposition temperatures are determined, on heating, for only a very few samples.

The solidus temperatures are utilized only as an aid in determining the monotectic temperature and the p-tristeric point. This point is estimated to be 1.65 ±0.08 in all three systems. The data in Figs. 54 through 56 indicate a somewhat smaller range of O/U ratio, but the analytical errors discussed in Sections 6.2 and 6.3 impose the error listed above. The monotectic temperature is estimated to be 2400° ±60°C for all three systems. Once again the liquidus temperatures appear to be depressed by ~100°C relative to the unstabilized system.

The decomposition temperatures agree with those of the unstabilized U-UO_2 system within the estimated composition error of ±0.04 in O/U ratio.

7.3.4. Phase Boundaries in the Thoria-stabilized U-O System

In both thoria- and ceria-stabilized systems, it was easier to obtain data on the decomposition temperatures. This is shown by the fact that it was possible to determine the decomposition temperature on heating for most of the compositions in these two series.

The phase boundaries for the thoria-stabilized series are shown in Figs. 57, 58, and 59 for the 2.5, 5.0, and 10.0 mol-% thoria series, respectively. The improvement in the determinations of the decomposition temperatures in the thoria-stabilized series was not accompanied by an analogous improvement in the solidus temperatures. Thus, they are used again only as guidelines.

The decomposition temperatures of samples with all three thoria contents are in agreement within the estimated error in O/U ratio, and the three series are, in turn, in agreement with the unstabilized U-O system.

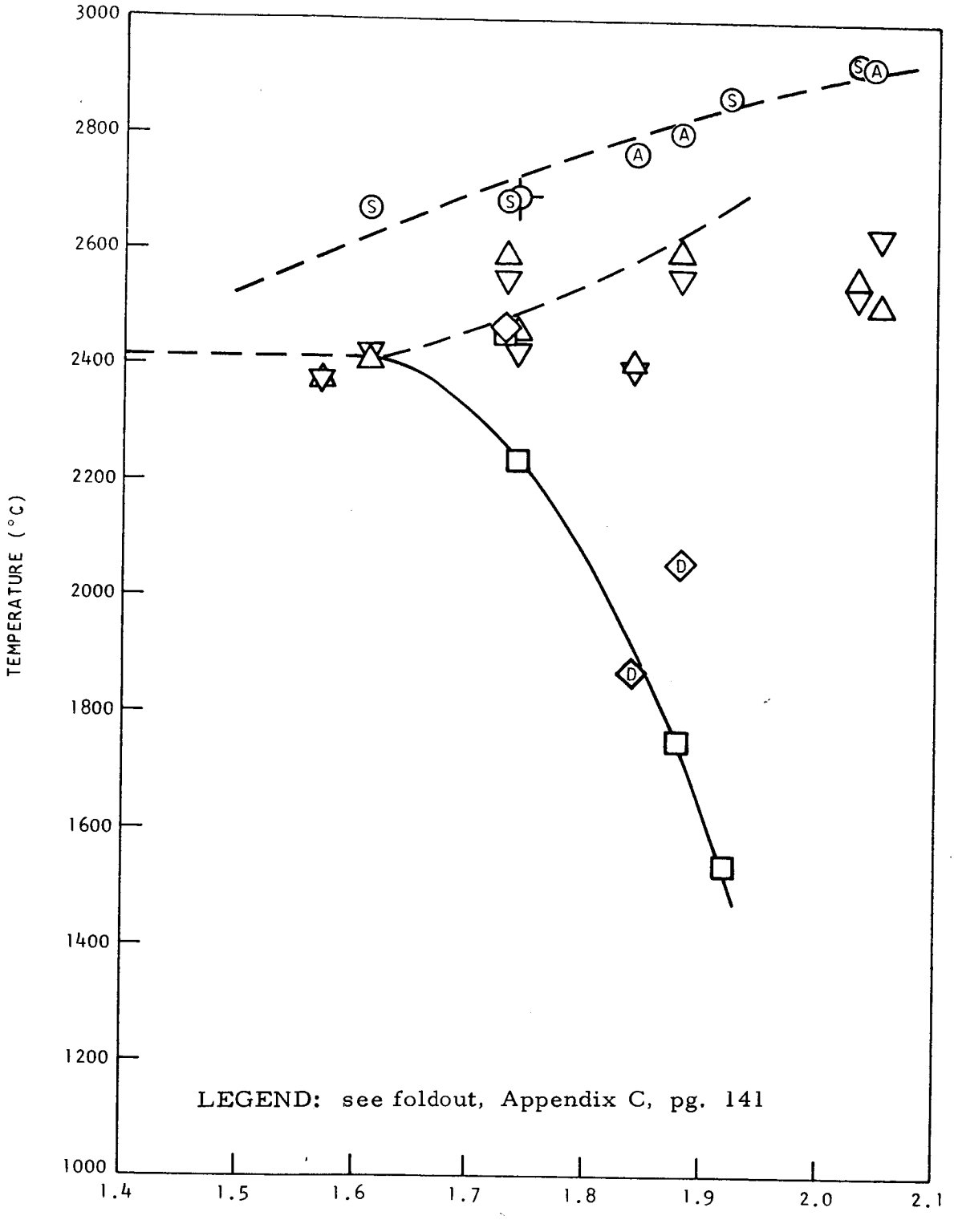

Fig. 54--Phase boundaries in the uranium-yttrium-oxygen system (2.5 mol-% yttria)

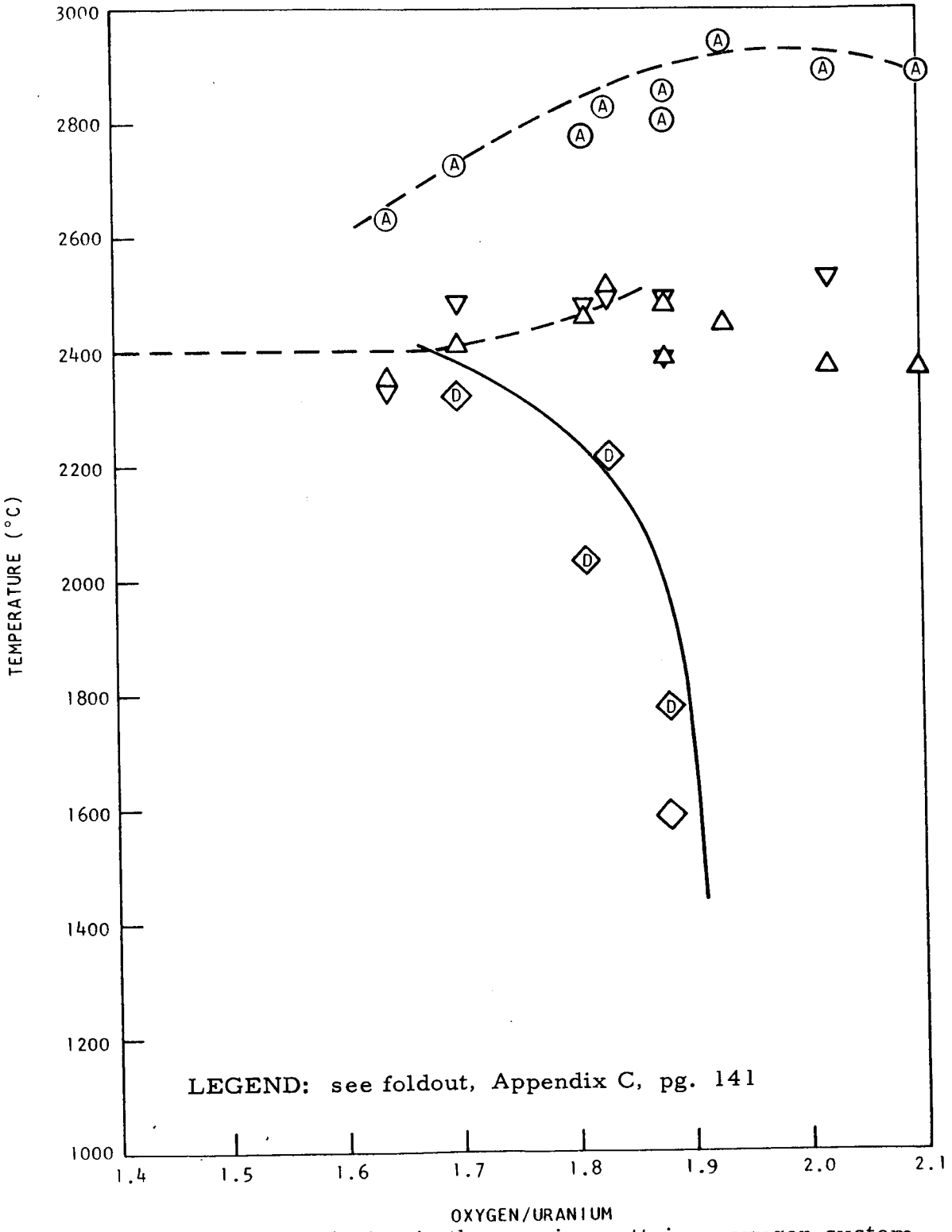

Fig. 55--Phase boundaries in the uranium-yttrium-oxygen system (5.0 mol-% yttria)

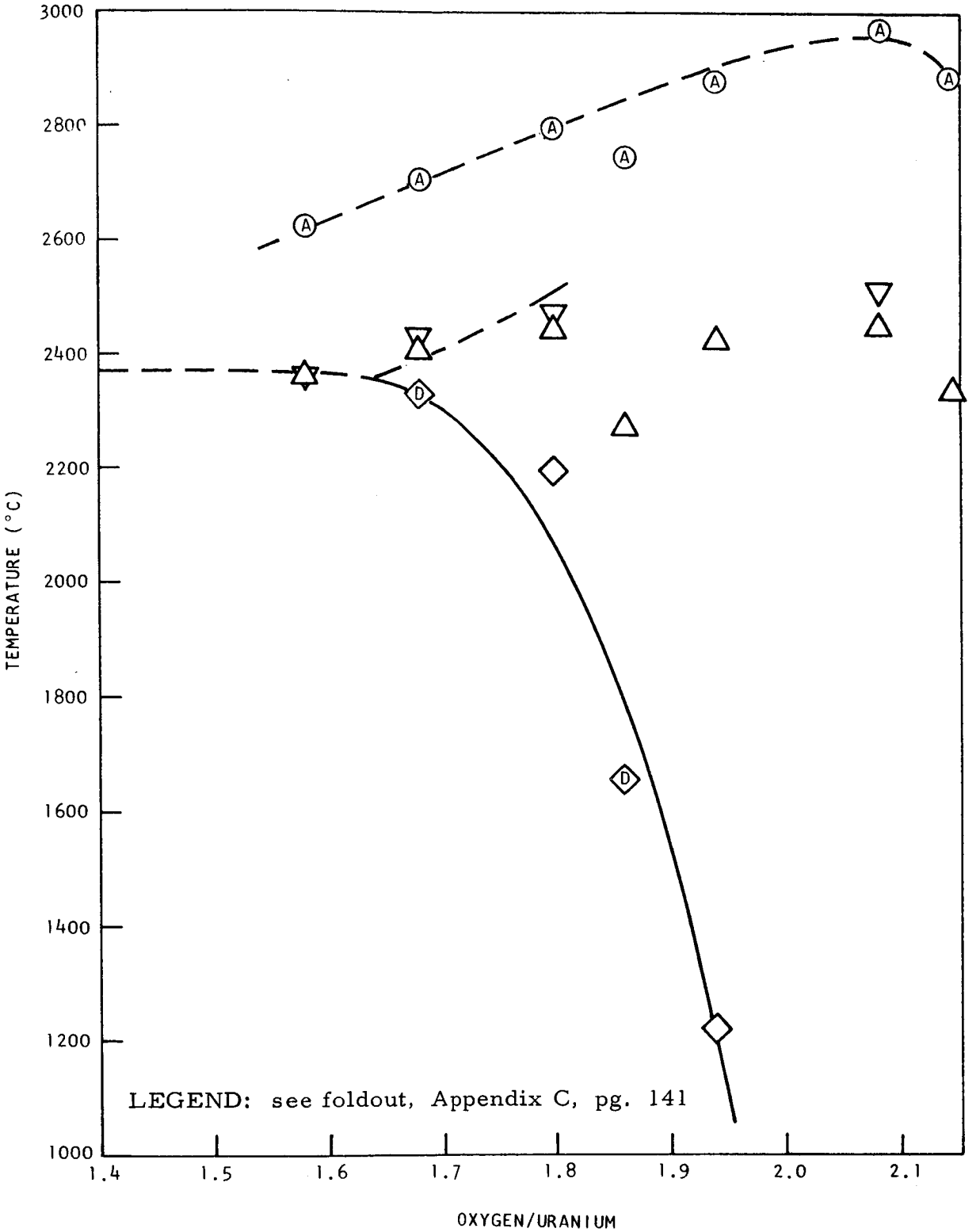

Fig. 56--Phase boundaries in the uranium-yttrium-oxygen system (10.0 mol-% yttria)

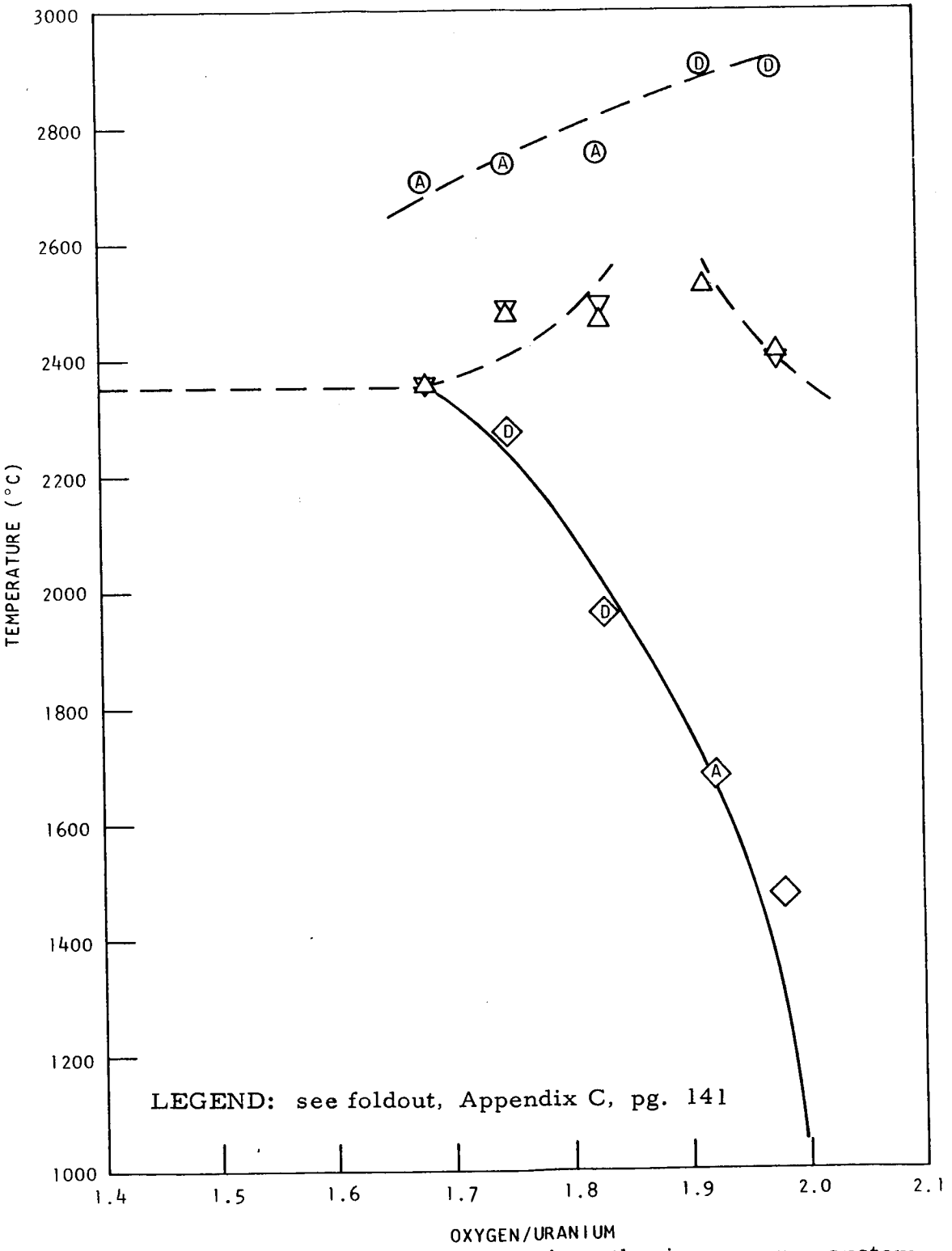

Fig. 57--Phase boundaries in the uranium-thorium-oxygen system (2.5 mol-% thoria)

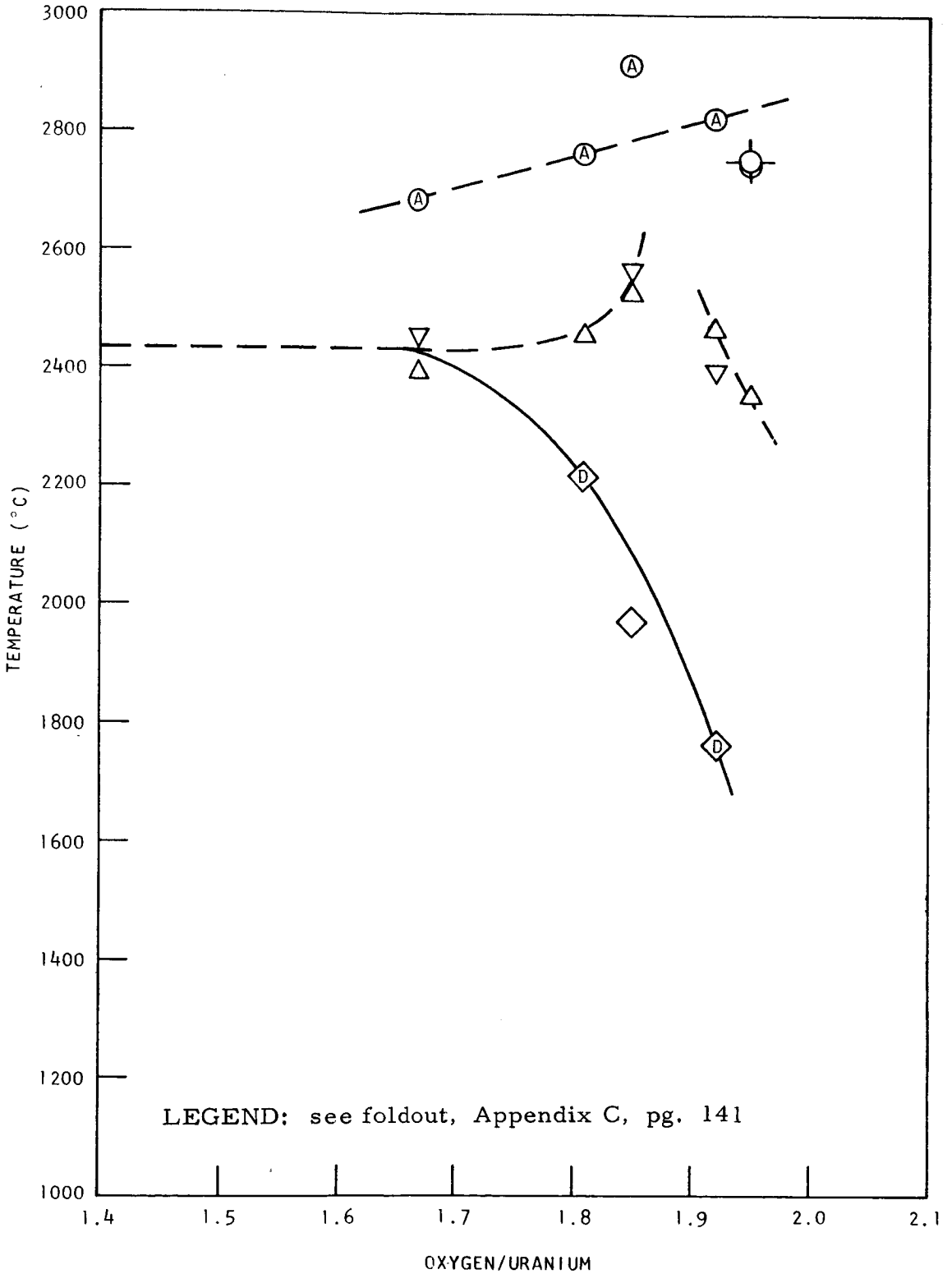

Fig. 58--Phase boundaries in the uranium-thorium-oxygen system (5.0 mol-% thoria)

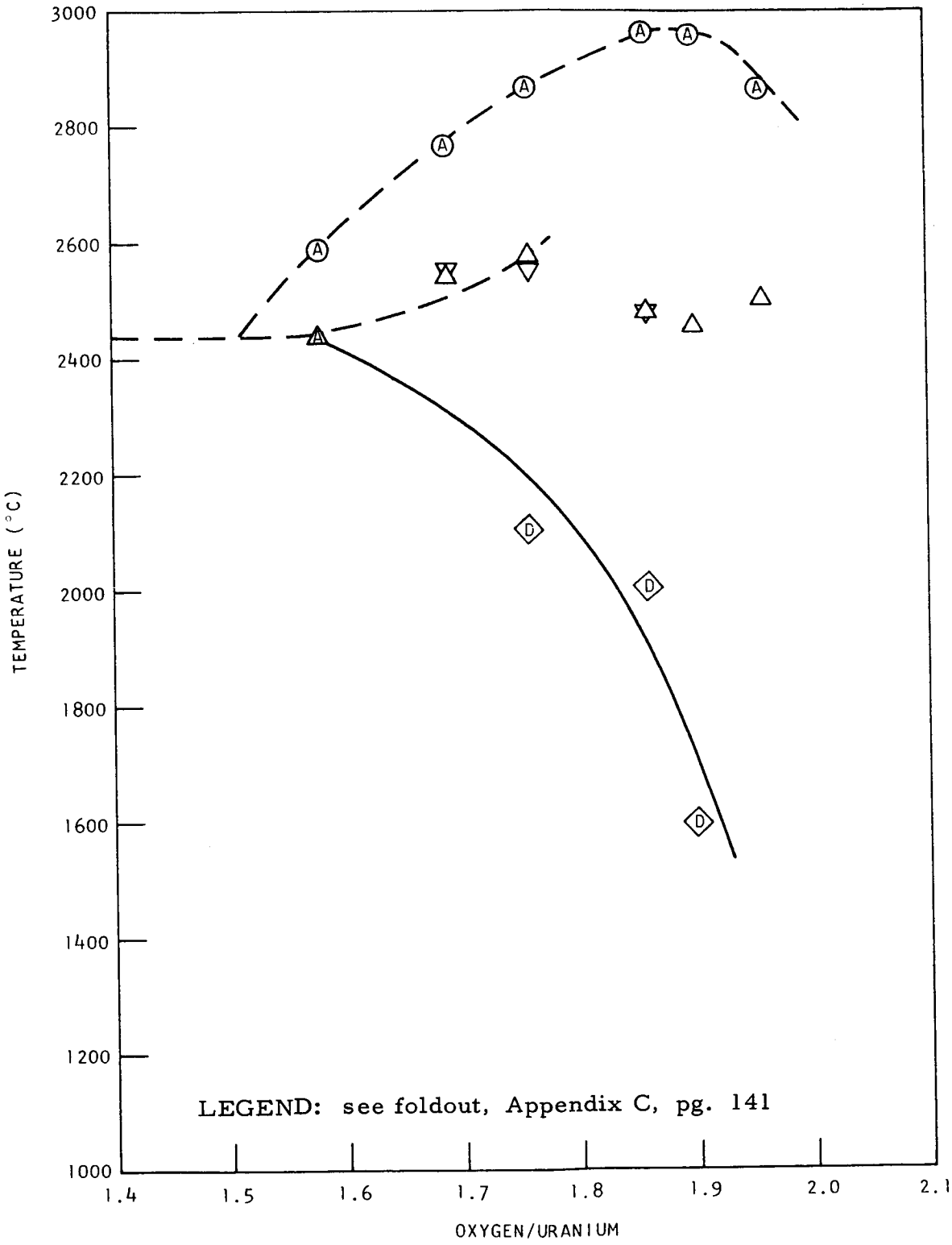

Fig. 59--Phase boundaries in the uranium-thorium-oxygen system (10.0 mol-% thoria)

The monotectic temperature is estimated to be 2380 ±80°C, and the p-tristeric point between 1.60 and 1.70. The liquidus curves for the 2.5 and 5.0 mol-% thoria series are somewhat lower than the liquidus of the unstabilized system at low O/U ratios, but equal to or higher than the U-O system at $UO_{2.0}$. In the 10 mol-% thoria series, at the higher O/U ratios; to exceed that of the unstabilized system.

7.3.5. Phase Boundaries in the Ceria-Stabalized U-O System

The averaged values for the liquidus, solidus, and decomposition temperatures for the ceria-stabilized samples are plotted in Fig. 60, 61, and 62 for the 2.5, 5.0, and 10.0 mol-% ceria samples. Once again it was possible to determine the decomposition temperatures on the heating cycle for most of the samples.

The best curves have been drawn through the data for the liquidus and decomposition temperatures, and the solidus points have been used to help estimate the monotectic temperature as 2360 ±100°C and the p-tristeric point between 1.60 and 1.70, for all three series.

The decomposition temperatures for all three series are in agreement with each other within the estimated errors in O/U ratio, and in turn are in agreement with the unstabilized U-O system.

As in the calcia and yttria series, the liquidus temperatures appear to be depressed by 100°C or more.

The data presented for the five systems investigated are summarized in Section 8.

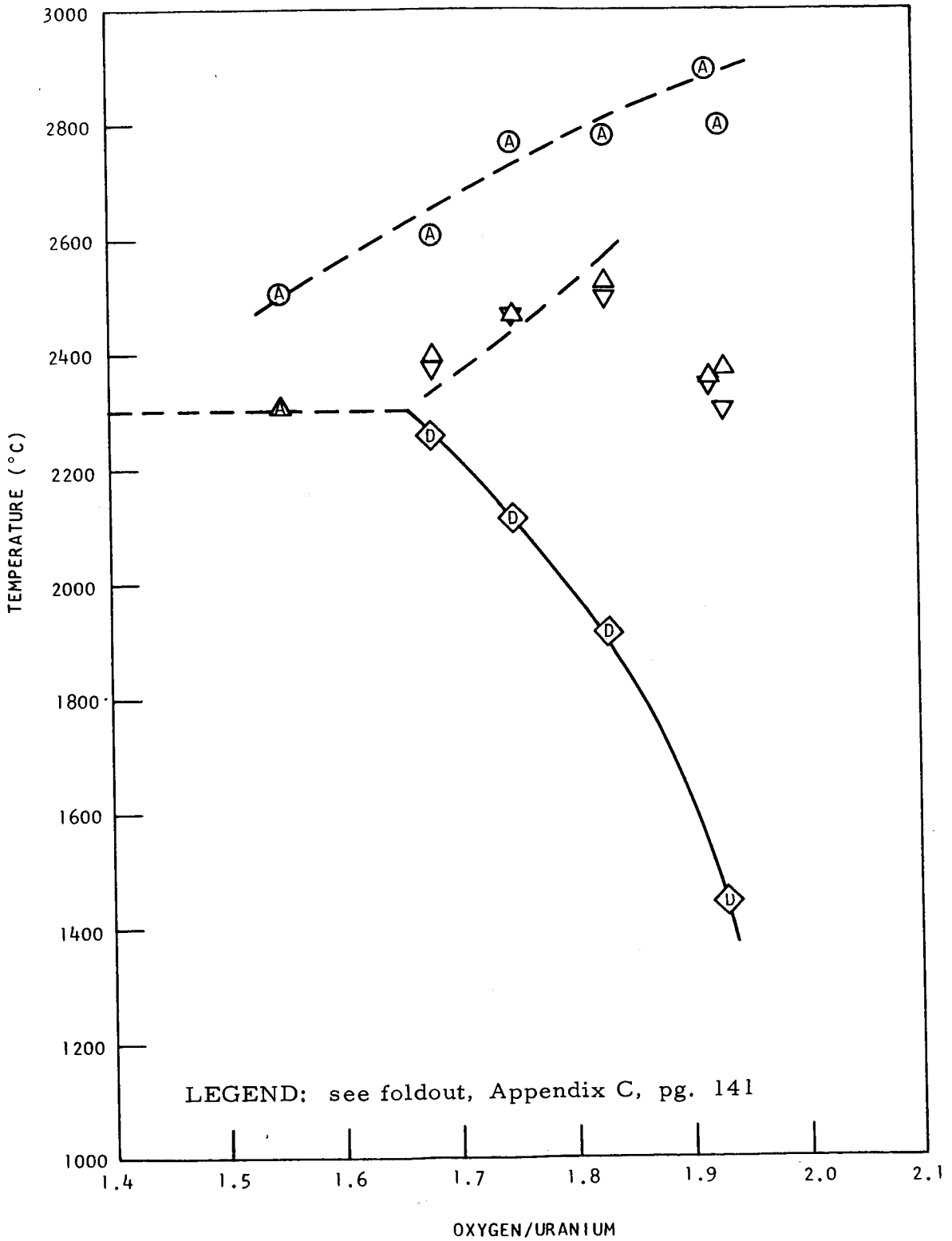

Fig. 60--Phase boundaries in the uranium-cerium-oxygen system (2.5 mol-% ceria)

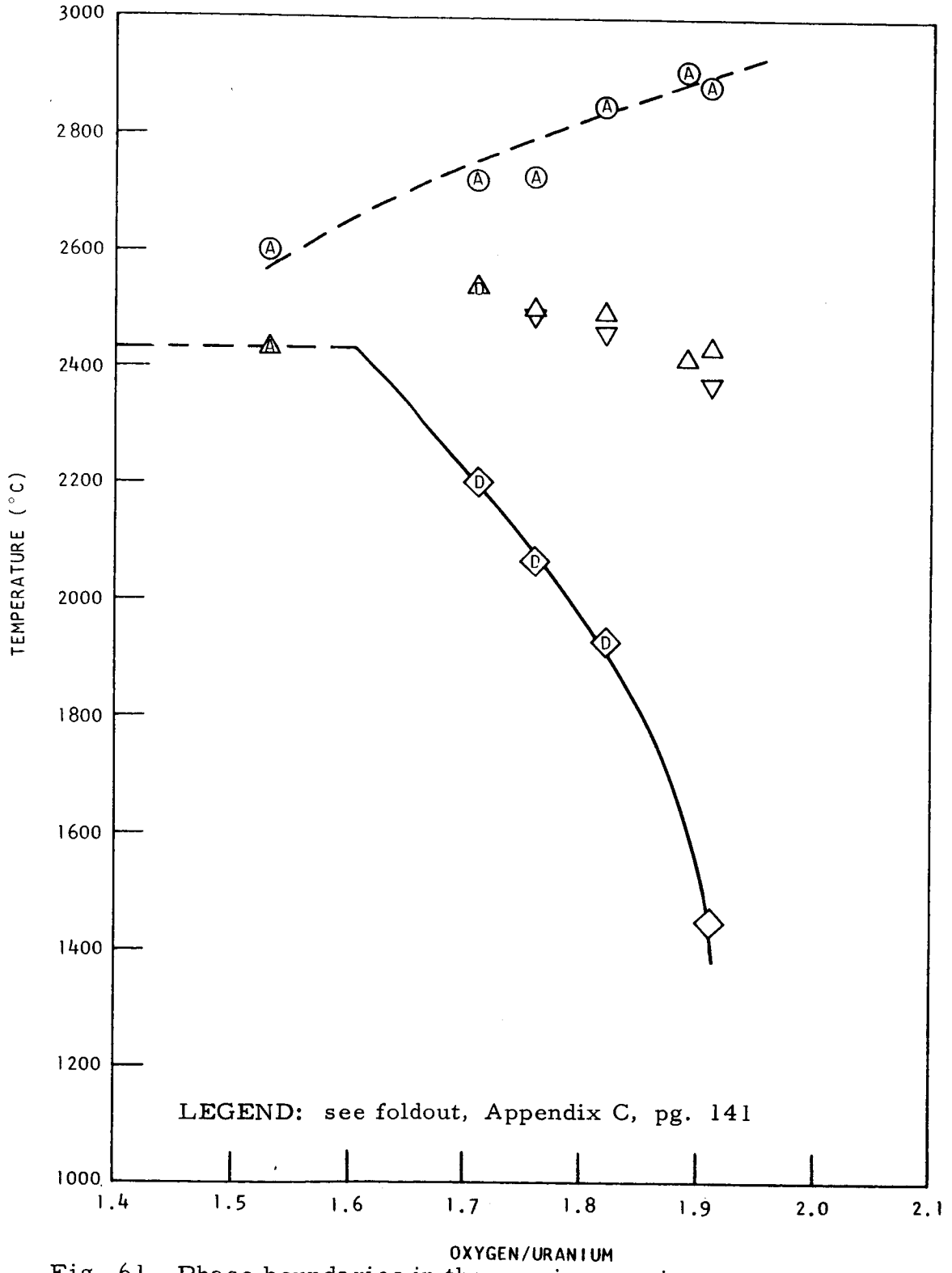

Fig. 61--Phase boundaries in the uranium-cerium-oxygen system (5.0 mol-% ceria)

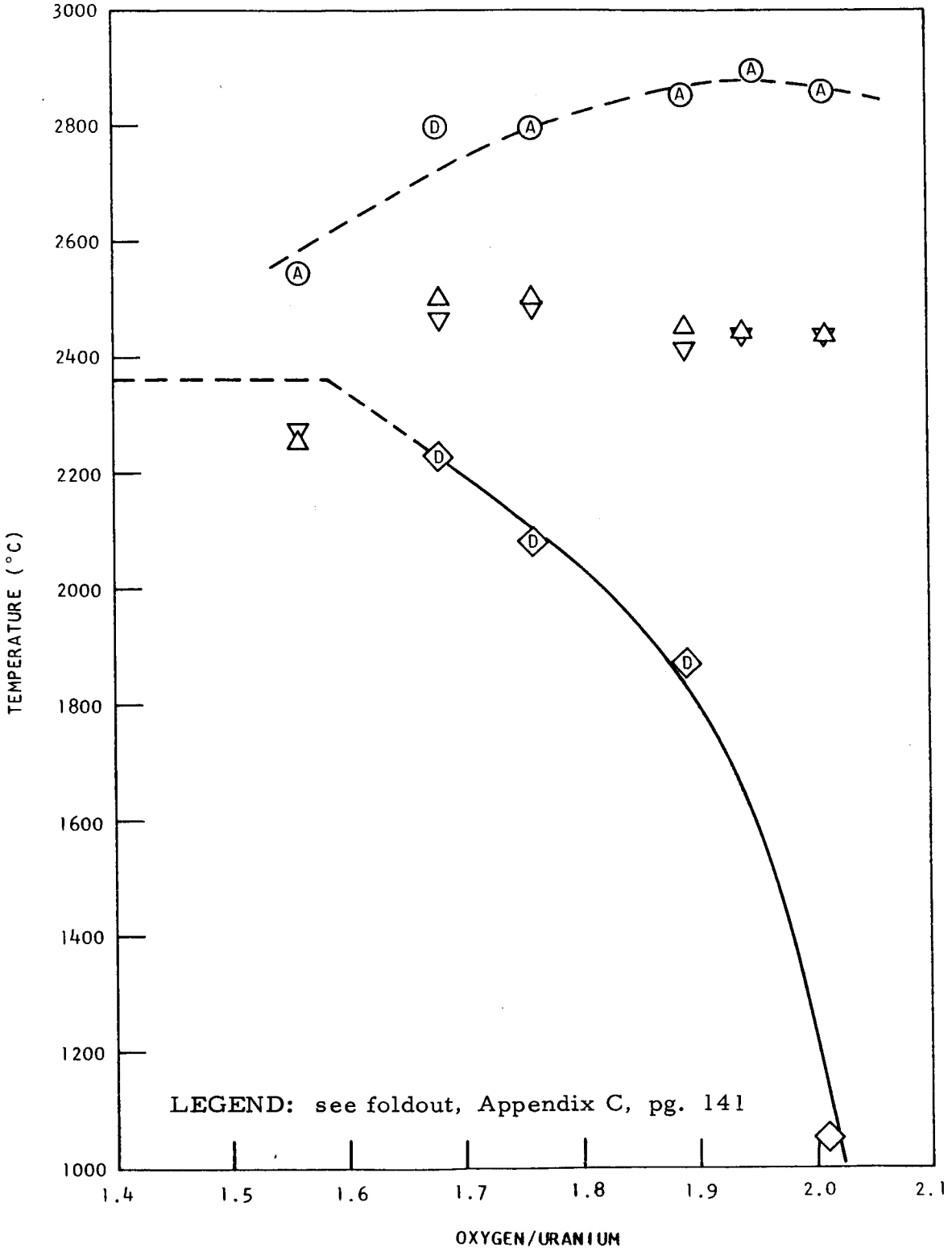

Fig. 62--Phase boundaries in the uranium-cerium-oxygen system (10.0 mol-% ceria)

8. DISCUSSION AND CONCLUSIONS

The phase boundaries shown in Figs. 47 through 62 of Section 7 indicate that within the experimental error, the decomposition temperatures of hypostoichiometric UO_2 are unaffected by the addition of CaO, Y_2O_3, ThO_2, and CeO_2. This is demonstrated in the following paragraphs.

If an error of ±0.04 in the O/U ratio is assigned to the decomposition curve for the unstabilized U-UO_2 system shown in Fig. 47, and a similar error is assigned to the liquidus temperatures, then these two phase boundaries, as determined by this study, can be represented by the bands shown in Fig. 63.

Assignment of compositional errors of ±0.04 in the O/U ratio, as discussed for the additive oxides in Section 6.2, yields similar "bands" representing the decomposition temperatures for the stabilized series containing CeO_2 and ThO_2. The scatter of the data in the yttria-stabilized series yields a somewhat wider band while the large deviations in composition in the calcia-containing series produce an even wider band. The probable phase boundary limits are shown for the calcia, yttria, thoria, and ceria systems in Figs. 64 through 67, respectively. It should be noted that these bands encompass the probable ranges of the phase boundaries for all compositions (2.5, 5.0, and 10.0 mol-%) in each series. That is, the phase boundaries are not concentration dependent.

Since the addition of the various stabilizing oxides did not affect the decomposition temperature of UO_{2-x}, within the experimental error, it is clear that there can be no dependence on the oxidation state of the stabilizer.* The decomposition bands in Figs. 64 through 67 can be reasonably well superimposed, indicating no measurable difference between the behavior of the various stabilizers.

The principal effect of the oxide additions is depression of the liquidus and monotectic temperatures of hypostoichiometric UO_2. This is primarily true for calcia additions and secondarily for yttria additions. Thoria may increase the temperature of the liquidus curve slightly, but any effect is certainly within the experimental error. Within experimental error, ceria has no effect.

The detection of the polymorphic and solid ↔ liquid phase transitions of uranium metal had added confirmatory evidence for the disproportionation of hypostoichiometric UO_2 into U (liquid) plus $UO_{2.0}$ (solid). Since these

*Reduction of CeO_2 to Ce_2O_3 is possible, but this resultant calculated change in the O/U ratios is within experimental error.

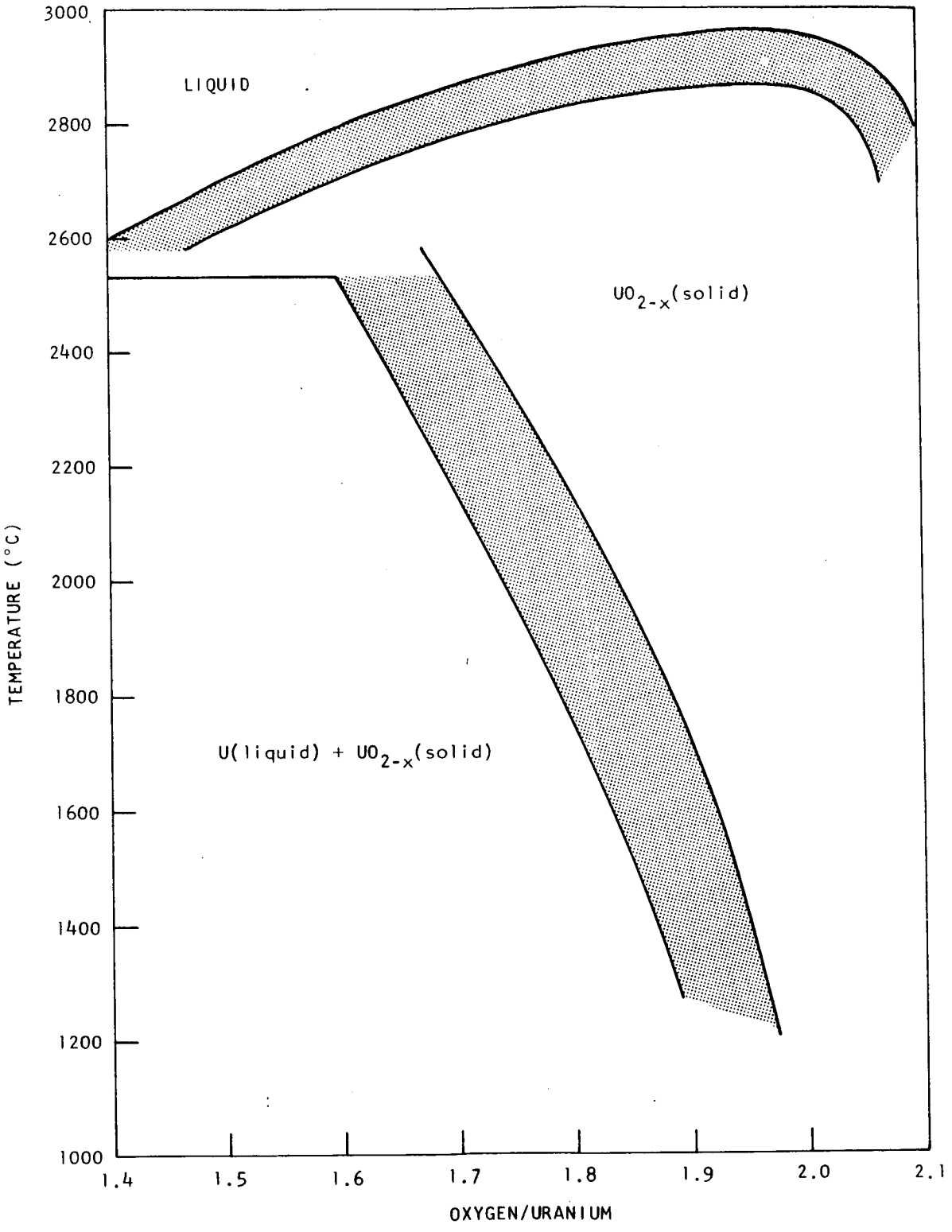

Fig. 63--Probable phase boundaries for the unstabilized U-O systems

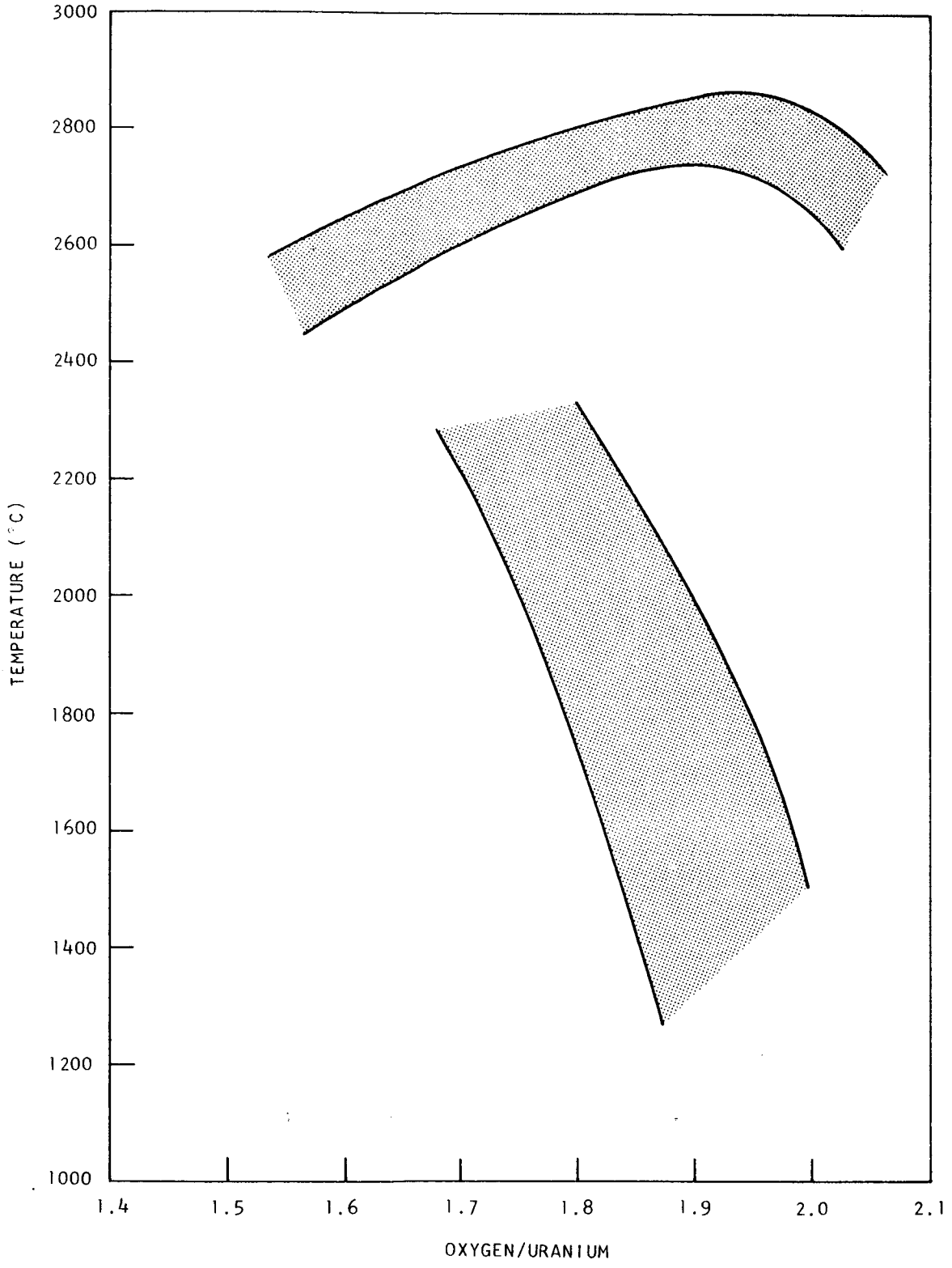

Fig. 64--Probable phase boundaries for the uranium-calcium-oxygen systems

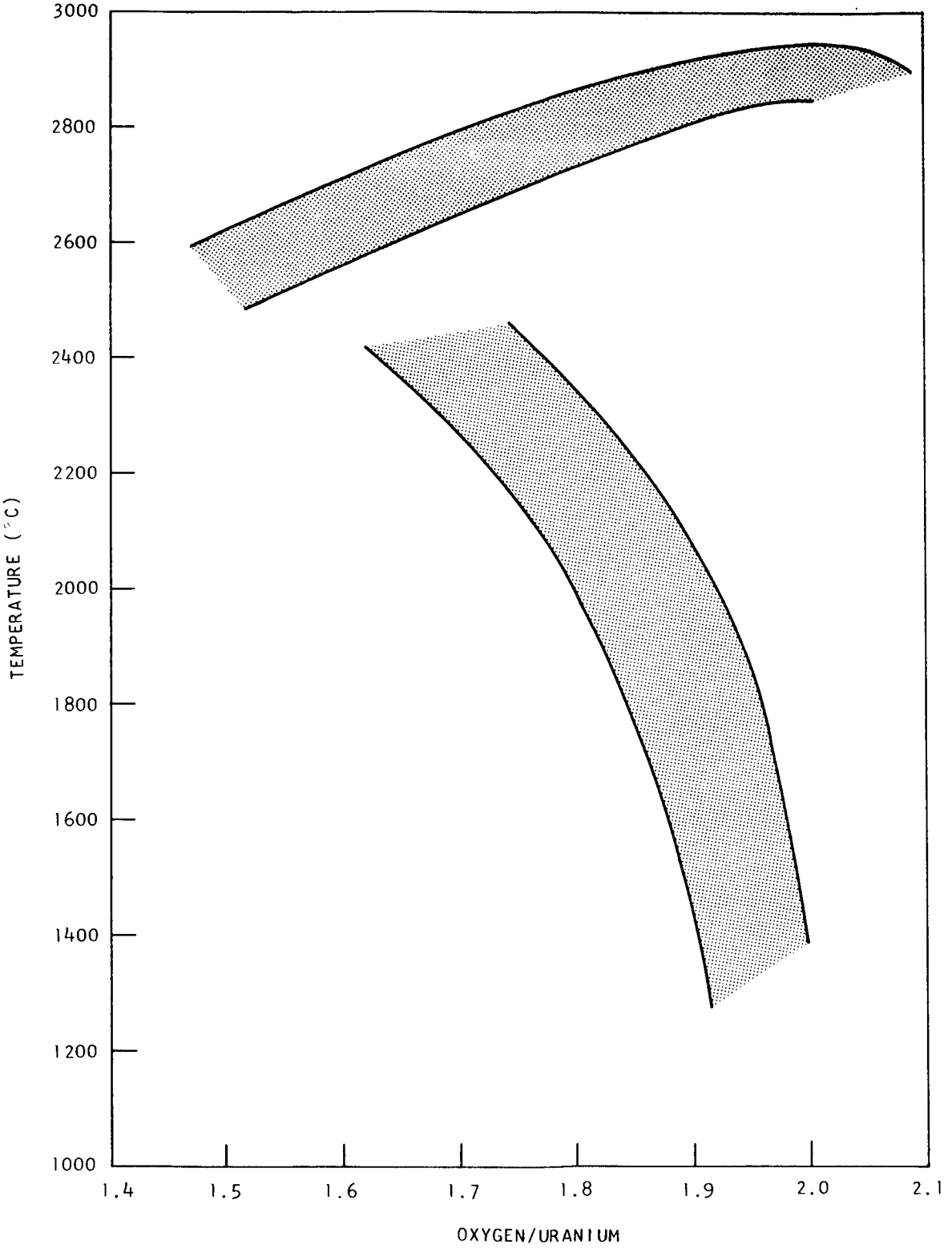

Fig. 65--Probable phase boundaries for the uranium-yttrium-oxygen systems

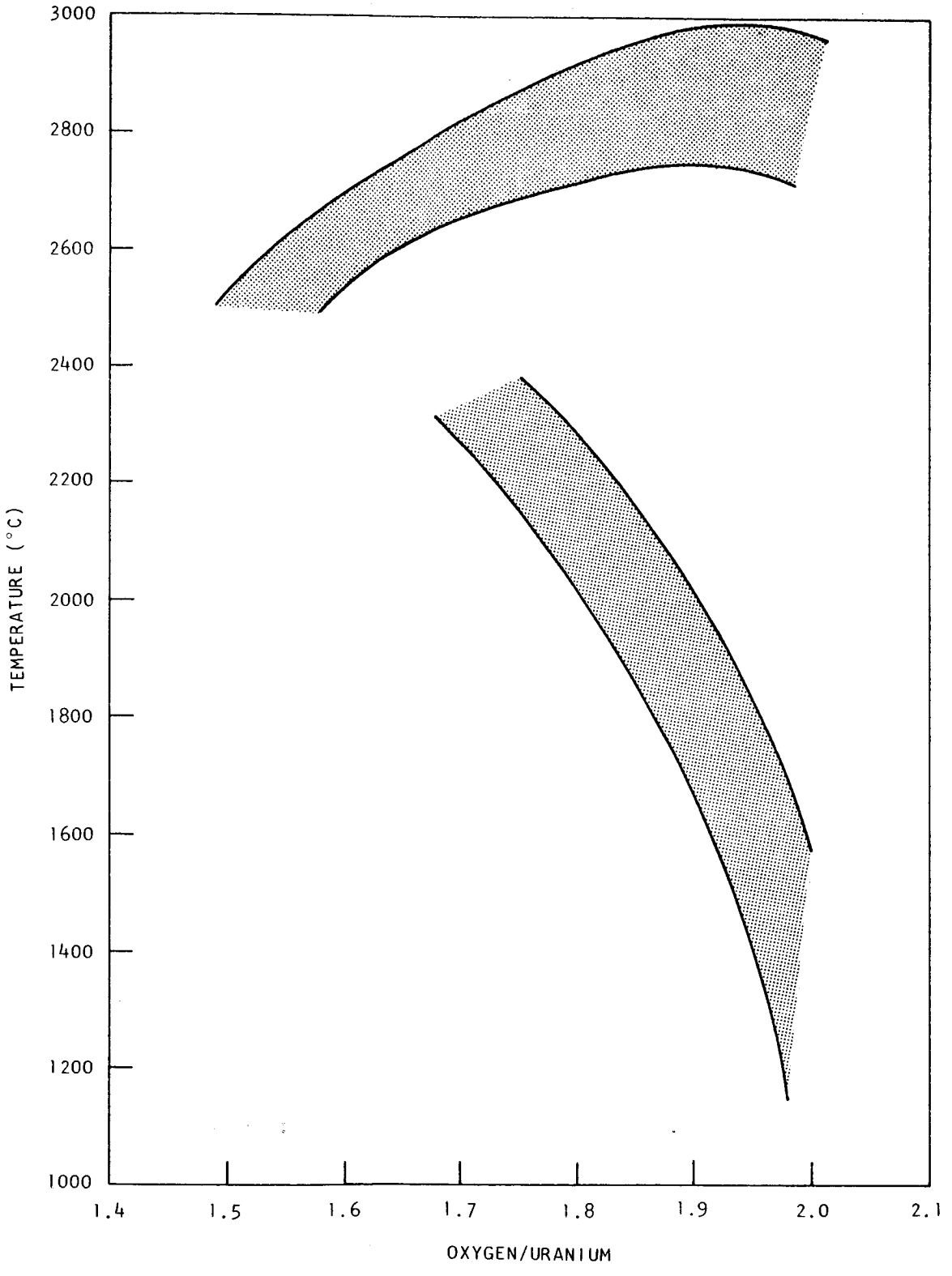

Fig. 66--Probable phase boundaries for the uranium-thorium-oxygen systems

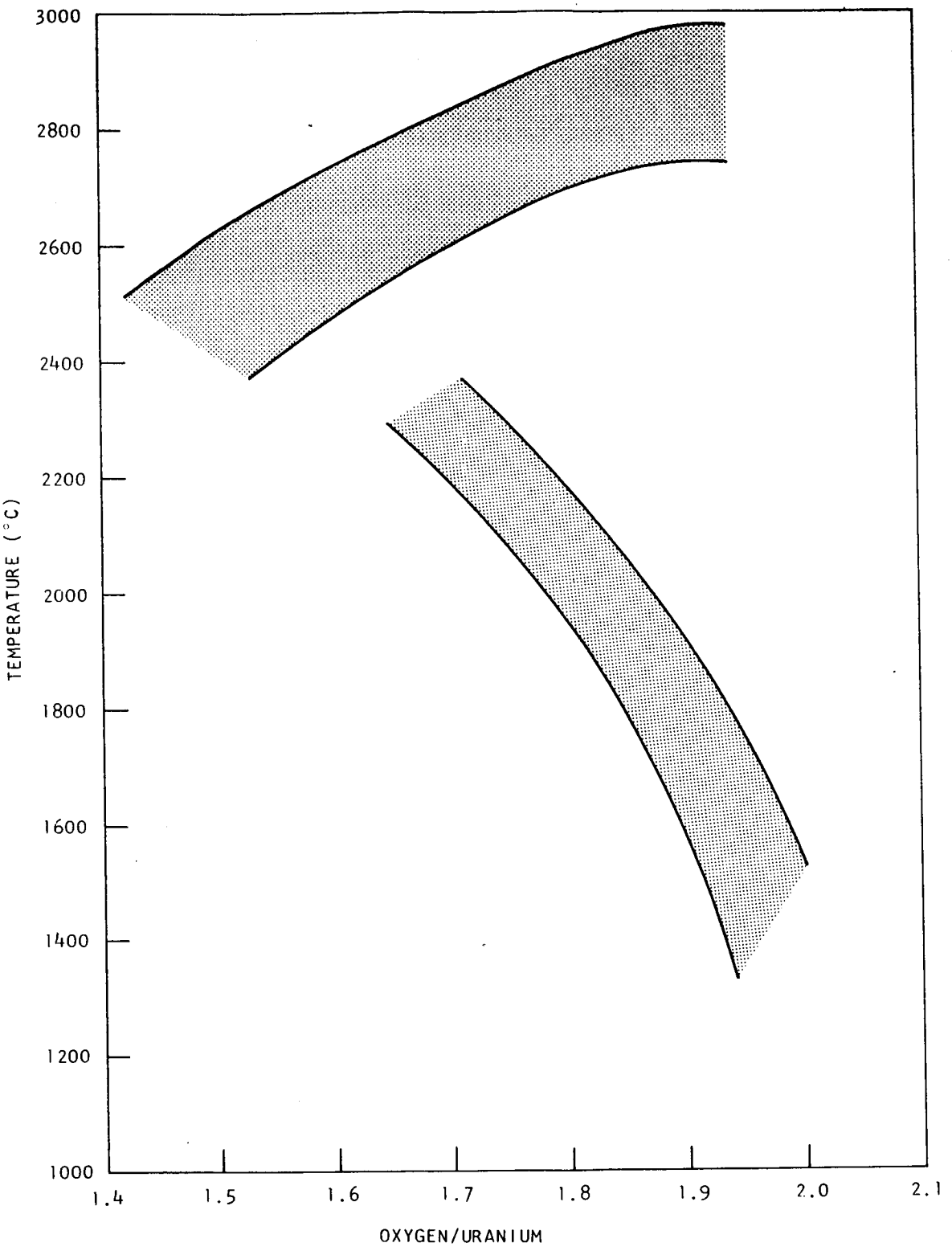

Fig. 67--Probable phase boundaries for the uranium-cerium-oxygen systems

phase transitions of uranium are isothermal reactions, they are readily detected by infrared thermal analysis, even though the enthalpy changes associated with the processes are small. On the other hand, the study of a nonisothermal precipitation reaction (basically a solubility) over a range of $\sim 1000^{\circ}C$ is more difficult and is probably better suited to equilibrium techniques.

The two final conclusions relate to the practical problem of the use of UO_2 as a high-temperature nuclear fuel. First, on the basis of the results of this study, the decrease in the amount of precipitated uranium metal observed in stabilized substoichiometric samples of UO_2 cannot be attributed to a shift in the location of the phase boundary between the single-phase region, UO_{2-x}, and the two-phase region U (liquid) plus $UO_{2.0}$ (solid). Finally, the use of calcia (and possibly yttria) as a stabilizer for UO_2 may substitute problems associated with the loss of the stabilizing oxide from the fuel by volatilization. Ceria and thoria do not present a volatilization problem.

9. RECOMMENDATIONS

A large body of data on the effectiveness of the various oxides as stabilizers for UO_2 has been compiled by the GE-NMPO (4, 23, 18, 13, 24, and 25). Restricting the discussion to the four oxides studied in this investigation, a table can be compiled which summarizes the important properties of these materials on the basis of the GE-NMPO results and the present work. These properties are given in Table 27.

Table 27

PROPERTIES AND EFFECTIVENESS OF SEVERAL STABILIZING OXIDES

Oxide	Reduces Precipitation of U Metal [a]	Reduces Fuel Loss by Volatilization [a]	Reduces Melting Point of UO_2 [b]	Additive Oxide Volatilizes [b]
CaO	Yes	No	Yes	Yes
Y_2O_3	Yes	Yes	Yes	Slightly
ThO_2	No	Yes	No	No
CeO_2	Yes	Yes	No effect	No

[a] Compiled from the NMPO references listed above.
[b] This study, and in some instances confirmed by GE-NMPO.

While thoria has excellent properties with regard to fuel and additive volatilization and melting point, the GE-NMPO data indicate that it is ineffective in reducing uranium precipitation. A major problem is thus left unsolved and thoria alone is, therefore, unsatisfactory. Calcia and yttria both present the problems associated with the volatilization of the stabilizer and reduction of the melting point of UO_2. In addition, calcia enhances fuel loss. Certainly calcia and possibly yttria are, therefore, unsatisfactory. Ceria, on the other hand, exhibits beneficial effects in all four of the properties listed on the basis of data presently available. The stabilizing ability of ceria should be investigated further. Other tetravalent oxides (thoria, zirconia, and hafnia) do not appear to reduce the precipitation of uranium metal, probably because they cannot reduce the oxygen deficiency of the

hypostoichiometric oxide by valence compensation as can trivalent and bivalent oxides. Ceria, as is well known, can be easily reduced to the plus three state, and it is likely that this property distinguishes it from the other tetravalent oxides in its ability to stabilize by valence compensation.

10. ACKNOWLEDGMENTS

The authors are indebted to many people for assistance and helpful discussions during the course of the study.

The analytical chemistry group under A. W. Mosen is due especial thanks, since a considerable part of this program involved analysis of samples. Mr. Ray E. Kelley carried out the direct oxygen determinations, Mr. Gordon Rankin and Mr. Robert Morrissey performed the x-ray spectrographic determinations for uranium, the additive metals, and tungsten impurity. Mrs. Elizabeth Salkeld was responsible for the carbon determinations.

Drs. John H. Norman, Wayne E. Bell, and Ulrich Merten have contributed much to helpful discussions and criticisms of the manuscripts.

Appendix A

The calibration curves for the two quartz and two pyrex windows which were used in the present study are given in Figs. A. 1 to A. 4. These windows were calibrated by standard procedures which measured the absorptions of the windows as a function of temperature by determining the decrease in observed temperature of a tungsten filament. The pyrometer mirror was calibrated by a similar procedure and the data are given in Fig. A. 5.

The brightness pyrometer was calibrated by standard procedures in the Calibration Section of the General Atomic Standards Laboratory. The data obtained in the two calibrations are given in Figs. A. 6 and A. 7.

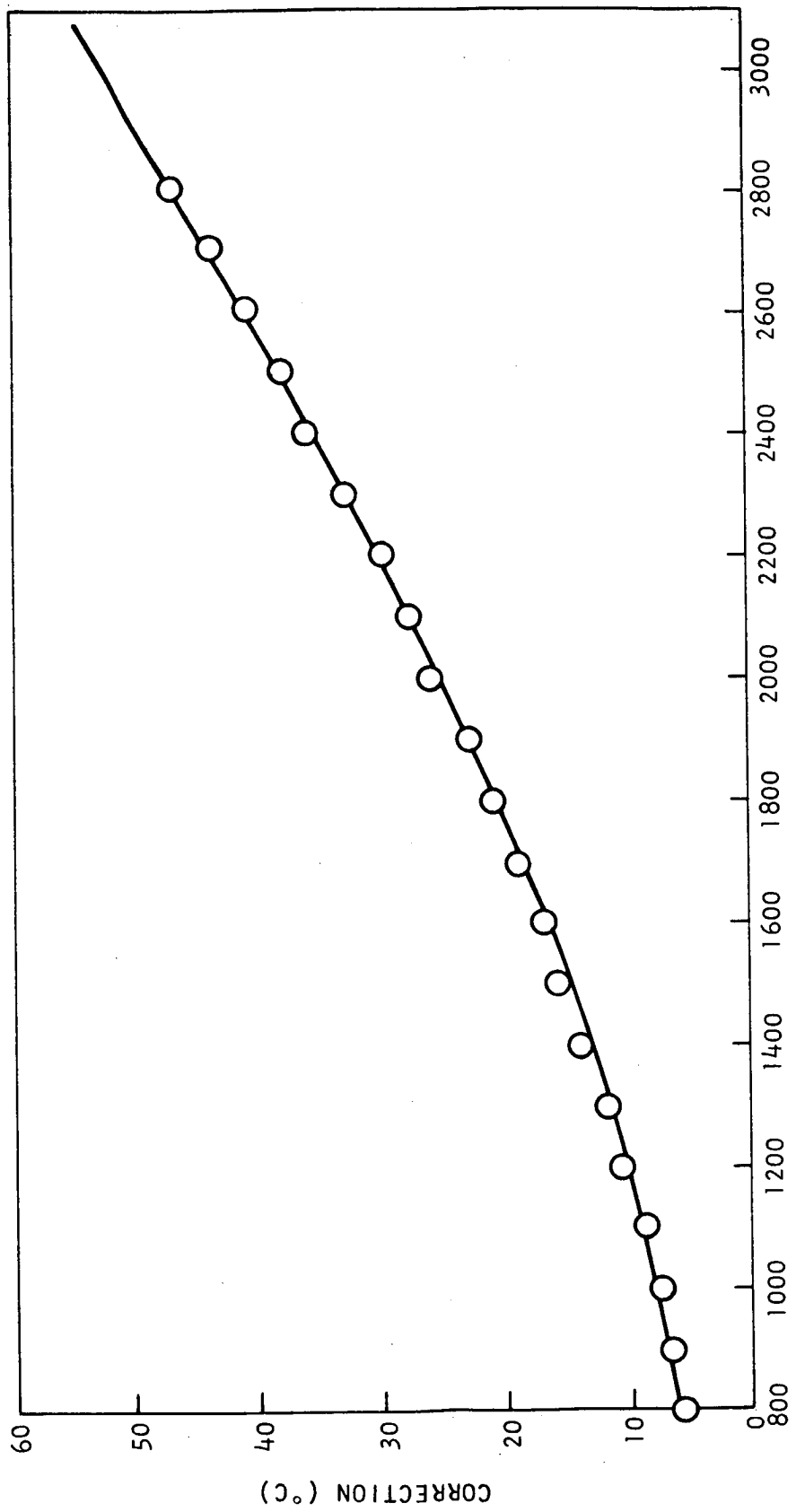

Fig. A.1--Calibration of window P-7

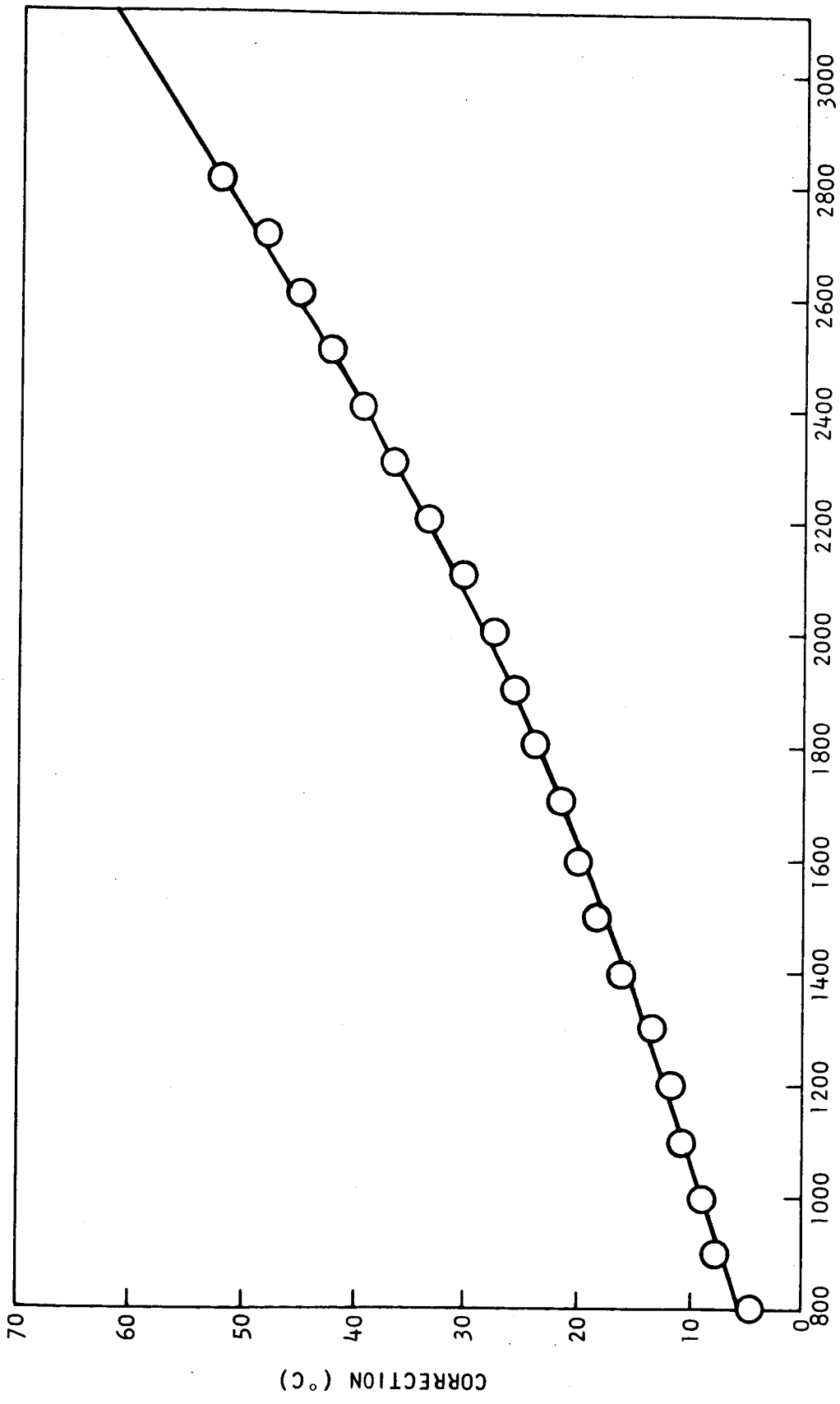

Fig. A.2--Calibration of window P-8

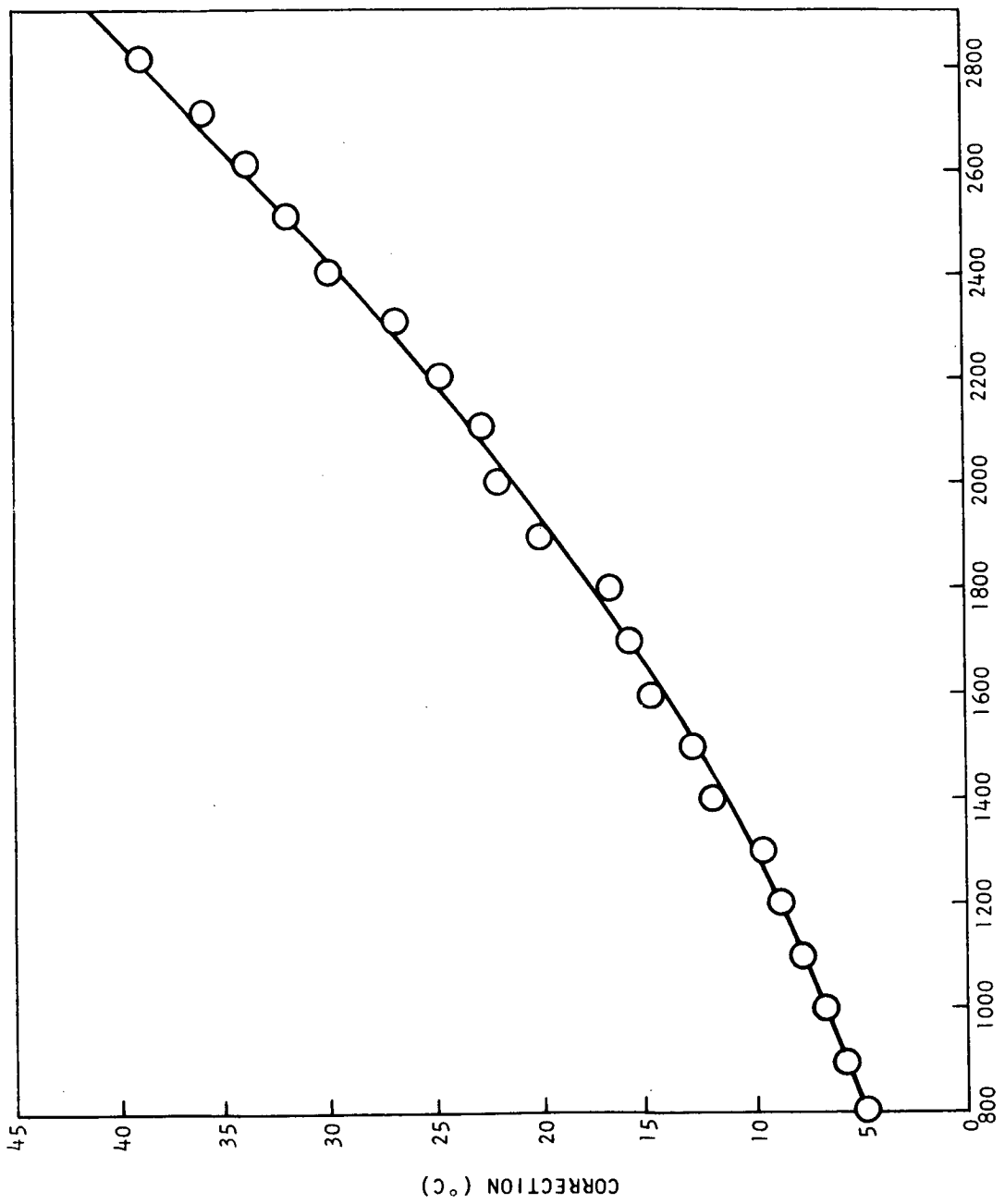

Fig. A.3--Calibration of window Q-1

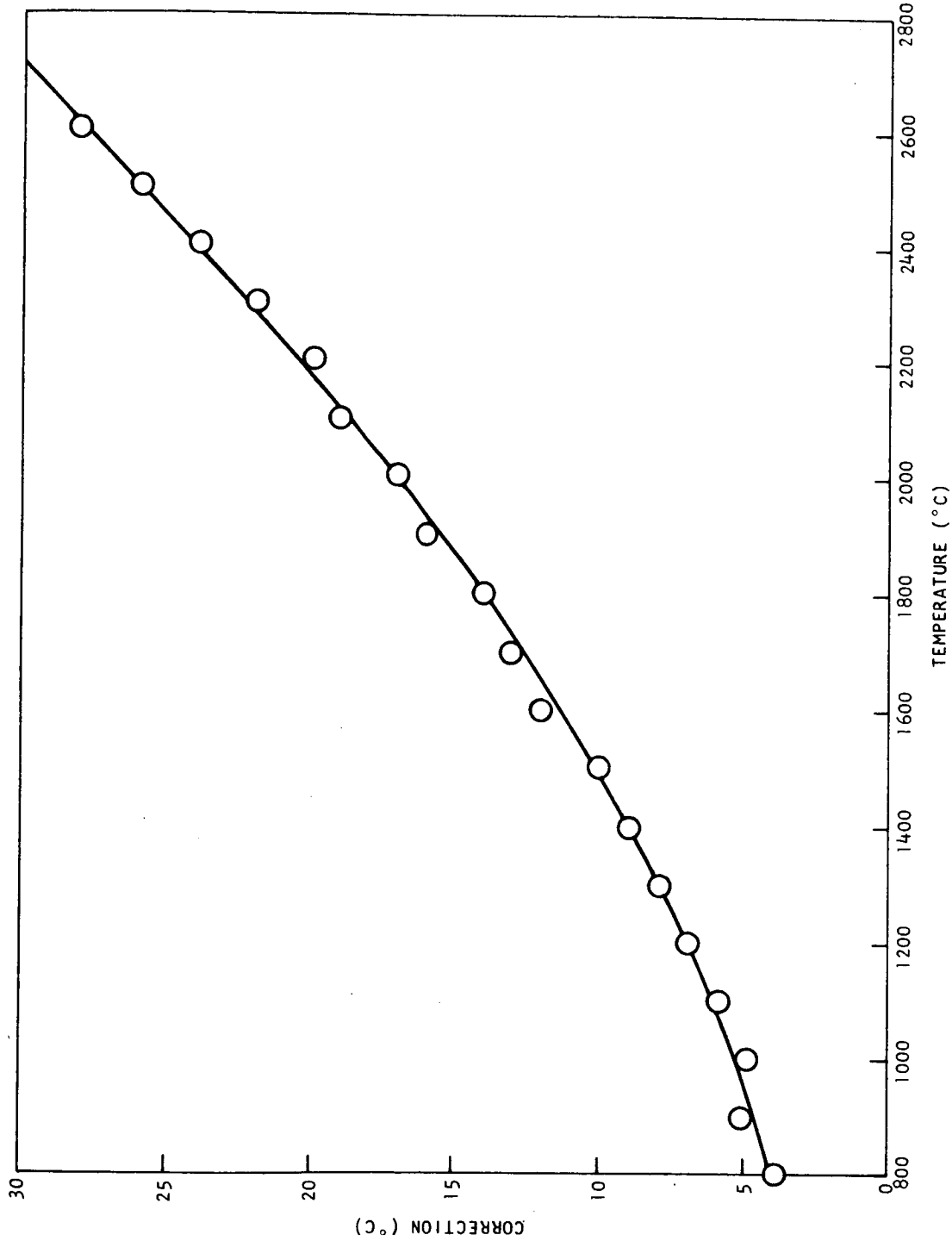

Fig. A.4--Calibration of window Q-2

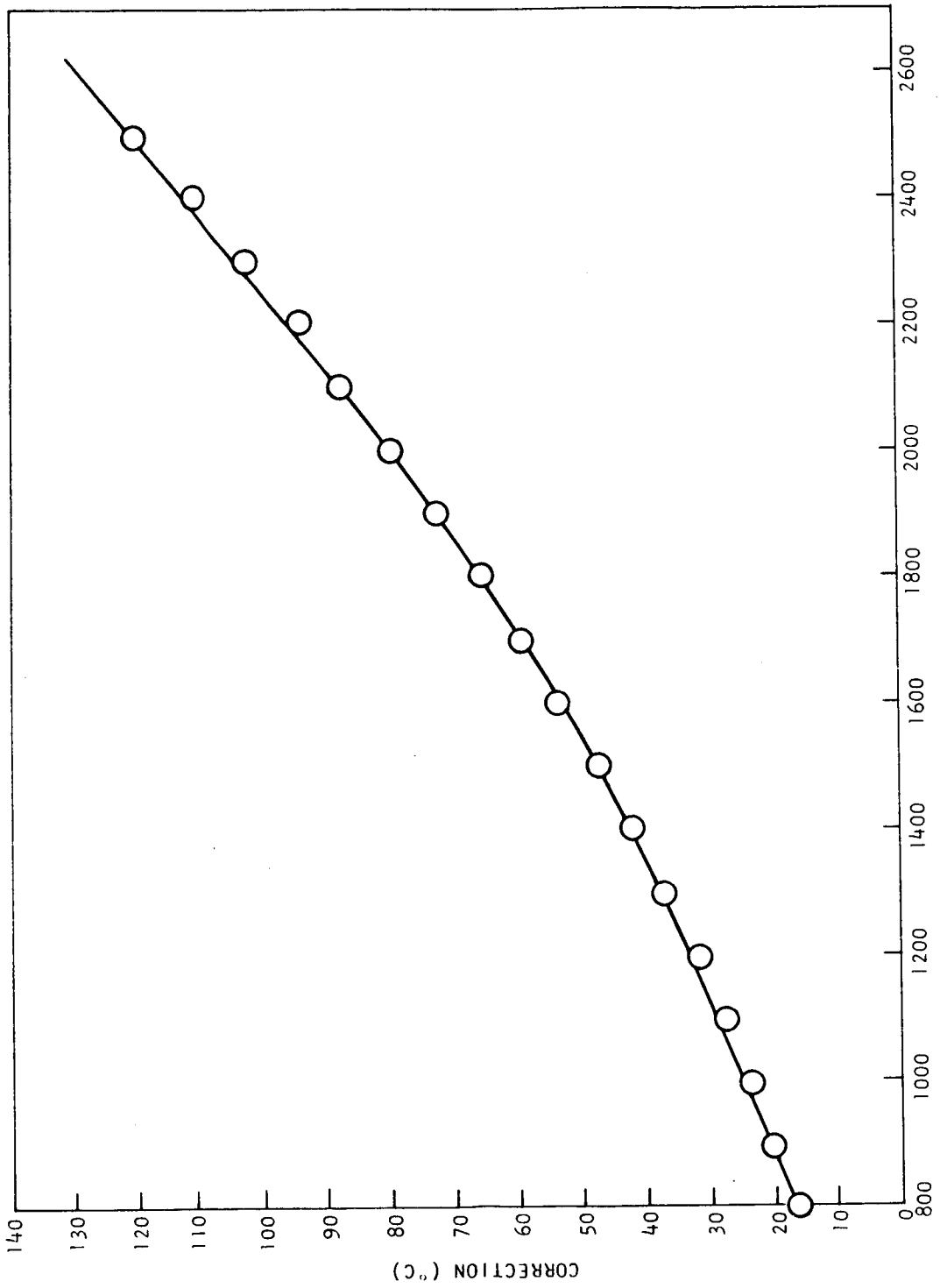

Fig. A.5--Calibration of pyrometer mirror PM-3

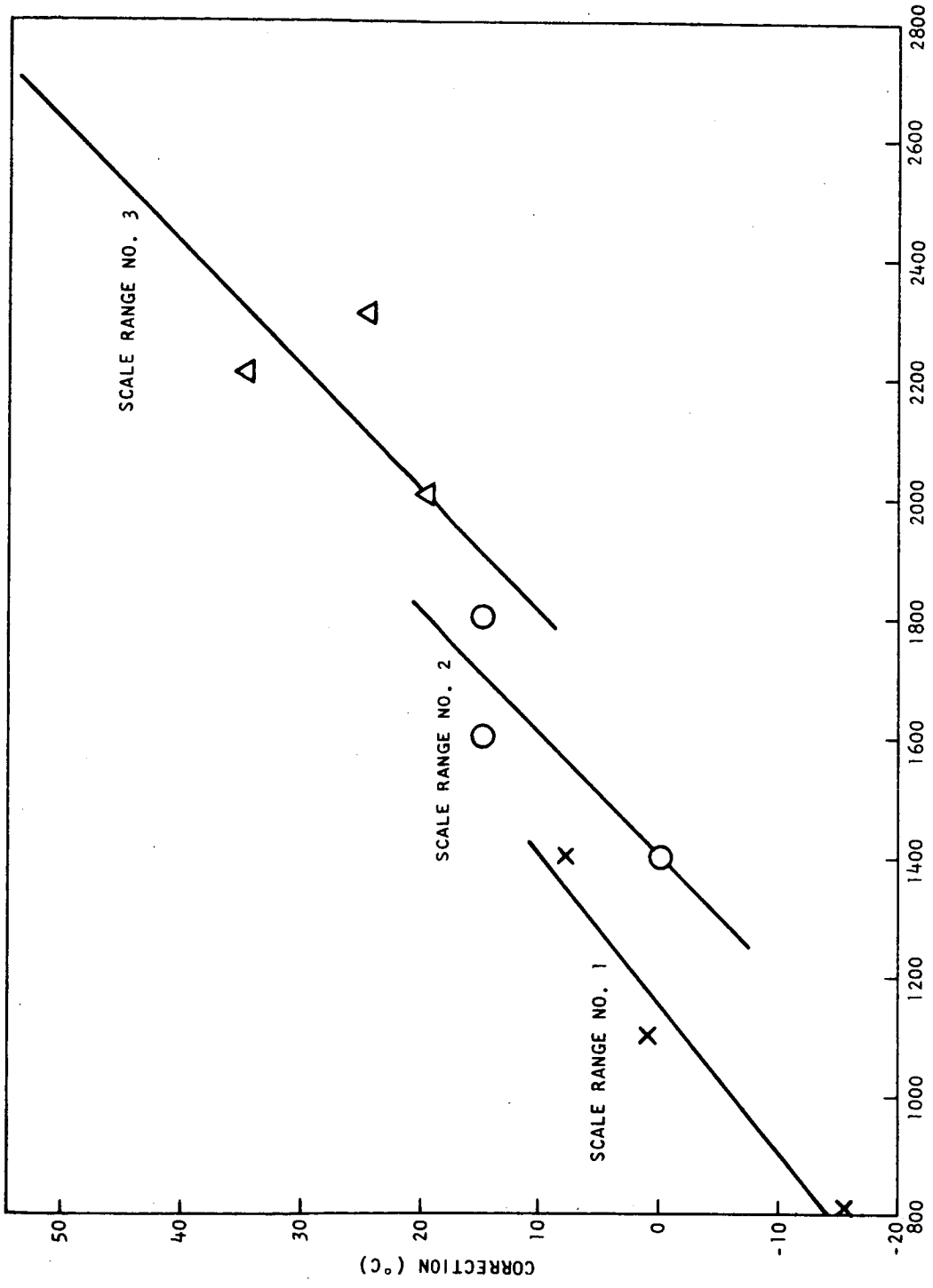

Fig. A.6--Calibration of pyrometer Mod-95 (6-30-65)

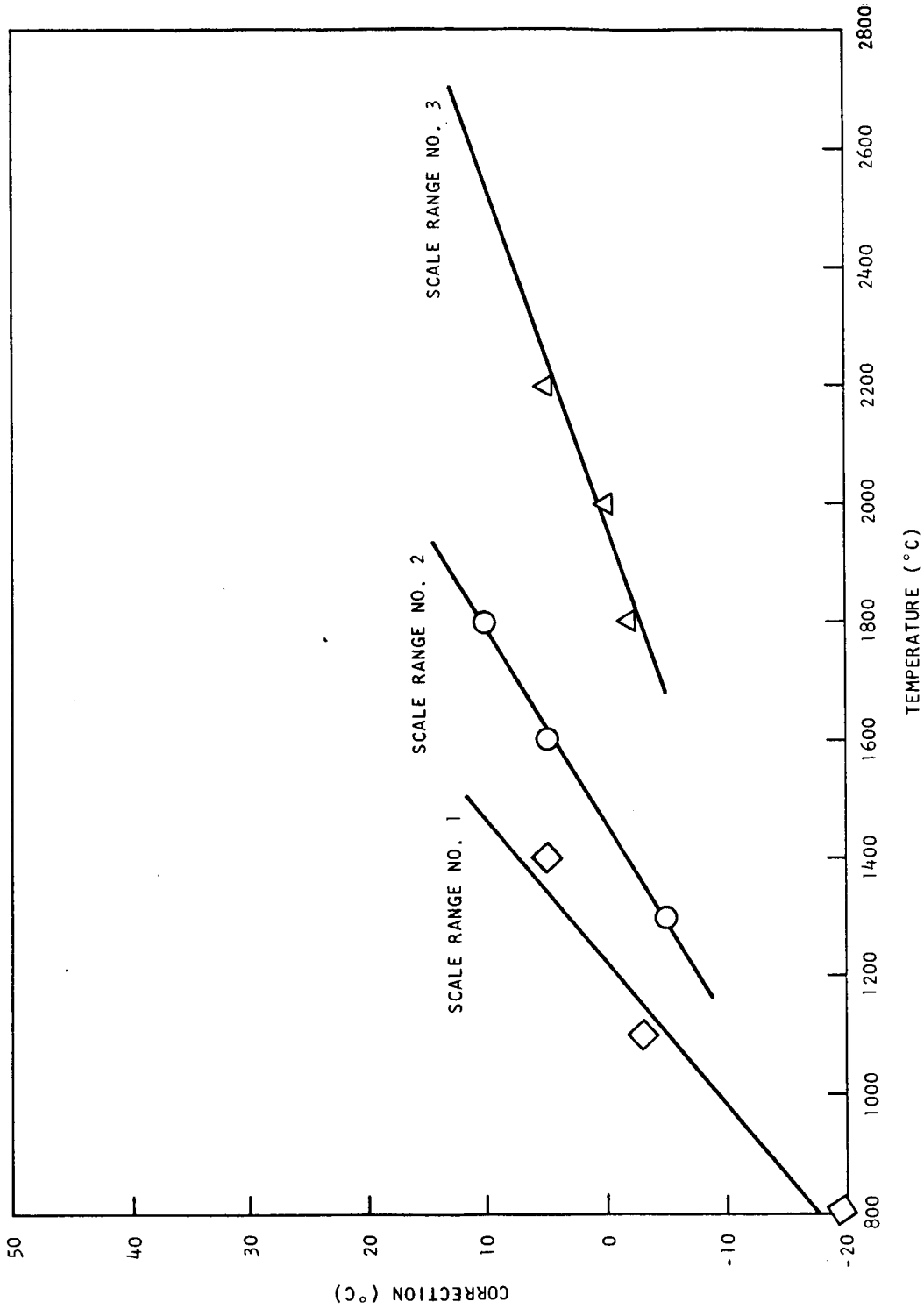

Fig. A. 7--Calibration of pyrometer Mod-95 (11-23-65)

Appendix B

ANALYTICAL PROCEDURES

The detailed analytical procedures used for the analysis of samples for oxygen, the metals, and carbon are described below.

B.1 THE DETERMINATION OF OXYGEN IN UO_2-M_xO_y SYSTEMS

An inert gas fusion-gravimetric procedure was used for the determination of oxygen in the metal oxides. This procedure was basically that described by Holt and Stoessel (26), which depends on the reduction of the oxide by carbon with the formation of CO which is converted to CO_2 and determined gravimetrically.

A sample of the oxide was heated in a covered graphite crucible to reduce the oxide and liberate carbon monoxide. The carbon monoxide was swept by a stream of helium through a furnace tube packed with hot copper oxide where it was oxidized to carbon dioxide. The carbon dioxide was absorbed on ascarite and weighed.

B.2 THE DETERMINATION OF CARBON IN UO_2-M_xO_y SYSTEMS

Carbon was determined in the metal oxides using a Low Carbon Analyzer. This instrument determines carbon by converting it quantitatively to CO_2, which is determined chromatographically.

The samples were weighed in a silica crucible along with a gram of tin metal. The crucible was placed in an induction furnace where the tin was was ignited and burned in a stream of oxygen. The carbon dioxide was collected in a molecular sieve trap. After the ignition was completed, the molecular sieve was heated to release the carbon dioxide which was then measured with a gas chromatograph.

B.3 THE DETERMINATION OF URANIUM AND ADDITIVE ELEMENTS IN THE SYSTEM UO_2-M_xO_y

An x-ray spectrographic procedure was used for the analysis of the oxide systems: UO_2-ThO_2, UO_2-Y_2O_3, UO_2-CeO_2, and UO_2-CaO with varying oxygen contents.

Samples of these materials were fused in sodium tetraborate and cast into beads. After cooling, the beads were polished to give a flat surface. The polished beads were then analyzed by x-ray spectroscopy. The intensities of the appropriate uranium and additive element lines were measured and compared with those of standard beads prepared by fusing known amounts of the oxides of uranium and the additive in sodium tetraborate. These standard beads served as permanent standards.

The spectrographic parameters are given in Table B.1.

Table B.I

SPECTROGRAPHIC PARAMETERS

Element	Analytical Line	Wavelength	Diffraction Crystal	Detector
U	L	0.91053	LiF	NaI(Tl) scintillation counter - air atmosphere
Th	L	0.95598	LiF	NaI(Tl) scintillation counter - air atmosphere
Y	K	0.83019	LiF	NaI(Tl) scintillation counter - air atmosphere
Ce	L	2.56116	LiF	Gas flow proportional counter - helium atmosphere
Ca	K	3.35936	LiF	Gas flow proportional counter - helium atmosphere

APPENDIX C

DERIVATIVE CURVE

	Heating	Cooling
Decomposition temperature	◆	◇
Monotectic and solidus temperature	▲	△
Liquidus temperature	●	○

STANDARD CURVE

	Heating	Cooling
Decomposition temperature	■	□
Monotectic and solidus temperature	▼	▽
Liquidus temperature	⊕	⊕

AVERAGES

	Decomposition Temperature	Monotectic or Solidus Temperature	Liquidus Temperature
Derivative curve average only	[D]	▽D	(D)
Standard curve average only	[S]	▽S	(S)
Average of standard and derivative	[A]	▽A	(A)

REFERENCES

1. Lenz, W. H., "Improved Performance of W-Based UO_2 Fuel Materials," (U) Los Alamos Scientific Laboratory Report LA-3329-MS, July 27, 1965. (C/RD)

2. Gedwill, Michael A., Paul F. Sikora, and Robert M. Caves, "Fuel Retention Properties of Tungsten-Uranium Dioxide Composites," (U) National Aeronautics and Space Administration Report NASA-TM-X-1059, February, 1965. (C/RD)

3. Ackermann, R. J., E. G. Rauh, and M. S. Chandrasekharaiah, "A Thermodynamic Study of the Urania-Uranium System," Argonne National Laboratory Report ANL-7048, July, 1965. (U)

4. "Fourth Annual Report, High Temperature Materials and Reactor Component Development Programs," (U) USAEC Report GEMP-334B, Vol. 2, Nuclear Materials and Propulsion Operation, General Electric Company, February 26, 1965. (S/RD)

5. Martin, A. E., and R. K. Edwards, "The Uranium-Uranium Dioxide Phase Diagram at High Temperatures," J. Phys. Chem. 69, 1788 (1965).

6. Edwards, R. K., and A. E. Martin, "Phase Relations in the Uranium-Uranium Dioxide System at High Temperatures," presented at the Symposium on Thermodynamics with Emphasis on Nuclear Materials and Atomic Transport in Solids, International Atomic Energy Agency, Vienna, July 22-27 (1965). (To be published in the Proceedings of the Symposium.)

7. Bates, J. L., and J. L. Daniel, "Irradiation Damage in UO_2," Ceramics Research and Development Quarterly Report, USAEC Report BNWL-91, Pacific Northwest Laboratory, Battelle Memorial Institute, p. 38. (U)

8. "High Temperature Materials Program Progress Report No. 50, Part B" (U) USAEC Report GEMP-50B, Nuclear Materials and Propulsion Operation, General Electric Company, August 20, 1965. (C/RD)

9. Cohn, C., et al., "Basic Material Resulting from ANL Rocket Study," Argonne National Laboratory Report ANL-6656, May 1963. (U)

10. Langer, S., et al., "Studies in the Thorium-Carbon Binary Systems," in Compounds of Interest in Nuclear Reactor Technology (Proceedings of an International Symposium held August 3-5, 1964, at Boulder, Colorado), J. T. Waber, P. Chiotti, and W. N. Miner, eds., Metallurgical Society of the American Institute of Mining, Metallurgical and Petroleum Engineers, New York, 1964, pp. 359-394.

11. Langer, S., N. Baldwin, and F. Kester, "High-Temperature Thermal Analysis and Differential Thermal Analysis Using Infrared Detection," (to be submitted to Rev. Sci. Instr.).

12. Wolten, G. M., "Diffusionless Phase Transformations in Zirconia and Hafnia," J. Am. Ceram. Soc. 46, 418 (1963).

13. "High Temperature Materials Program Report No. 51, Part B," (U) USAEC Report GEMP-51B, Nuclear Materials and Propulsion Operation, General Electric Co., September 30, 1965. (C/RD)

14. Laitinen, H. A., Chemical Analysis, McGraw-Hill Book Company, New York, 1960.

15. Bockris, J. O'M., J. L. White, J. D. MacKenzie, eds., Physico-chemical Measurements at High Temperatures, Academic Press, Inc., (1959).

16. Ackermann, R. J., P. W. Gilles, R. J. Thorn, J. Chem. Phys. 25, 1089 (1956).

17. Ötvos, J. W. and D. P. Stevenson, J. Amer. Chem. Soc. 78, 546 (1956).

18. "High Temperature Materials Program Report No. 49, Part B," (U) USAEC Report GEMP-49B, Nuclear Materials and Propulsion Operation, General Electric Co., July 28, 1965. (C/RD)

19. Gschneidner, K. A., Rare Earth Alloys, Van Nostrand Company, Inc., Princeton, N. J., 1961, p. 329.

20. Rand, M. H., and O. Kubaschewski, Thermochemical Properties of Uranium Compounds, Interscience Publishers, New York, 1963, p. 8.

21. Marsh, J. S., Principles of Phase Diagrams, McGraw-Hill Book Co., New York, (1935) p. 94ff.

22. "High Temperature Materials Program Report No. 54, Part B," (U) USAEC Report GEMP-54B, Nuclear Materials and Propulsion Operation, General Electric Co., December 20, 1965. (C/RD)

23. "Third Annual Report, High Temperature Materials and Reactor Component Development Programs," (U) USAEC Report GEMP-270B, Vol. 2, Nuclear Materials and Propulsion Operation, General Electric Company, February 28, 1964. (S/RD)

24. "High Temperature Materials Program Report No. 53, Part B," (U) USAEC Report GEMP-53B, Nuclear Materials and Propulsion Operation," General Electric Co., November 26, 1965. (C/RD)

25. "High Temperature Materials Program Report No. 47, Part B," (U) USAEC Report GEMP-47B, Nuclear Materials and Propulsion Operation," General Electric Co., May 28, 1965. (C/RD)

26. Holt, B. D., J. E. Stoessel, Anal. Chem. 36, 1320 (1964).

(This page intentionally left blank.)